

# Polymer bonding and adhesion on aluminium and magnesium alloys

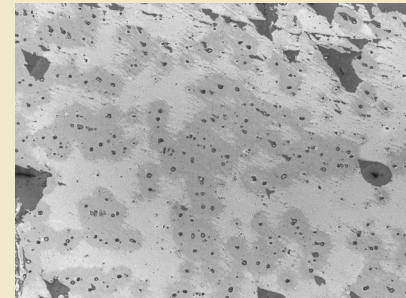
Polymer bonding and adhesion on aluminium and magnesium alloys - F.M. de Wit

F.M. de Wit

## Uitnodiging

voor het bijwonen van de  
openbare verdediging van mijn  
proefschrift:

*Polymer bonding  
and adhesion  
on aluminium and  
magnesium alloys*



op maandag  
5 november 2012  
om 15.00 uur

De promotie zal plaatsvinden  
in de Senaatszaal van de Aula  
van de Technische Universiteit  
Delft aan de Mekelweg 5, Delft

Aansluitend op de promotie-  
plechtigheid wordt een receptie  
gehouden, ook in de Aula.

**Frederik de Wit**

Propositions, part of the thesis: **Polymer bonding and adhesion on aluminium and magnesium alloys**

1. Without chemical bonding, adhesion cannot exist.

2. Contrary to what is usually assumed, the quality of adhesion of coatings on metal substrates is mainly determined by the local (oxide) composition of the substrates.

3. Improving adhesion on metals through roughening is not due to “mechanical interlocking”, but mainly because removing the top layer creates a fresh oxide and removes organic contamination.

A.F. Harris, A. Beevers, *International Journal of Adhesion and Adhesives* **1999**, *19*, 445.

4. It is wrong to assume bonding of PET molecules on aluminium is through molecular end-groups only since saponification of the ester groups can also lead to bonding possibilities.

F.M. De Wit, Ö. Özkanat, J.M.C. Mol, H. Terryn, J.H.W. De Wit, *Surface and Interface Analysis* **2010**, *42*, 316.

5. It is not possible to measure delamination with Scanning Kelvin Probe (SKP) for systems where the delamination mechanism is dominated by displacement of polymer-metal bonds by water.

6. Rights are not social privileges but objective facts, identifying the freedoms we need to live our lives - whether a majority in society agrees or not.

Thomas A. Bowden in “Supreme Disappointments”, Ayn Rand Center for Individual Rights, November 3rd, 2008, <http://tinyurl.com/9fr3lga>

7. Persuasion is clearly a sort of demonstration, since we are most fully persuaded when we consider a thing to have been demonstrated.

Aristotele’s Rethoric, Book 1, 1355a (translation by W. Rhys Roberts)

8. Since mobile phone use by children increases the chances of brain tumors, more public information on the risks in the Netherlands is urgently needed.

F. Soderqvist, M. Carlberg, K.H. Mild, L. Hardell, *Environmental Health* **2011**, *10*.

9. "Green" subsidies on electric cars are misplaced, because "electrifying" all cars would result in a worldwide depletion of lithium or nickel resources in around 15 years if the number of new cars stays at the level of 2010.

H. Wouters and D. Bol in *Material Scarcity An M2i study* **2009**

10. The importance of adhesion is usually only noticed, when it is not present.

*These propositions are regarded as opposable and defensible, and have been approved as such by the supervisors prof. dr. R. Boom and prof. dr. ir. H. Terryn*

Stellingen behorende bij het proefschrift: **Polymer bonding and adhesion on aluminium and magnesium alloys**

1. Zonder chemische binding kan er geen hechting zijn.
2. In tegenstelling tot wat doorgaans gedacht wordt, wordt de kwaliteit van hechting van organische deklagen op metalen wordt hoofdzakelijk bepaald door de lokale samenstelling van de substraten
3. Het verbeteren van hechting op metalen door opruwen kan niet worden toegeschreven aan “mechanische interlocking”, maar is voornamelijk het gevolg van het verwijderen van de oppervlaktelaag, wat een vers oxide creëert en organische vervuiling verwijdert.
4. Het is verkeerd om aan te nemen dat binding van PET moleculen op aluminium alleen door moleculaire eindgroepen tot stand komt, omdat verzeeping van de ester groepen ook kan leiden tot bindingsmogelijkheden.

F.M. De Wit, Ö. Özkanat, J.M.C. Mol, H. Terryn, J.H.W. De Wit, *Surface and Interface Analysis* **2010**, *42*, 316.

5. De kwaliteit van de hechting van organische deklagen op metalen substraten wordt hoofdzakelijk bepaald door de locale samenstelling van de substraten.
6. Rechten zijn geen sociale privileges maar objectieve feiten, die de vrijheden definiëren die we nodig hebben om onze levens te leven - of de meerderheid het daar nou mee eens is of niet.

Thomas A. Bowden in “Supreme Disappointments”, Ayn Rand Center for Individual Rights, November 3rd, 2008, <http://tinyurl.com/9fr3lga>

7. Overtuiging is een soort bewijs, want we zijn het meest overtuigd als we aannemen dat iets bewezen is

Aristoteles' Rethoric Book 1 1355a, 11

8. “Groene” subsidies op elektrische auto’s zijn misplaatst, omdat het elektrisch maken van alle auto’s tot gevolg zou hebben dat de wereldwijde voorraden lithium of nikkel binnen circa 15 jaar uitgeput zijn als het aantal nieuwe auto’s gelijk zou blijven aan het niveau van 2010.

H. Wouters and D. Bol in *Material Scarcity An M2i study* **2009**

9. Omdat het gebruik van mobiele telefoons bij kinderen de kans op hersentumoren vergroot, is er dringend meer openbare informatie over de risico’s in Nederland nodig.

F. Soderqvist, M. Carlberg, K.H. Mild, L. Hardell, *Environmental Health* **2011**, 10.

10. Het belang van hechting wordt meestal pas opgemerkt bij het ontbreken ervan.

*Deze stellingen worden opponeerbaar en verdedigbaar geacht en zijn als zodanig goedgekeurd door de promotoren prof. dr. R. Boom en prof. dr. ir. H. Terryn*

# **Polymer bonding and adhesion on aluminium and magnesium alloys**

## **Proefschrift**

ter verkrijging van de graad van doctor  
aan de Technische Universiteit Delft,  
op gezag van de Rector Magnificus prof.ir. K.C.A.M. Luyben,  
voorzitter van het College voor Promoties,  
in het openbaar te verdedigen  
op maandag 5 november 2012 om 15.00 uur

door

**Frederik Mathijs DE WIT**  
materiaalkundig ingenieur  
geboren te Utrecht

Dit proefschrift is goedgekeurd door de promotoren:  
Prof. dr. R. Boom  
Prof. dr. ir. H. Terryn

Samenstelling promotiecommissie:

Rector Magnificus,	voorzitter
Prof. dr. R. Boom,	Technische Universiteit Delft, promotor
Prof. dr. ir. H. Terryn,	Vrije Universiteit Brussel, België, promotor
Prof. dr. J. Sietsma,	Technische Universiteit Delft
Prof. dr. ir. R. Benedictus,	Technische Universiteit Delft
Prof. dr. J.T.M. de Hosson,	Rijksuniversiteit Groningen
Prof. dr J. Watts,	University of Surrey, Verenigd Koninkrijk
Dr. ir. D.H. van der Weijde,	Tata Steel Europe

This research was carried out under project number MC6.04196 in the framework of the Research Program of Materials innovation institute M2i in the Netherlands ([www.m2i.nl](http://www.m2i.nl))

ISBN 978-90-77172-84-1

Copyright © 2012 by F.M. de Wit

*Printed by: Ipskamp Drukkers, Enschede, The Netherlands*

## Table of contents

<b>Chapter 1 - Introduction</b>	<b>7</b>
<hr/>	
<b>Chapter 2 - Background</b>	<b>13</b>
<b>2.1 Introduction and scope</b>	<b>15</b>
<b>2.2 Materials used</b>	<b>15</b>
2.2.1 Aluminium, magnesium and alloys	15
2.2.2 Applications of aluminium-magnesium and magnesium-aluminium alloys	19
2.2.3 Protection (from corrosion) of aluminium-magnesium and magnesium-aluminium alloys	20
<b>2.3 Aluminium and magnesium oxides</b>	<b>23</b>
2.3.1 Composition of aluminium and magnesium alloy oxides	23
2.3.2 Chemical properties of aluminium-magnesium oxide surfaces	25
2.3.3 Influences of pretreatments on the oxides of aluminium and magnesium alloys	30
<b>2.4 Theories of bonding and adhesion of organic molecules and coatings on metals</b>	<b>32</b>
2.4.1 Definitions	32
2.4.2 Bonding physics and chemistry of polymers on metals: interaction at oxides	33
2.4.3 Organic coatings and representative molecules	40
2.4.4 Macroscopical mechanical adhesion testing	41
2.4.5 Failure	42
2.4.6 Relation between bonding and adhesion	43
<hr/>	
<b>Chapter 3 - Experimental</b>	<b>51</b>
<b>3.1 Introduction</b>	<b>53</b>
<b>3.2 Materials</b>	<b>53</b>
3.2.1 Substrates	53
3.2.2 Preparation	54
3.2.3 Molecules	55



3.2.4 PETG coatings	57
<b>3.3 Pre-treatments and application methods</b>	<b>57</b>
3.3.1 Pre-treatments of alloys	57
3.3.2 Application of molecules	58
<b>3.4 Experimental equipment and methods</b>	<b>59</b>
3.4.1 Auger Electron Spectroscopy (AES) depth profiling	59
3.4.2 Fourier Transform Infrared - Reflection Absorbtion Spectroscopy (FTIR-RAS)	59
3.4.3 Asymmetrical Double Cantilever Beam	60
3.4.4 Potentiodynamic measurements	61
<b>Chapter 4 - Analysis of the surface composition of pre-treated aluminium alloys</b>	<b>63</b>
<hr/>	
<b>4.1 Introduction</b>	<b>65</b>
<b>4.2 Results...</b>	<b>65</b>
4.2.1 AES analysis of chemically pre-treated samples	67
4.2.2 AES analysis of heat pre-treated samples	70
<b>4.3 Discussion</b>	<b>73</b>
4.3.1 AES analysis of chemically pre-treated samples	73
4.3.2 AES analysis of heat pre-treated samples	74
<b>4.4 Conclusions</b>	<b>76</b>
<b>Chapter 5 - Electrochemical behavior of pre-treated aluminium and aluminium magnesium alloy in neutral and acidified saline environments</b>	<b>79</b>
<hr/>	
<b>5.1 Introduction and background</b>	<b>81</b>
<b>5.2 Results</b>	<b>85</b>
<b>5.3 Discussion</b>	<b>89</b>
<b>5.4 Conclusions</b>	<b>91</b>
<b>Chapter 6 - Bonding of succinic acid and di-methyl terephthalate</b>	<b>95</b>
<hr/>	
<b>6.1 Introduction</b>	<b>97</b>
<b>6.2 Results</b>	<b>99</b>

6.2.1 FTIR-RAS analysis of bonding of succinic acid to chemically pretreated aluminium alloy surfaces	99
6.2.2 FTIR-RAS analysis of bonding of succinic acid on heat-treated aluminium alloy surfaces, vacuum evaporated magnesium and AZ31	103
6.2.3 FTIR-RAS analysis of bonding of dimethyl terephthalate (DMT) on pretreated aluminium alloy surfaces	105
<b>6.3 Discussion</b>	<b>107</b>
6.3.1 Bonding of succinic acid on heat-treated aluminium alloy surfaces, vacuum evaporated magnesium and AZ31	107
6.3.3 Bonding of dimethyl terephthalate (DMT) on pretreated aluminium alloy surfaces	107
<b>6.4 Conclusions</b>	<b>112</b>
6.4.1 Bonding of succinic acid on presented surfaces	110
6.4.2 Bonding of DMT on presented surfaces	110

## **Chapter 7 - Bonding and stability of succinic acid on magnesium alloy** **115**

---

<b>7.1 Introduction</b>	<b>117</b>
<b>7.2 Results</b>	<b>117</b>
7.2.1 FTIR-RAS analysis of bonding of succinic acid to chemically pretreated magnesium alloy surfaces	117
7.2.2 Aqueous stability of succinic acid on the differently prepared substrates	120
7.2.3 Influence of aging in air	122
7.2.4 Bonding of succinic acid molecules on aged samples	124
7.2.5 Morphological characterization	125
<b>7.3 Discussion</b>	<b>128</b>
7.3.1 Bonding of succinic acid on AZ31	128
7.3.2 Bonding stability of succinic acid on pretreated AZ31	129
7.3.3 Influence of aging on bonding	130
<b>7.4 Conclusions</b>	<b>130</b>

<b>Chapter 8 - Adhesion of PETG</b>	<b>133</b>
<b>8.1 Introduction</b>	<b>135</b>
<b>8.2 Results</b>	<b>136</b>
8.2.1 Energy release rates from ADCB	136
8.2.2 Morphological analysis of delamination on aluminium surfaces	139
<b>8.3 Discussion</b>	<b>141</b>
8.3.1 Interpretation of ADCB results	141
8.3.2 Morphological analysis of delamination on aluminium surfaces	143
8.3.3 Comparison to FTIR-RAS results from chapter 6	144
<b>8.4 Conclusions</b>	<b>145</b>
<b>Chapter 9 - Summarizing conclusions</b>	<b>149</b>
<b>Introductory chapters</b>	<b>151</b>
<b>Surface Characterization (chapters 4 and 5)</b>	<b>151</b>
<b>Nanosopic/molecular interactions at the interface (chapters 6 and 7)</b>	<b>154</b>
<b>Macroscopical/mechanical testing of adhesion (chapter 8)</b>	<b>156</b>
<b>Epilogue and outlook</b>	<b>159</b>
<b>Summary</b>	<b>161</b>
<b>Samenvatting</b>	<b>163</b>
<b>Publications related to this work</b>	<b>165</b>
<b>Dankwoord</b>	<b>167</b>
<b>Curriculum Vitae</b>	<b>169</b>

# Chapter 1 - Introduction



Adhesion is a vast field in science, with an increasing number of publications on different systems, ranging from atomic-size (modeling) research<sup>[1]</sup> to the testing of macroscopic systems like adhesively bonded tailor made blanks for the aircraft industry<sup>[2]</sup>. The importance of adhesion, i.e. the macroscopic behavior of an (organic) coating adhering to a metal, is usually only noticed, when it is *not* present: when systems start to fail and for instance, corrosion can take place on the freely accessible metal surface resulting in coating blistering and cracking. The results (of the failing) of adhesion are present all around us in our daily lives. Modern consumption patterns are very reliant on the durability of bonding between polymers and between polymers and metals. Examples are so numerous that it would be hard to name an activity in daily life that doesn't rely on the presence of adhesion. Construction activities, (food) packaging and transportation (trains, busses, cars, bikes and airplanes), just to name a few, would be much more expensive, nearly impossible or very risky at best, if the durability of the adhesion in these systems would not be well optimized. Not only mechanical failure of a system is a problem, but also mentioned before, the subsequent corrosion which can occur freely if the adhesion of an organic coating to a metal surface is not adequate. Preventable corrosion takes up 3 percent of the GDP of Western countries, which in the Netherlands roughly amounts to €18 billion *annually* (estimation by Dutch Corrosion Centre NCC<sup>[3]</sup>). Not all of this can be ascribed to adhesion failure, but nevertheless, improving adhesion of organic coatings can lower this figure considerably.

To be able to understand adhesion, one must go back to the basics of bonding. Why do materials stick to each other, what is the driving force and how can one influence it beneficially? These are broad questions, for which answers will be presented on specific systems of aluminium and magnesium alloys and particular molecules and coatings. Adhesion (macroscopic, mechanical testing) and bonding (nanoscopic, chemical interfaces), though related issues are discussed separately, which is also observed in literature (chapter 2 elaborates on this).

Previous research on aluminium has shown that increasing the OH concentration<sup>[4]</sup>, the hydroxides formed from the oxides by pre-treatment in for instance an alkaline solution, could improve the bonding of ester<sup>[5]</sup> and carboxylic acid<sup>[6]</sup> groups. Also, macroscopic adhesion of epoxy coatings could be improved by boiling aluminium in water<sup>[7]</sup>.

However, aluminium alloying elements and their effect on adhesion were not taken into consideration. Therefore, the research of this thesis started as an extension to the previous work, studying the adhesion of polymer coatings on two aluminium alloys. As alloying element magnesium was chosen because of its relatively high

solid solubility in aluminium and its homogeneous distribution (precipitates are approximately 1 - 5  $\mu\text{m}$ ). Moreover, from an industrial perspective, magnesium is a very relevant element, since AA5xxx series is used widely. More specifically, a nearly pure aluminium alloy (99.5 wt% Al), which was studied before and an Al-Mg alloy (AA5182, 4.8 wt% Mg) were compared. The pure metals, vacuum-evaporated onto glass slides were used as references. One chapter of this thesis is dedicated to the bonding behavior on an Mg-Al alloy. Pre-treatments were given to both alloys and the bonding of molecules was compared *qualitatively* while the macroscopic adhesion of two coatings was studied *quantitatively*. For one system both properties were coupled, i.e. the bonding of the molecules was linked to macroscopic adhesion, as expected from literature<sup>[8]</sup>, to study the influence of the alloying element magnesium.

In the next chapter (Chapter 2) an overview is given of the literature that forms the background of this thesis. It is focused on the relevant (chemical) properties of the aluminium alloy oxide surface, the methods to investigate these properties and summarizes previously obtained results and conclusions. Furthermore, the theories of bonding and adhesion are discussed. A prediction from theory is given for the bonding strength of succinic acid to the chosen alloys while a very weak bonding is expected for DMT on Al- and Mg-alloy. Finally, some macroscopical testing methods and results are evaluated. Chapter 3 then continues with the specific materials, (pre-treatment) methods and equipment used and mentioned in this thesis.

The approach followed in this thesis consists of three steps as also summarized in Fig 1.1. The first step starts with the understanding of the metal alloy oxides. In chapter 4, Auger Electron Spectroscopy (AES) depth-profiles are discussed, which reveal the chemical composition of the aluminium-magnesium alloy surfaces after simple pre-treatments, like acid and alkaline etching and heat pre-treatments. Chapter 5 is grouped with chapter 4 because it discusses the electrochemical characterization of the used surfaces. This adds to the understanding of certain concepts, which (indirectly) govern bonding or can be used as quantitative or qualitative indication of the possibility of metal-polymer compatibility, like the isoelectric point of the surface (IEPS).

The next step is to investigate the behavior of polymers on these surfaces at a microscopic (actually *nanoscopic*) level. Here, the method of virtually breaking down polymers into the molecules, which are held responsible for the bonding of the longer polymer chains, was chosen. This means that succinic acid was used to mimic the behavior of bonds added to otherwise a-polar polyethylene (PE). In a similar way, di-methyl-terephthalate (DMT) was used as a mimic molecule of polyethylene-terephthalate (PET). Chapter 6 gives various results obtained with Fourier

Transform Infrared Reflection Absorption Spectroscopy (FTIR-RAS) of succinic acid and DMT on the aluminium-magnesium alloy. Chapter 7 shows the behavior of magnesium-aluminium alloys as well as the stability of succinic acid molecules on the surfaces of these alloys in the presence of water. Also a comparison is made with the prediction in chapter 2 on water displacement.

The last part, finally, contains the third and last step of the approach followed. In chapter 8, the macroscopic adhesion behavior of a polymer film was tested. PET(G) was bonded to the pretreated alloys and the films were subsequently delaminated with the novel method of asymmetrical double cantilever beam (ADCB). The results are coupled to the chemical data collected in chapter 6 and compared with the theoretical values as calculated in Chapter 2. Finally, in chapter 9 a summary is given and conclusions are drawn following from the previous chapters with a holistic view on the future of adhesion science.

## References

- [1] K. L. Mittal, A. Pizzi, Adhesion promotion techniques: technological applications, Dekker, New York, **1999**.
- [2] A. A. Zadpoor, J. Sinke, R. Benedictus, *International Journal of Adhesion and Adhesives* **2009**, *29*, 558.
- [3] N. W. Buijs, *Voorkomen corrosie kan miljoenen euro schade besparen* Metaalmagazine 1, Eisma Industrialmedia BV, Doetinchem, **2007**.
- [4] J. van den Brand, P. C. Snijders, W. G. Sloof, H. Terryn, J. H. W. de Wit, *Journal of Physical Chemistry B* **2004**, *108*, 6017.
- [5] J. van den Brand, O. Blajiev, P. C. J. Beentjes, H. Terryn, J. H. W. de Wit, *Langmuir* **2004**, *20*, 6318.
- [6] J. van den Brand, O. Blajiev, P. C. J. Beentjes, H. Terryn, J. H. W. de Wit, *Langmuir* **2004**, *20*, 6308.
- [7] J. van den Brand, S. Van Gils, P. C. J. Beentjes, H. Terryn, V. Sivel, J. H. W. de Wit, *Progress in Organic Coatings* **2004**, *51*, 339.
- [8] E. McCafferty, *Journal of the Electrochemical Society* **2003**, *150*, B342.



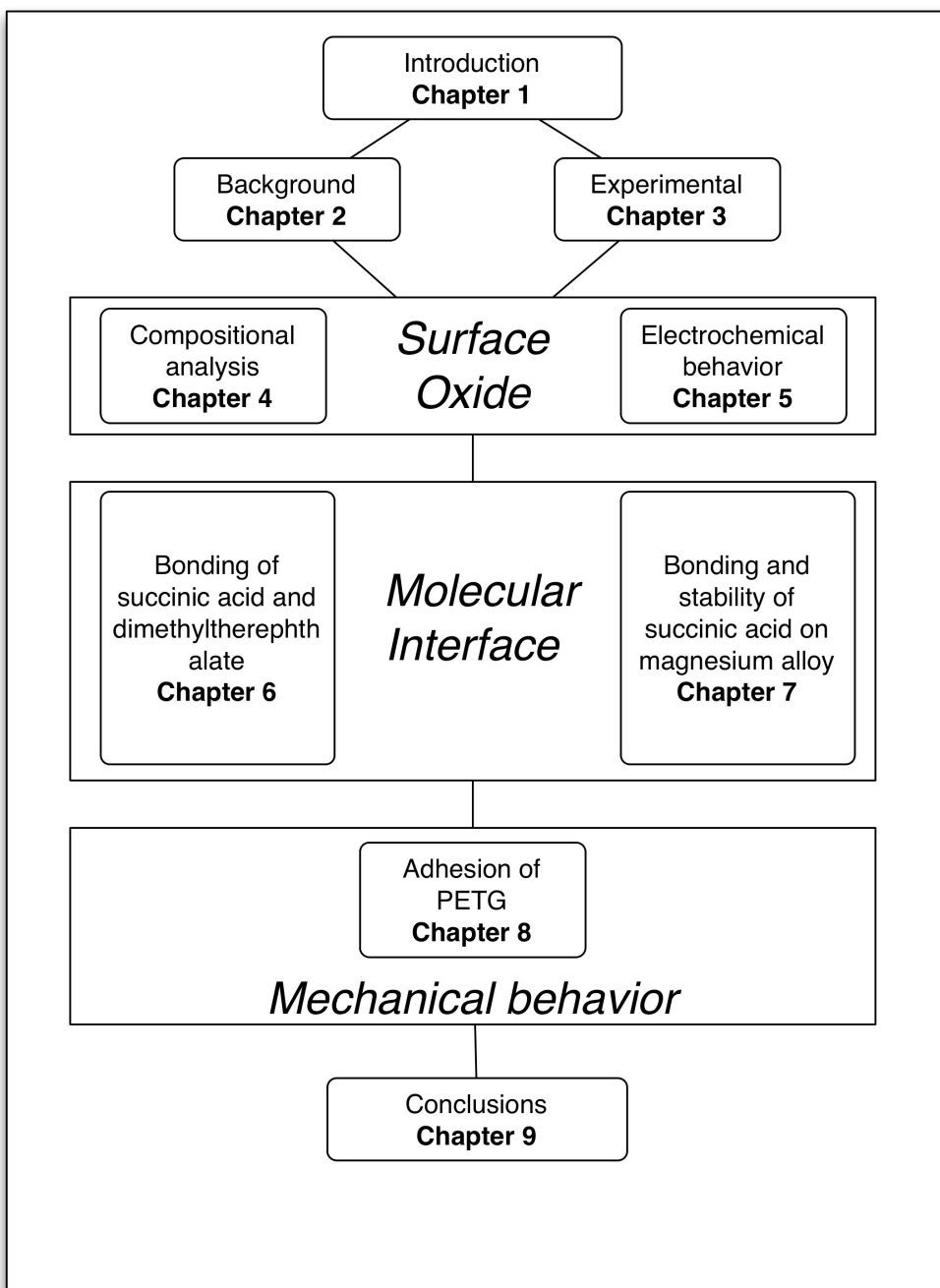


**Figure 1.1** Survey of the thesis with subdivision in three main subjects; Surface characterization; Nanoscopic/molecular interactions at the interface; Macroscopical mechanical testing of adhesion

## **Chapter 2 - Background**



---

## 2.1 Introduction and scope

The first part of this chapter gives an overview of properties of the used materials in this thesis: aluminium and magnesium. It starts with a broad and brief overview of the properties and applications of aluminium and magnesium and their alloys and discusses the possible protection measures against corrosion. In the second paragraph the composition and the properties of oxides on aluminium, magnesium and their alloys are discussed. Also most common pretreatments for aluminium alloys are briefly discussed.

The third paragraph focuses on adhesion and bonding of organic molecules/polymers on aluminium alloys in general and on aluminium-magnesium alloys specifically. Also the possible influence of pretreatments on adhesion on these alloys, as taken from literature, is discussed.

A description of the theory of adhesion and bonding, building on the previous work of Van den Brand<sup>[1]</sup> is given. Also several techniques to measure both bonding and adhesion directly and indirectly on aluminium alloys are revisited. And finally, in the last paragraph some mechanical testing methods used for delamination studies also delivering associated adhesion energies are evaluated for their usefulness for thin coatings.

## 2.2 Materials used

### 2.2.1 Aluminium, magnesium and alloys

Aluminium is the most abundant metallic element (if silicon is not considered a metal) on earth. It is also the second most produced structural metal worldwide. Nevertheless, on a yearly basis, the tonnage of aluminium in production (including recycled material) is only a small fraction of the amount of steel produced worldwide (see table 2.1). More exotic even in this sense is the use of magnesium (the main alloying element for one of the alloys used in this thesis, AA5182) of which production worldwide is less than 2 % of the aluminium production, and therefore far less than 1 ‰ of steel production in tonnage. In table 2.1, the production quantities in tonnes of other metals, which are either used as alloying elements or for completely different structural and engineering purposes are also given to put the abundance of materials into perspective. For instance, the total amount of lithium (used in rechargeable batteries) expected ever to be mined worldwide is about the same as the total worldwide annual production of aluminium. On a similar level are platinum group metals (PGM), which are currently abundantly used in fuel

cells. Some of these elements, like lithium and scandium are also used for alloying aluminium. The future availability is however uncertain because of economic and geopolitical reasons<sup>[2]</sup>. It is highly questionable if the mining of the minerals that contain these elements till the last gram to produce the aforementioned applications in energy storage or conversion systems is economically feasible. Recycling and optimizing the material use in applications seems like a much more sensible route to follow. Therefore the protection against corrosion for structurally used light metals like aluminium and magnesium is more urgent than ever.

**Table 2.1** Rough estimates of annual production and estimated worldwide reserve (years at “current rate”) of selected engineering metals. From Wouters et al.<sup>[2]</sup> and other sources.

Metal	Annual worldwide production (tonnes)	Estimated worldwide reserve
Steel	$>1000 \cdot 10^6$	50 - 119 years
Aluminium	$32 \cdot 10^6$	65 - 1027 years
Zinc	$10 \cdot 10^6$	$100 \cdot 10^6$ tonnes 15 - 46 years
Magnesium	$430 \cdot 10^3$	$>70 - >100$ years
Lithium	$85 \cdot 10^3$	$35 \cdot 10^6$ * tonnes $>70 - >100$ years
Copper	$15.6 \cdot 10^3$	25 - 61 years
Platinum	130	$14 - 48 \cdot 10^{6**}$ tonnes 42 - 360 years
Nickel	$1.2 \cdot 10^6$	$140 \cdot 10^6$ tonnes 30 - 100 years

\* Maximum, including  $15 \cdot 10^6$  tonnes already found.

\*\* Platinum group metals (PGM), i.e. Pd, Ru, Rh etc.

For aluminium the production and use in various applications has been commonplace for more than seven decades. The need for a light, formable metal has been high since World War II, when aluminium alloys were used mostly in aircraft structures and some cookware. Its production has increased explosively since then. See figure 2.1 for a historic overview.

Some features have gained importance, such as higher yield and ultimate tensile strength, while maintaining or improving formability properties, high fatigue life and better corrosion properties. In ten years time (1999-2009) the annual production of primary aluminium has almost doubled from 25.400 tonnes to 49.900 tonnes. From 2004, the (corrected) price for raw aluminium has steadily risen from \$1600 to \$3300 per tonne in the second quarter of 2008. After the crisis, in the second quarter of 2009, the price had dropped to \$1350 per tonne while it increased again

to about \$2100 november 2011. Secondary recycled aluminium (alloys mainly) is cheaper than pure primary aluminium by about 20%. Therefore, it is very interesting for aluminium manufacturers to experiment with compositions to get the required properties for the intended applications. Currently, from the total amount of aluminium in circulation, around 50% consists of recycled aluminium. Magnesium prices have followed the trend of aluminium prices.

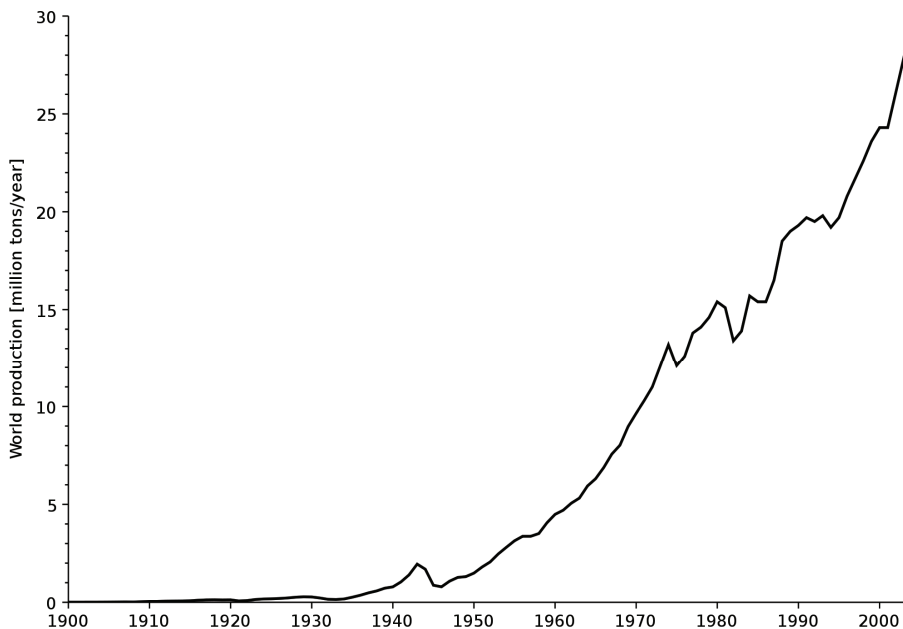


**Figure 2.1.** World production of aluminium, US geological survey<sup>[3]</sup>.

The influence of alloying elements on different properties of the resulting alloy is considerable<sup>[4]</sup>. There are many different aluminium alloys, wrought alloys classified by the International Alloy Designation System as AAxxxx, where xxxx is a number. Table 2.2 gives an overview of the compositions of the major alloying series and yield strengths. The most common alloying elements are: copper, magnesium, chromium, silicon, iron, nickel, zinc and lithium. Every element adds specific properties to the alloy. Magnesium for instance increases the weldability of the alloy. Silicon lowers the melting point and makes casting easier. Copper adds strength to the alloy. Also cadmium, manganese and titanium can be added, but in all cases, the total amount of alloying elements is less than 10% of the total alloy. Specifically for the experiments discussed this thesis, an alloy of the AA5xxx series was used, which contains magnesium as the major alloying element, improving the corrosion properties and resulting in a high formability and yield strength. There are many

applications where AA5xxx series is used, which will be discussed in the next paragraph.

**Table 2.2** Aluminium series description, common alloys and uses.

Series name	System	Common alloys	Used in	Yield strength (MPa), alloy
AA1xxx	Al > 99 wt%	AA1050	Foil	117 (AA1100-H14)
AA2xxx	Al-Cu	AA2024	Aerospace	324 (AA2024-H14)
AA3xxx	Al-Mn	AA3005	Packaging	145 (AA3003-H14)
AA5xxx	Al-Mg	AA5182	Can ends, automotive	214 (AA5052-H34)
AA6xxx	Al-Mg-Si	AA6061	Construction, transportation	276 (AA6061-T6)
AA7xxx	Al-Zn-Mg	AA7075	Aerospace, personal transportation	503 (AA7075-T6)

Magnesium is alloyed with aluminium, zinc, silicon, zirconium, silver and manganese. Alloys are usually named with the first letters of the main alloying components. See table 2.3 for the most commonly used names. Magnesium alloy prices are about twice as high as aluminium alloy's. Aluminium is used to increase the yield strength of magnesium. AZ91 for example has twice the yield strength of pure magnesium<sup>[5]</sup>. Combining both aluminium and zinc in an alloy increases the maximum deformation, so products don't rupture easily when extruded. Manganese for instance is added to improve corrosion properties. An overview of the AA5xxx aluminium-magnesium family of alloys with selected properties is given in Table 2.4.

**Table 2.3** Magnesium series description and common alloys.

Series name	System	Common alloys
AMxx	Mg-Al-Mn	AM60
ASxx	Mg-Al-Si	AS21
AZxx	Mg-Al-Zn	AZ91, AZ31
WExx	Mg-RE*-Zr-Y	WE54
ZExx	Mg-Zn-RE-Zr	ZE63
ZKxx	Mg-Zn-Zr	ZK21
ZMxx	Mg-Zn-Mn	ZM21

\* RE = rare earth elements

**Table 2.4** AA5xxx aluminium-magnesium family of alloys with selected properties

Series name	System	Applications
AA5005	0.8% Mg	Piping, tubing, marine and offshore superstructures
AA5049	2.1% Mg, 0.8% Mn	Transport containers
AA5052	2.5% Mg	Pressure vessels, rivets; industrial and architectural uses as plates and pipes
AA5083	4.5% Mg-RE*-Zr-Y	Welded pressure vessels, marine, auto aircraft cryogenics, TV towers, drilling rigs, transportation equipment, missile components
AA5086	4% Mg-Zn-RE-Zr	
AA5154A	3.5% Mg-Zn-Zr	Welded structure, storage tanks, pressure vessels, salt water service
AA5182	5% Mg-Zn-Mn	Automobile body sheets, can ends
AA5454	2.5% Mg	Welding electrodes, welded structures, storage tanks for heated products, pressure vessels, truck bodies for hot oil or asphalt applications

\*RE = rare earth elements

## 2.2.2 Applications of aluminium-magnesium and magnesium-aluminium alloys

Sometimes aluminium is not visible in end-products or not commonly recognized. Examples include printing plate material, used for printing-to-plate for books. Another example of “hidden” use is in packaging material, like chips bags and recently food and beverage pouches.

More obvious examples (although not always to the public!) of aluminium use include (parts) of beverage cans to transportation systems (bikes, airplanes and parts of cars). Some parts in transportation have “magically changed” to aluminium or more recently, fiber metal laminates like Glare®, which combine low weight with high (impact) strength.

Aluminium-magnesium alloys are used often in daily life. The most common, but fairly well hidden application of AA5182 is in the ends of beverage cans. While the tabs are made from AA5042 or AA5082, AA5182 containing approximately 4.5% magnesium and 0.35% manganese has very high strength and sufficient formability to permit making the integral rivet in the easy open end<sup>[6]</sup>. The alloy was actually designed specifically with that purpose in mind<sup>[7]</sup>, requiring maximum strength with minimum thickness because of cost and because the consumer needs to be able to open the score. With a steel lid, a completely different design is required, as was



done for the “easy open end” steel can<sup>[8]</sup>. Other uses include some inner car door frames because of the good formability. In shipbuilding and architecture AA5xxx series alloys are popular because of their good weldability, fatigue properties and inherent corrosion resistance, as compared to other available alloys<sup>[9]</sup>.

Magnesium alloys have even lower densities than aluminium alloys (1740 vs. 2700 kg/m<sup>3</sup>). Usually, magnesium alloys appear in consumer electronics like camera bodies and personal audio (see fig 2.2), (race) car parts (rims, engine blocks, body parts in F1) and military applications. Also, because of its low density and still relatively high melting point it is used in (aero)space applications like missiles and rockets and also in nuclear facilities.



**Figure 2.2** Philips AX7201 portable CD player with diecast magnesium lid.

### **2.2.3 Protection (from corrosion) of aluminium-magnesium and magnesium-aluminium alloys**

Most of these mentioned structural applications could not be achieved if aluminium or magnesium alloys would be used as-cast or only rolled. Multiple corrosion problems occur with unprotected alloys, even in mild environments. Aluminium and magnesium alloys were previously studied extensively and are prone to various forms of corrosion even in mild environments (low salinity, pH neutral): intergranular, pitting, crevice<sup>[10-12]</sup>. Therefore, in most cases aluminium and magnesium alloy surfaces are protected by layers which are not, or less affected by the environment. One of the common ways of protection is to clad high-strength alloys with relatively poor corrosion properties with an aluminium alloy which is not so prone to corrosion. One of the examples is AA2024 which is used in aerospace

industry and is commonly clad with AA1100, an alloy with 99% aluminium. AA1100 does not have favorable mechanical properties relatively unimportant for cladding applications, but due to its high purity it will not suffer from pitting corrosion because there is only a very small number of precipitates that can act as initiation sites for that type of attack. For AA5xxx, however, this is not always deemed necessary, as some alloys in shipbuilding and architecture are used without protection, with some foreseeable corrosion problems<sup>[9]</sup>.

Another way of protection is to apply another layer to the surface which has protective properties to the alloy underneath. This can either be an organic or an inorganic layer. Inorganic layers are usually produced by creating a thicker and denser aluminium oxide layer by anodizing. Anodizing involves an electrolyte which will facilitate the build up of the layer. Chromic acid anodizing (CAA) has been used for decades in the aerospace industry, but is under scrutiny because the anodizing baths that are used contain Cr(VI), chromate ions. These ions are considered a health problem and therefore are to be banned in the near future. CAA leads to a porous structure, where the bottom of the pores is sealed off by a dense barrier layer. Pores of about 30 nm wide and an oxide thickness of 1  $\mu\text{m}$  are typically used in the aerospace industry providing an extremely stable surface to be adhesively bonded to a (chromate containing) organic primer. Other techniques can create thicker layers of oxides, which can be either sealed in boiling water, forming pseudoboehmite inside the pores, or by introducing pigments in boiling water during sealing. More recently, because of the pending ban on chromates in industrial processes, alternatives to CAA have been explored, which were historically actually already available. These include anodizing in phosphoric (PAA), sulphuric (SAA), boric acid or a combination thereof, e.g. phosphoric/sulfuric acid (PSA). Although these alternatives are viable industrial-scale possibilities, the corrosion protection, or rather prevention, is much worse than that of CAA. Recently, Zhang et al.<sup>[13]</sup> have shown that in a potentiodynamic experiment of AA2024 in an 3.5% NaCl solution anodic current densities of layers produced by CAA were a factor 10 to 105 lower than those produced by all the other processes. Also, the current density did not rise above  $10^{-7}$  A/cm<sup>2</sup> even at 0.6 V vs. SCE. It was argued that the density of the barrier layer and the overall higher density of the oxide were the main contributing factors. This particular inertness is one of the reasons this process is so well embedded in the production of aerospace materials. There are other ways of protection of aluminium with inorganic layers, which are not further discussed here, but reference is made to Sheasby<sup>[9]</sup>.

The other way of protection of aluminium and magnesium (with or without anodizing) is through the use of organic coatings. These have since long been used and depending on the application, a wide variety of properties can be chosen. Multiple layers can be applied where each layer has specific properties, e.g. a hydrophobic top layer to protect water from entering into the system. The surfaces of the alloys can be tailored to provide the proper circumstances for the organic coatings to bond to. In general it is a proper “configuration” of the oxide in combination with well selected organic molecules that gives the best combination of properties. The oxide might however not have the proper configuration, or there might be oils or old oxide skins rolled into the surface<sup>[14]</sup>. Therefore, the surfaces need to be “cleaned”. This can be done with acid or alkaline cleaners or etching baths. There are many industrial processes where both are applied. In general the advantage of alkaline cleaners is that the treatments are more thorough. This will be further discussed in 2.3.3.

The specific application of AA5182 in can ends, requires a coating with a sealant top coat. These are modified epoxy or a vinyl organosol coatings<sup>[15]</sup>, but because of environmental interests improvement of these coatings continues.

## 2.3 Aluminium and magnesium oxides

Because bonding of organic coatings takes place on the oxide layers present, the composition of these oxide layers is very relevant for adhesion. The composition of the aluminium-magnesium oxides, which are always present at the surface of the Al-Mg alloys, is therefore discussed.

Next the chemical properties of these oxide layers are shortly discussed and the expected influence of different surface pretreatments is examined.

### 2.3.1 Composition of aluminium and magnesium alloy oxides

The main goal of the investigations was to compare a range of materials varying from pure aluminium to Al-Mg, Mg-Al and finally pure magnesium. Therefore, it is necessary to understand the behavior of all oxide surfaces which are possible.

#### *Aluminium alloys*

Oxide surfaces of commercial aluminium alloys (e.g. AA2024<sup>[16, 17]</sup>, AA7075<sup>[17]</sup> and AA5754<sup>[18]</sup>) have different compositions due to incorporation of alloying elements, like copper, zinc and magnesium. Preferential dissolution or surface enrichment of alloying elements can be induced by chemically pre-treating the surfaces or by anodizing<sup>[16, 19]</sup> in acid and alkaline solutions. Preferential surface enrichment can also be achieved with heat treatments<sup>[16]</sup>.

Natural oxide film on Al-Mg alloys which are formed below 300°C have a thickness of 1 - 3 nm, while these can be significantly thicker above 300°C up to 3 µm depending on temperature and bulk Mg content<sup>[9]</sup>. Magnesium can not only segregate on grain boundaries and form precipitates (Mg<sub>2</sub>Al<sub>3</sub>)<sup>[20]</sup> but it can also diffuse into the surface-oxide at elevated temperatures<sup>[21]</sup>, which either occurs after casting or during the tempering step to influence mechanical properties. At temperatures above 340°C, magnesium diffuses from the bulk of the alloy to the surface. There is a competitive oxidation reaction between magnesium and aluminium due to outward diffusion of magnesium and oxygen diffusion inwards, even at levels less than 50 ppm magnesium. Several authors<sup>[22, 23]</sup> have shown by means of AES and XPS that the oxide layer of an Al-Mg alloy can be enriched in Mg by subjecting the material to a prolonged heat treatment even at temperatures below 200°C if the alloy contains more than 4.5 wt% magnesium. At these higher levels of bulk magnesium, sometimes a duplex film of aluminium oxide close to the metal and an outer layer of MgO results. Wefers<sup>[24]</sup> and Field<sup>[25]</sup> have summarized the oxidation of aluminium magnesium alloys at higher temperatures previously.

Lea and Molinari<sup>[26]</sup> have also extensively studied the diffusion of magnesium in aluminium AA5657 and AA5252 alloys (lower alloyed 0.8 and 2.5 wt% magnesium) and have found that considerably higher temperatures (up to 600°C) are needed for magnesium surface enrichment of these alloys.

### *Magnesium alloys*

Several studies were performed to understand the mechanism of film growth on magnesium and its alloys in different environments. Nordlien et al.<sup>[27]</sup> found an oxide film morphology on pure magnesium consisting of three layers, see also figure 2.3.

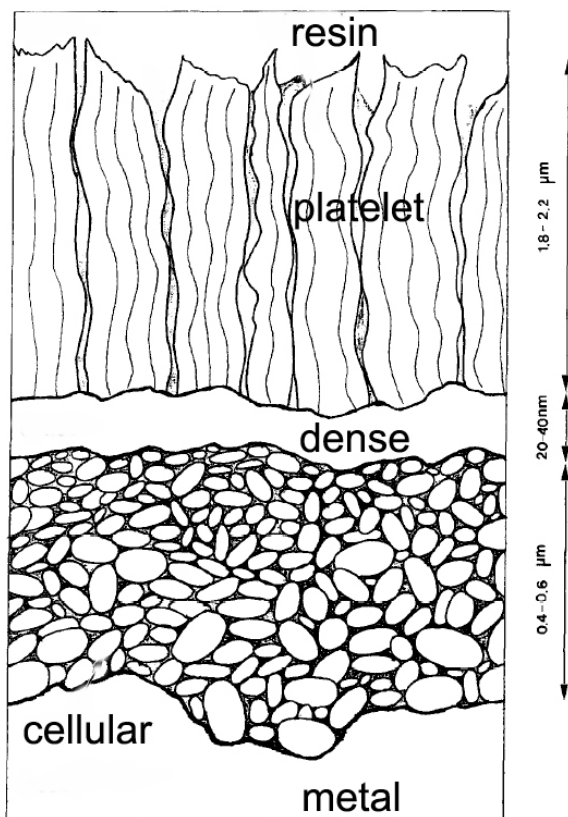


**Figure 2.3** Three-layer oxide structure on magnesium (schematic), Nordlien et al. <sup>[27]</sup>.

Pure magnesium is protected by a stable air-formed dense oxide in dry environments. In humid air and aqueous environments, the air-formed film is undermined by formation of a less stable hydrated cellular oxide resulting from electrochemical metal oxidation. A platelet-like outer layer is formed to give a three-

layer film morphology in water by precipitation of oxides on the air formed film. The air-formed film, although characterized by a dense morphology, plays an important role in the formation of the inner and outer layers, by allowing water ingress and dissolution of Mg.

In general similar layers were found on MgAl-alloys, but these were significantly thinner than layers on pure magnesium, mainly due to a smaller platelet thickness of the alloys. Increasing the aluminium content of binary magnesium alloys caused a significant reduction of the overall thickness and of the platelet layer in particular. The presence of zinc in alloys with more than 4% aluminium caused a significant increase in thickness of the inner layer as compared to alloys containing manganese. The platelet layers on the AZ series alloys are appreciably thinner than the platelet layers on AM or AS series with similar amounts of Al while the inner layers are thicker. A significant enrichment of aluminium oxide in the inner most layer occurs, especially on alloys containing more than 4% aluminium. Aluminium concentrations in the order of 35% were detected in the inner layer for alloys exceeding the 4% threshold concentration. This resulted in increased stability of the oxide and consequently an improved corrosion resistance. It was suggested, that the 4% limit for the alloy giving about 35% of aluminium in the oxide corresponded to some sort of percolation threshold for the passivating  $\text{Al}_2\text{O}_3$  component of the oxide<sup>[28]</sup>.

### **2.3.2 Chemical properties of aluminium-magnesium oxide surfaces**

Because aluminium is amphoteric, aluminium oxide dissolves in aqueous solutions below  $\text{pH} = 4$  and above  $\text{pH} = 8,5$ , where the  $\text{Al}^{3+}$  ions act as acid and  $\text{AlO}_2^-$  as base (see Pourbaix diagram in fig 2.4).

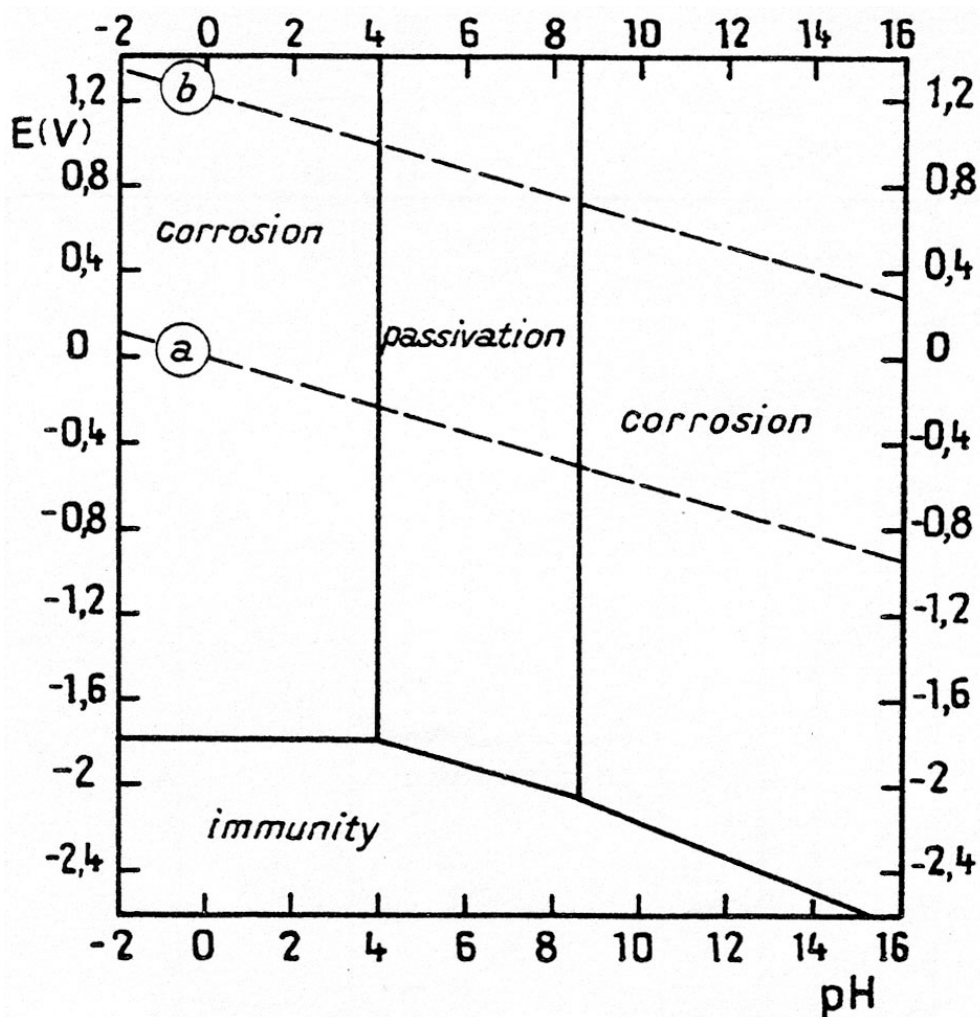


**Figure 2.4** Potential-pH diagram for the system Al water at 25°C, activity 1, Pourbaix<sup>[29]</sup>.

Dissolution may be slow if a well adhering oxide layer is present (passivity). Breakdown of the oxide film can result from mechanical rupture or from chemical attack by anions such as chloride ions. In most cases repair is instantaneous and, depending on the moisture content of the environment, can either be accompanied by the oxygen reduction reaction or the hydrogen evolution reaction:



Both  $\text{Al}_2\text{O}_3$  and  $\text{Al}(\text{OH})_3$  can be formed as well as many other complex oxyhydroxide species<sup>[30]</sup>.

Magnesium on the other hand only forms a stable hydroxide above  $\text{pH} = 12$  (see figure 2.5). Under normal atmospheric circumstances, magnesium therefore needs to be covered in a stable oxide layer. It is suggested that this is a complex oxide made up of magnesium hydroxides and carbonates<sup>[30]</sup>. Magnesium hydroxides and carbonates protect the metal up to a certain level, but when these layers are damaged, corrosion will occur very rapidly, since magnesium corrosion is extreme fast. Higher temperatures accelerate this even further<sup>[31]</sup>. Next to the film formation as described by Nordlien and given above in figure 2.3, Koppers et al.<sup>[32]</sup> developed an electrochemical model for the formation of different layers on Mg in air and water<sup>[32]</sup>. In dry air a thin oxide layer is formed on magnesium:



In contact with water, magnesium oxide reacts with water to form magnesium hydroxide, while the volume of the layer is growing:



In water without chlorine, Mg reacts to  $\text{Mg}^{2+}$  and water is reduced to hydrogen and hydroxide ions:



$\text{Mg}^{2+}$  and  $\text{OH}^-$  then recombine to  $\text{Mg}(\text{OH})_2$



In Figure 2.6 theoretical domains of corrosion ( $\text{Mg}^{2+}$ ), immunity (Mg) and passivation ( $\text{Mg}(\text{OH})_2$ ) of magnesium at  $25^\circ\text{C}$  are given in the Pourbaix diagram.



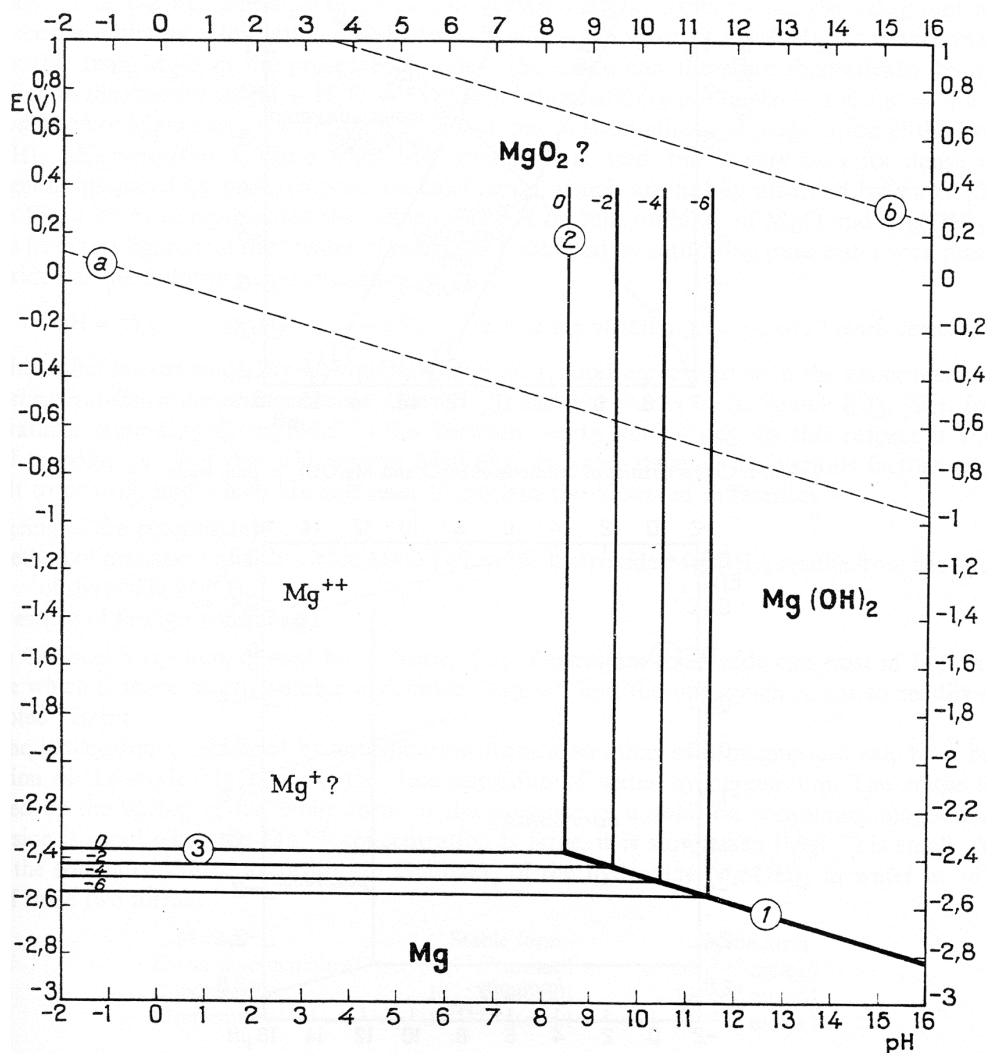


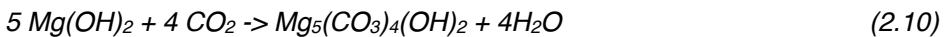
**Figure 2.5** Potential-pH diagram for the system magnesium-water at 25°C, Pourbaix<sup>[29]</sup>.

So far, only processes in controlled environments without CO<sub>2</sub> are described. Under atmospheric conditions, the formation of oxide layers on magnesium and its alloys is more complex. Adding ambient concentrations of carbon dioxide to humid air results in slower corrosion and in a less localized mode of attack<sup>[33]</sup>. Blücher argued that the inhibitive effect of CO<sub>2</sub> seen for a Mg/Al model and alloy AZ91D is partly explained by its acidic properties<sup>[34]</sup>.

Carbon dioxide tends to neutralize the surface electrolyte by reaction:



The atmospheric corrosion of pure magnesium is reported to be inhibited by carbon dioxide. This was attributed to the slightly protective nature of magnesium hydroxyl carbonate that tends to accumulate on the surface.  $\text{Mg}(\text{OH})_2$  reacts with  $\text{CO}_2$  to form magnesium hydroxyl carbonate according to the following reaction:



It is suggested that this effect contributes to the slow corrosion of the magnesium aluminium model alloy used by Blücher et al.<sup>[30]</sup>. A similar mechanism is suggested for AZ91D, see also Figure 2.6. Carbon dioxide neutralizes the surface electrolyte and forms complex hydroxy carbonates e.g.  $\text{Mg}_5(\text{CO}_3)_4(\text{OH})_2$ <sup>[30, 35]</sup>.

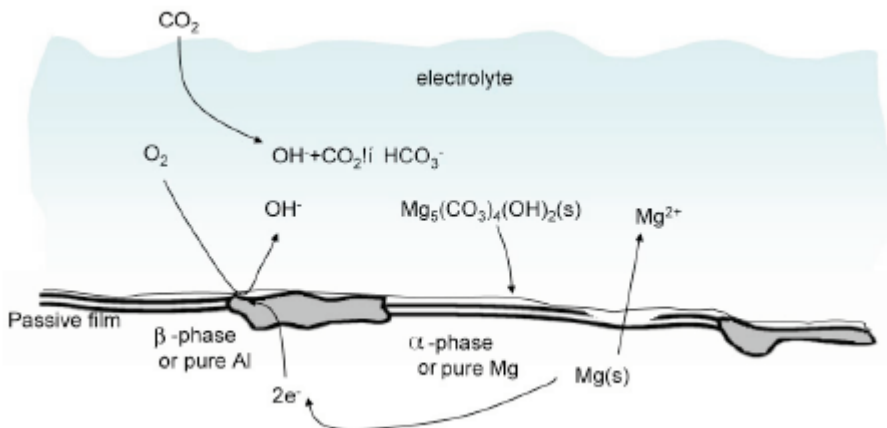


**Figure 2.6** Suggested corrosion mechanism of AZ91D in humid air at ambient levels of CO<sub>2</sub>. Blücher et al.<sup>[30]</sup>.

Alloying elements usually increase the corrosion rate, since local corrosion occurs when galvanic coupling takes place between the precipitates or other discontinuities and the matrix material. The oxides on these precipitates are usually not closed or well-adhering, therefore leaving the bare metal and surroundings exposed to the (aggressive) aqueous environment. Another problem consists of the interference of anions, especially Cl<sup>-</sup> ions, which block or hinder the re-oxidation of the metal if the native oxides have disappeared<sup>[24]</sup>.

### 2.3.3 Influences of pretreatments on the oxides of aluminium and magnesium alloys

Aluminium alloys in general are extensively chemically cleaned and etched before coating or adhesive bonding. Sheasby<sup>[9]</sup> has given an extensive overview of these pretreatments in chapter 4 of the mentioned reference. Most of the pretreatments are applied to ensure a more durable bond of coatings and adhesives in practical applications.

In literature some pretreatments for the AA5xxx series alloys were described in more detail. Next to mechanical pretreatments, which remove the top layer of (contaminated) oxides, there are several mechanisms by which the oxide composition can be altered. Commonly used pretreatments include alkaline or acid cleaning plus etching and the application of several conversion coatings. Especially in the last type there has been progress in recent years to replace the chromate conversion coatings as mentioned under 2.1.3. Several researchers have looked into properties of non-chromate containing self-assembling monolayers (SAMs) with different functionalities, in general<sup>[36]</sup>, to act as corrosion protection or for improving the bonding of coatings or adhesives. For each category of these treatments there are many commercial products available, which work with standard<sup>[9]</sup> or patented<sup>[37]</sup> recipes. These usually contain extra chemicals to form complexes with the contamination or reaction products, to influence the kinetics (e.g. wetting agents) of the reactions or to stabilize the pre-treatment baths. Commonly, after a pre-treatment step, the substrates are rinsed (thoroughly) with (deionized) water to prevent the reactions from continuing and producing over-etched surfaces<sup>[9]</sup>.

To clean the as-rolled alloys of oil and grease, alkaline pretreatments are used. These have the advantage that, especially at elevated temperatures<sup>[9]</sup>, etching is very rapid. As disadvantage, these pretreatments might leave a smut layer when larger amounts of aluminium are etched, e.g. at longer etching times. Typically, sodium hydroxide (NaOH) is used to create an aqueous solution of high pH > 12). As a de-smutting treatment after alkaline cleaning, several acid solutions are used. These can contain phosphoric, nitric, hydrofluoric, chromic acid or combinations thereof.

Acid pretreatments are also being used separately with a similar composition of the baths.

In the beginning of the 1980s, Kinloch and coworkers have extensively studied the relation between pretreatments and the oxide composition of various aluminium-

magnesium alloys<sup>[22, 38]</sup>. The goal of these investigations was to relate the pretreatments and the (durability) of adhesion to aluminium-magnesium alloys with two magnesium concentrations (ca. 2 and 5 wt% Mg) in comparison to an alloy without magnesium. They found with XPS measurements that solvent cleaning and grit-blasting did not result in a lowering of the amount of magnesium at the surface; on the contrary they always found an increased magnesium content at the surface as compared to the bulk. Acid pretreatments, however, removed magnesium completely. Their main conclusion was also that the lower strength of joints could be explained by the presence of magnesium oxide.

Moffit and coworkers<sup>[17]</sup> studied AA2024-T3 (1.2 - 1.8 wt% Mg) and found that an alkaline (commercial, caustic) pretreatment removed a large part of magnesium from the surface. Also, alkaline and acid ("deoxidiser") treatments combined as well as all other acid pretreatments completely removed magnesium from the surface. They attributed the original increased magnesium surface concentration to the processing of the sheets. Combining these papers, it can be concluded that, because magnesium can lead to poorer durability of the (adhesively) bonded system, it should be removed by an acid pretreatment. As was discussed before, higher temperatures can lead to an increased level of magnesium at the surface. Nevertheless a already four times increase of magnesium content at the surface was shown by Sun et al.<sup>[16]</sup> after bonding had taken place at relatively low temperatures and short times (~ 180°C, 4 hours). This occurred for FPL etched (acid) AA2024-T3 samples. Next to the increase in Mg content, also a Cu content increase was found, which is also detrimental to the durability of the adhesive bonds.

## 2.4 Theories of bonding and adhesion of organic molecules and coatings on metals

### 2.4.1 Definitions

Allen<sup>[39]</sup> summarized in his 1987 overview the phenomenon of adhesion with the following statements: "...it has been suggested that there is not an accepted explanation of adhesion because people have not recognized the multi-component nature of the problem" and "For these various mechanisms (*of adhesion* – FdW) the relative importance and the proper way in which they should be combined will vary from one example to another, but none should be excluded without very careful consideration and exploration."

Bonding and adhesion are sometimes used interchangeably. In general the distinction is made between the two using the following definitions: bonding is the phenomenon where two molecules or atoms are (semi) permanently attached to each other by physical or chemical interaction. Adhesion on the other hand deals with the macroscopical interaction between phases, where also dissipation of energy and mobility of atoms and molecules are involved. In literature, most articles either address one or the other.

For this thesis the following definitions of bonding and adhesion of organic groups to metals will be used:

**Bonding** is the interaction of an organic molecule with the surface species on the metal, e.g. oxides, hydroxides, carbonates, etc. This is by definition a single attachment, while the bond strength is usually averaged out over many bonds. There are weak and strong bonds, which will be discussed below and an overview is given in Table 2.5. Bonding is expressed in J/mol.

**Adhesion** is the macroscopic behavior of an (organic) coating adhering to a metal. Adhesion manifests itself by definition as a number of attachments, averaged out over a larger surface area when loaded macroscopically. Without bonding, adhesion cannot exist. It includes (micro) material properties and behavior comparable to bulk materials, e.g. E-moduli, tensile strength, necking, etc. and therefore adhesion is expressed as energy or force per square surface area, e.g. J/m<sup>2</sup> or N/m<sup>2</sup>

The scientific field is therefore split in two: one consists of the theory of bonding of molecules and the other of the mechanical properties of the whole system. The

latter usually includes studies of the durability of the systems exposed to more or less severe and practical environments like high or low temperatures, humidity combined with mechanical (fatigue) forces.

The next two sections contain examples of both fields; 2.3.2 addresses the theoretical of bonding and adhesion on metals while 2.3.3 deals with mechanical adhesion. Since during this thesis work no durability studies have been performed, these have been omitted from this chapter, although they are essential when looking at practical coating adhesion<sup>[40, 41]</sup>. Finally 2.3.3 gives an overview of the few studies that have combined molecular bonding and mechanical adhesion quantitatively.

**Table 2.5** Overview of bonds and their strength

Type	Specific	From <sup>[44]</sup> kcal/mol*	From <sup>[58]</sup> kJ/mol	From <sup>[46]</sup> kcal/mole
<i>Primary bonds</i>	Ionic	150-250	600-1100	140-250
	Covalent	15-170	60-700	15-170
	Metallic	27-83	110-350	27-83
<i>Donor-acceptor bonds</i>	Brønsted acid-base interactions	N/a	up to 1000	N/a
	Lewis acid-base interactions		up to 80	
<i>Secondary Bonds</i>				
<i>Hydrogen bonds</i>	Hydrogen bonds involving fluorine	< 12	up to 40	Up to 10
	Hydrogen bonds excluding fluorine		10-25	5-8
<i>Van der Waals bonds</i>	Permanent dipole-dipole	< 5	4-20	1-5
	Dipole induced dipole	< 0.5	less than 2	< 0.5
	Dispersion (London) forces	< 10	0.08-40	0.02 - 10

\*1 kcal = 4,184 kJ

## 2.4.2 Bonding physics and chemistry of polymers on metals: interaction at oxides

Models for interaction between two phases in literature (from almost all references) fall into three categories:

- Mechanical anchorage: macroscopic or microscopic intertwining of two phases due to roughness.

- Chemical adsorption, or chemisorption: covalent or ionic bonds
- Physical adsorption, or physisorption: physical attractive forces Van der Waals forces including permanent dipole-dipole interactions (Keesom), dipole-induced dipole (Debye) and dispersion forces (London). Hydrogen bonds fall in the category of Van der Waals bonds (see also table 2.5).

Mechanical anchorage or mechanical interlocking exists supposedly where coatings attach well to rough surfaces. Allen<sup>[42]</sup> argued that a naive belief in this explanation persists even in the face of clear evidence that surface roughness and bond strength correlate negatively in many examples. In some specific cases, although he mentions no metal-polymer systems, on this macroscopical scale, the interpenetration did make a positive difference on the adhesion. However more recently, Harris et al. have not found any correlation between the roughness of a surface and the total energy for delamination<sup>[43]</sup>. On a microscopic or even on a nm scale intertwining through oxide “whiskers” penetrating the coating can prove beneficial to adhesion but only if the increased effective interfacial area is substantial. Also, oxides have to have strong bonds with the underlying metal (adhesive) and high internal (cohesive) strength. In the rest of this paragraph this contribution on adhesive forces is neglected, since it is normally very small.

The total work of adhesion incorporates all types of interaction at the interface and takes adhesion to the level of molecules interacting with the surface of the metal(oxide). Hare<sup>[44]</sup> states that when molecular bonding predominates, it results from chemical linkages (primary valence bonding) between reactive species on binder and substrate, or from molecular associations (secondary valence bonding) between the two. Such forces operate only across very limited distances. For adhesion of any kind, the coating and the substrate must approach each other extremely closely. Separation must reach less than 5Å, three times the diameter of an oxygen ion. These attracting forces also diminish in proportion to the sixth power of the distance. To achieve this level of approach, the coating must wet the substrate and spread across it. Wetting is the result of the surface/interface energy that is related to the relative values of the surface free energy of the coating and the substrate. For any given coating and substrate system, the coating will wet the substrate only when the interfacial energies match. Molecules at the surface of a liquid tend to orient themselves to minimize the surface energy of the liquid. For quantifying this property, one must turn to:

$$W_A = \gamma_1 + \gamma_2 - \gamma_{12} (+\pi_e) \quad (\text{Dupr  equation}) \quad (2.11)$$

$$W_A = \gamma_2(1 + \cos\theta_{12}) \quad (\text{Young-Dupr  equation}) \quad (2.12)$$

in which  $W_A$  (work of adhesion) shows the energy of adhesion between a solid substrate 1 and a wetting liquid 2, which follows from the surface energies (in  $\text{mJ}\cdot\text{m}^2$ )  $\gamma_1$  and  $\gamma_2$  and their interfacial energy  $\gamma_{12}$ . Equation 2.12 expresses this from the point of view of measurable contact angles.  $W_A$  gives the macroscopic measure of the energy required to reversibly remove the two phases into separate enclosures. Adhesion becomes cohesion when the physical-chemical properties of the interacting molecules become identical and equilibrium conditions for bonding exist. The factor  $\pi_e$  accounts for the reduction of the surface free energy of the solid in vacuum on immersion in the saturated vapor of the liquid. For low-energy surfaces,  $\pi_e = 0$ .

The actual measured adhesion force often exceeds the calculated value based on the contact angles between two phases, mainly due to energy dissipation in the coating during mechanical testing.

However, the calculated work of adhesion can give useful information (although not necessarily accurate) on the relative adhesive strength. When the calculation of  $W_A$  results in negative values, separation should occur.

Fowkes<sup>[45]</sup>, in agreement with Hare as stated above, showed that a variety of contributions from a number of interactions results in the work of adhesion:

$$W_A = W^d + W^h + W^{ab} + W^p + W^i \quad (2.13)$$

In fact these include all the contributions from table 2.5, including the primary and secondary bonds.

The superscripts in Eq. 2.13 represent: d the London Dispersion forces, h the hydrogen bonding, ab the acid-base interactions, p the dipole-dipole interaction (Keesom) and i the dipole-induced dipole (Debye) interactions.

Allen<sup>[42]</sup> states that hydrogen bonds form a sub-set of acid-base interactions when following the Lewis approach, which means regarding an acid as a electron acceptor and a base as a electron donor. Equation 2.13, furthermore neglecting the small contribution by Debye and Keesom forces, then reduces to:

$$W_A = W^d + W^{ab} \quad (2.14)$$



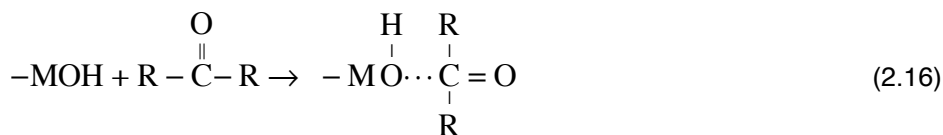
He concludes that the demonstration of recognizable chemical bonding as a significant component of adhesion forms one of the major advances in theoretical discussions in the last four decades.

Thus the work of adhesion is now to be considered as effectively arising from two components; the dispersion forces and the polar forces to be considered as acid/base interactions. In support of the previous, Bolger and Michaels<sup>[46]</sup> suggested that, considering the case of (acidic) polar polymers and (basic) metallic oxides, the only forces other than dispersion forces came from hydrogen bonds. They regarded these using the Brønsted proton definition and theories of acid/base relationships, which gave satisfactory results for these particular examples of adhesion. They recognized that this sort of treatment might extend to a wider field by use of the Lewis acid/base definitions and theories that consider electron donor/acceptor interactions.

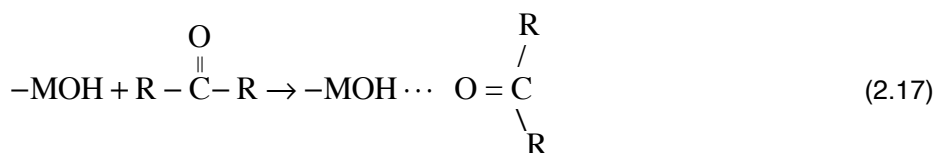
Organic polar groups can interact with oxide surfaces in various ways<sup>[46]</sup>. Either the surface hydroxyl or the organic group can act as the acid (as the proton donor in the Brønsted sense or the electron acceptor in the Lewis sense) or as the base (proton acceptor or electron donor). The bond between the surface group and the organic group can range anywhere from fully ionic to very weakly ionic, as illustrated in:



To find a general relationship that can predict which of the many possible will predominate in any given surface-organic group combination, Bolger and Michaels<sup>[46]</sup> have distinguished between two general interaction types. For type A interactions the surface provides the basic group which interacts with an organic acid, as in:



For type type B interactions the surface provides the acidic group which interacts with an organic base:



Within each type, Bolger and Michaels further distinguish two extreme conditions wherein the interaction appears predominantly ionic or non-ionic:

Type A-1: Dipole interaction with an organic acid (Lewis):



Type A-2: Ionic interaction with an organic acid (Brønsted):



Type B-1: Dipole interaction with an organic base (Lewis):



Type B-2: Ionic interaction with an organic base (Brønsted):



X represents an electronegative atom, usually oxygen or nitrogen, sometimes chlorine.

Parks<sup>[47]</sup> reviewed the isoelectric points of solid oxides (IEPS), hydroxides and aqueous hydroxo complex systems. He stated that solid oxides in aqueous suspensions generally have an electrical charge. For this he gave two explanations from literature:

- a. amphoteric dissociation of surface M-OH groups
- b. adsorption of the metal hydroxo complexes dissolved from the solid

Both mechanisms explain quantitatively the pH dependence of surface charge and the existence of a pH resulting in zero net charge, called the isoelectric point (IEP) or zero point of charge (ZPC). The term "isoelectric point" represents both the pH at which an immersed solid oxide surface has zero net charge and the pH resulting in (electrically) equivalent concentrations of positive and negative complexes. For solids the IEP becomes the IEPS. From this data one can qualitatively order bond strengths, like Bolger and Michaels<sup>[46]</sup>, see figure 2.7 for these bonds on magnesium. In this figure the interaction types and dipole orientations for water and other polar compounds predicted from the tables 2.6 for several organic molecules on SiO<sub>2</sub>, Al<sub>2</sub>O<sub>3</sub> and MgO surfaces are shown schematically. To predict the

interaction for a given oxide surface-polar group combination, they expressed the equilibrium constant for type A or type B interactions as:

$$\Delta_A \equiv \log \kappa_A = \log \frac{[\text{MOH}_2^+][\text{X}^-]}{[\text{MOH}][\text{HX}]} = \text{IEPS} - \text{pK}_{A(A)} \quad (2.22)$$

$$\Delta_B \equiv \log \kappa_B = \log \frac{[\text{MO}^-][\text{HX}^+]}{[\text{MOH}][\text{X}]} = \text{pK}_{A(B)} - \text{IEPS} \quad (2.23)$$

Where  $\text{pK}_{A(A)}$  and  $\text{pK}_{A(B)}$  represent acid-base constants, defined as:

$$\text{pK}_{A(A)} = -\log \frac{[\text{H}^+][\text{X}^-]}{[\text{HX}]} \quad (2.24a)$$

and

$$\text{pK}_{A(B)} = -\log \frac{[\text{X}][\text{H}^+]}{[\text{HX}^+]} \quad (2.24b)$$

If  $\Delta_A$  or  $\Delta_B$  have large positive values, the ionic reactions (type A-2 or B-2) predominate, whereas if  $\Delta_A$  or  $\Delta_B$  have negative values, the dipole type should predominate. An overview of  $\Delta_A$  and  $\Delta_B$  values is given in tables 2.6.

At very negative  $\Delta$  values, ionic forces become negligible and dipole forces are weak. Non-polar polymers such as polyethylene have very weak acid properties ( $\text{pK}_{A(A)}$  large and positive) and weak base properties ( $\text{pK}_{A(B)}$  large and negative) giving large negative values of  $\Delta_A$  and  $\Delta_B$  with surfaces of any IEPS and leading to the prediction that London forces (only) should exist across such interfaces.

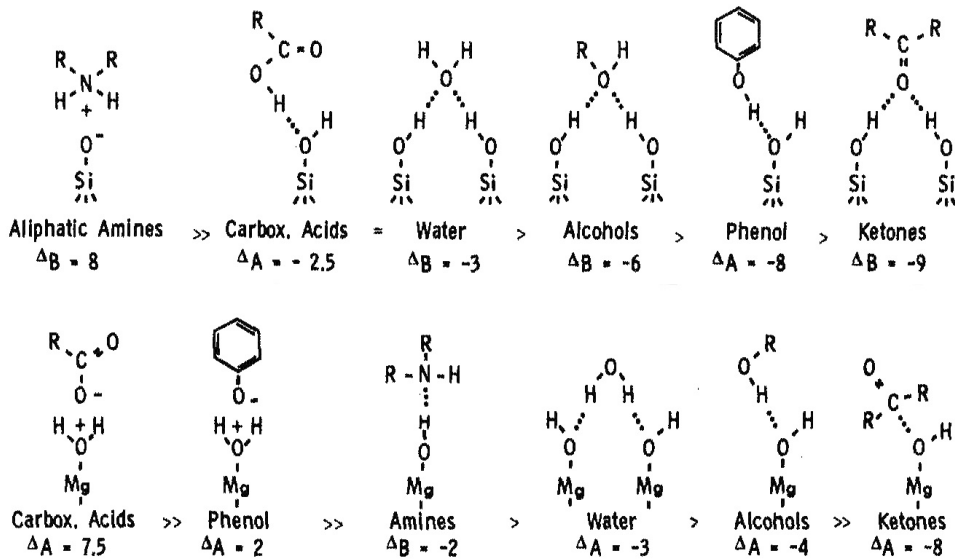


**Figure 2.7** Theoretical configuration of several organic molecules on an acid Si oxide surface and an alkaline Mg oxide surface, Bolger and Michaels<sup>[46]</sup>.

The ability of all such bonds to resist water displacement depends strongly on the pH in the aqueous phase. If the pH at the interface changes by the addition of extraneous potential-determining ions (such as  $H^+$  or  $OH^-$ ) the theory predicts that maximum resistance to displacement by water should occur only over the pH ranges<sup>[46]</sup>:

$$\text{For type A interactions: } IEPS > pH > pK_{A(A)} \quad (2.25a)$$

$$\text{For type B interactions: } pK_{A(B)} > pH > IEPS \quad (2.25b)$$

True covalent bonds can only form on a surface when a pre-treatment with silanes has taken place<sup>[46, 48]</sup>. Bolger and Michaels<sup>[46]</sup> stated that, typically, the magnitude of the interaction term attributable solely to London dispersion force interaction comes close to about  $0.01 \text{ N/cm}^2$  for either water, polar or non-polar organic materials in contact with a large number of metals, oxides and silicate surfaces. For such surfaces in contact with a non-polar organic (for example, polyolefins), only the London force interactions exist and the total interfacial interaction term remains  $0.01 \text{ N/cm}^2$ .

The total free energy of interaction for such surfaces with water, however, generally reaches  $0.05 \text{ N/cm}^2$ . This means that the surface interactions due to hydrogen bonding and other dipole interactions will form preferentially to the simple London

force interactions. Thus, while non-polar polymers such as polyethylene, polypropylene and polytetrafluoroethylene can adhere relatively well to high-energy surfaces, such non-polar polymers do not keep their adhesion to metals after extended immersion in water.

For stronger bonds, like Lewis acid-base interactions (80 kJ/mol), the total energy for de-adhesion can be calculated by using the theoretical maximum density of bonds at the surface, on an average of 15 hydroxyl groups per nm<sup>2</sup> for aluminium<sup>[49, 50]</sup>. This results (with the use of Avogadro's number) in a de-adhesion energy of 2 J/m<sup>2</sup>. This will prove to be much lower (see under 2.3.6) than the total de-adhesion energy of a practical system.

### 2.4.3 Organic coatings and representative molecules

Various organic coatings are used to protect aluminium alloys, as mentioned before. In the next paragraph the configurations of the model systems, as they will be used in the rest of this thesis, will be discussed. Since adhesion of coatings takes place at the interface through molecular bonding, the bonding behavior of coatings can be interpreted by using organic molecules.

The approach for this thesis was to examine organic coatings on the basis of their availability and the possible use of molecules representing the functional groups of the coatings. An approach similar to Van den Brand<sup>[51]</sup> was taken to use succinic acid molecules to represent the grafting molecules used for otherwise non-polar coatings and adhesive, e.g. polypropylene. Additionally, a poly-ethylene-terephthalate (PETG) film was used as a model system to study coating adhesion on the prepared aluminium-magnesium samples. As representative molecules for PETG, dimethyl-terephthalate (DMT) was used.

Following equations 2.22 and table 2.6a (at the end of the chapter) this means that for succinic acid (please refer to Chapter 6 and 7 for the experimental results) with pK<sub>a</sub> equal to benzoic acid, a predominant ionic interaction will take place with good adhesion as a possible result on aluminium and magnesium alloys. For DMT following equation 2.23 and table 2.6b (at the end of the chapter) (please refer to Chapter 6 for the experimental results) on the other hand with very negative  $\Delta B$  of -15 to -18 for respectively Al<sub>2</sub>O<sub>3</sub> and MgO as substrate, no strong bonding may be expected.

When following equations 2.25a and b, in competition with water at the surface, for succinic acid on Al<sub>2</sub>O<sub>3</sub> this means that resistance to water displacement at the interface is limited to the pH range of 4-8 and for Mg(OH)<sub>2</sub> of 4 to 12. Of course in practice Mg(OH)<sub>2</sub> is not stable below pH = 12, therefore bonding will be undermined

by magnesium dissolution. For DMT, this means that water displacement, if adhesion takes place at all before decomposition of DMT (see chapter 6), will take place over the full practical pH range.

#### **2.4.4 Macroscopical mechanical adhesion testing**

Macroscopical testing is per definition dealing with adhesion of a system, not with bonding, although the latter does play a very important role, especially when durability is involved. The methods discussed here are specific for testing of (initial) adhesion of coatings and thus not used primarily for adhesives. Nonetheless, there are some standard methods for both types of layers, which will be briefly summarized here.

There are many methods available that are primarily aimed at adhesives, but can also be applied to coatings, if a two-sided test is selected. Especially the loading mode (I, II or mixed-mode) is a parameter with which one can determine under what type of load a system might fail. Examples are DCB, (floating) roller peel and cleavage tests. These will not be further elaborated upon. A review of these methods can be found in literature by e.g. Anderson et al.<sup>[52]</sup>.

In testing coating adhesion, several methods are available for one-sided systems. In table 2.7, some test methods are presented which are commonly used to test coating adhesion, i.e. to measure the force one needs to separate an organic coating from a substrate. Some more or less established tests available, are marked as ASTM or other standards. The advantages are just mentioned in Table 2.7, without further elaboration, since emphasis later on will be on the specific method used for this thesis.

All of these test methods can be used at different stages of exposure tests, therefore marking also the decline of properties. In recent years however, there have been novel ways in which coating adhesion has been studied. One method, which can also be visualized clearly is the Scanning Kelvin Probe method. For instance, Wapner et al.<sup>[53]</sup> have used this to show coating delamination for organically coated steel and galvanized substrates. This method allows for testing the coatings under water pressure and the combined delamination/corrosion process. However, no quantitative data for coating adhesion can be deduced from these measurements.

**Table 2.7** Overview of various macroscopical mechanical tests methods for organic coating adhesion

Test	Test standard or reference	Advantage	Disadvantage
Tape Test	ASTM D3359	Quick; flexible in configuration; quantitative strength	Large statistical deviation in results; n/a for brittle coatings
Cross hatch NMP	Van den Brand et al. <sup>[44]</sup>	Quick; easily repeatable	No quantitative strength
“Dolly” test	ASTM D4541; ISO 4624	Industry standard; universal application; quantitative strength	Requires altering the system by adhesively bonded dollies

Polymers in general respond differently to applied strain than metals. Like in metals elastic deformation exists until a yield strain is reached and necking starts. For higher strain values necking does not continue however. Instead of additional necking, drawing or strain softening occurs; polymer chains will realign and stretch to reduce stress. The yield stress and the amount of strain softening increases with decreasing temperatures and increasing strain rate, which was shown for PETG by Dupaix et al.<sup>[54]</sup>. When all polymer chains are realigned, strain hardening occurs, characterized by a rapid increase in stress for increasing strain. Plastic deformation of the polymer is then manifested as shear banding or crazing. Shear bands are generally formed in regions with high compression or shear, where crazing occurs in regions with high hydrostatic tension. During crazing, fibrils and micro-voids are formed in the polymer, leading to volumetric growth and eventually to cracks.

Van den Bosch et al.<sup>[55]</sup> showed that during a 180° peel test of a PET coating on a steel sheet, these fibrils were formed at the delamination front, and were considered the main delamination mechanism.

#### 2.4.5 Failure

While the tests mentioned in the last paragraph deliver a value for the delamination force or stress, also the failure *mode* is of great importance, as it offers a way of determining the locus of failure. This might be important if the total system is to be improved. Failure in coatings specifies the weakest link in the total system, albeit locally. Fracture usually occurs at a discontinuity in the system, whether it is a natural one like an edge or a production flaw like a bubble or uncured part of the

coating due to imperfect mixing for instance. In general, three types of failure are recognized: adhesive, cohesive and mixed failure. Usually a mixed failure mode means that locally adhesive or cohesive failure occurred. Sometimes it is not clear with the bare eye if any polymer remains from the coating are on the surface after failure, so several methods are then used to check this. SEM or more sensitive and quantitative, XPS or local FTIR can be deployed to show the presence of remains of coating. This is an important step, since true adhesive failure (a “clean” surface after detachment) is usually attributed to an improper pretreatment. And therefore, the coating or adhesive system, where this plays an even more important role, is not loaded during testing to its full potential. Cohesive failure however, which can occur in general in any solid, be it the substrate, the primer or the coating/adhesive, usually indicates the pretreatments have been sufficient to ensure optimal bonding of the polymer molecules to the substrate. Mixed mode of failure is a locally varying mechanism by which the system catastrophically gave in to the stresses imposed.

#### **2.4.6 Relation between bonding and adhesion**

For adhesion to be present, bonding needs to have taken place between the organic coating or adhesive and the oxide surface. As mentioned at the end of 2.3.2, bonding is relatively weak, in the order of  $2 \text{ J/m}^2$  for acid/base type bonds. Macroscopical adhesion forces for adhesive systems however can reach more than  $1000 \text{ J/m}^2$ , even in mode I (normal stress, butt joints). The main reason for of this discrepancy in orders of magnitude is the distribution of forces inside the coating or adhesives. The results of macroscopic tests are usually depicted in stress-strain diagrams, as schematically shown in figure 2.8. On the horizontal axis is the strain in % elongation, while the vertical axis shows an arbitrary stress in MPa. When stress is put on an adhesively bonded joint (or tape in peel, coating in pull tests, etc.), deformation increases linearly with that stress. However, at some point the elastic (reversible) part of the stress is reached just before point A. Point A is the intersection of a line drawn parallel to the curve, starting at 0.2% strain per definition. This is defined as the modulus of elasticity (E-modulus or Young’s modulus) of the tested system. Below this triangular shaped form (called roman I) is the energy that goes into the system due to reversible elastic deformation. Beyond this triangle, the curve can show a variety of behavior, including lowering of stress because of necking. In this theoretical case, the ultimate stress is reached in point B and finally catastrophic failure in point C. Because of rubbery behavior of a coating or adhesive, the distance between point A and C can be more than 100% strain, however at limited stresses. Area II therefore represents the plastic deformation



energy. The total energy that the system can dissipate until failure is obviously the sum of area I and II. It is therefore not realistic to evaluate the total adhesion energy with respect to bonding, since the area II is contributed totally to the plastic deformation in the system at strains which are not supported by bonds. However, if the mode of failure is cohesive in the coating or in the adhesive, bonding has obviously sufficed to transfer the energy to the coating, where it can be dissipated. Apparently the bonds are able to form anchor points (the type and number tailorable) at the surface where the macroscopic system can attach to and three-dimensionally transfer the stresses in the surrounding matrix through covalent bonds. Two-dimensionally this can be demonstrated by pulling on a knitted sweater, where the single threads will distribute the force to the surrounding area because they are either attached or they overlap. The stresses are also not mode I, but because of the flexibility of the strands directed in all ways, except towards the source of the force.

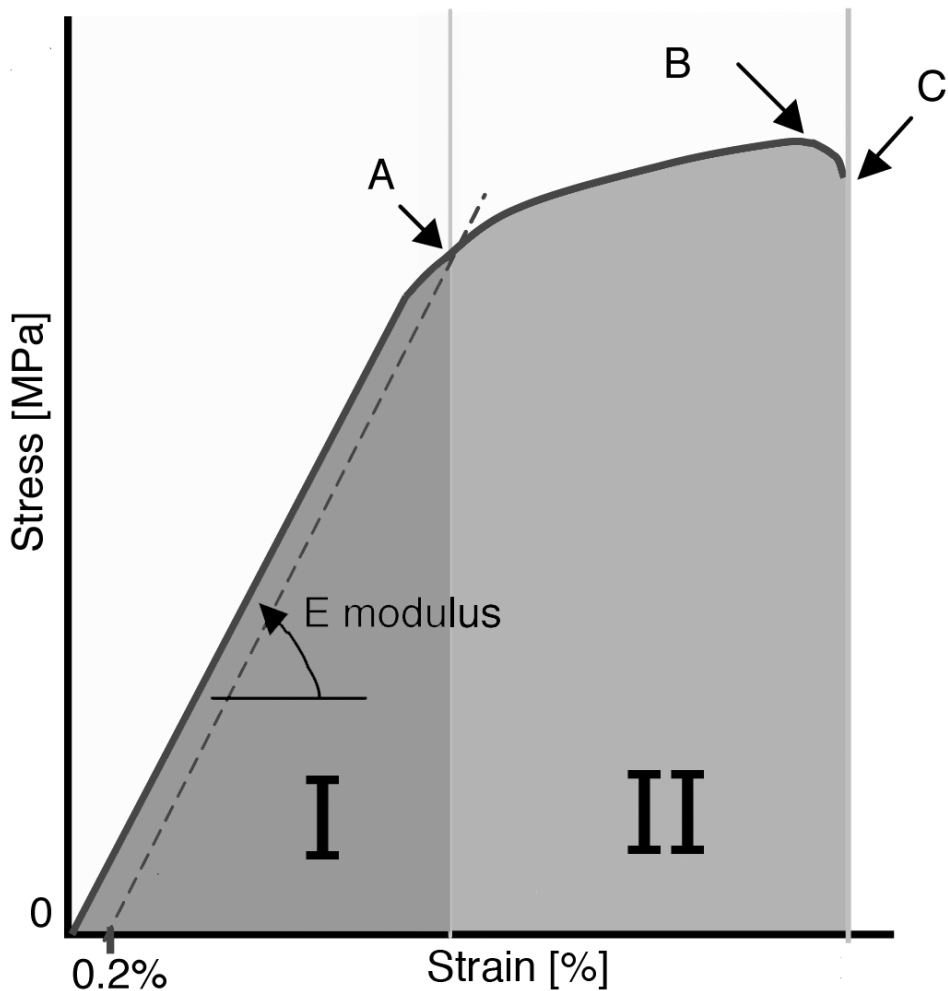


**Figure 2.8** Schematic of theoretical stress-strain curve; A: yield point, B: ultimate stress, C: failure, area I: elastic deformation, area II: plastic deformation

Because the type and number of bonds are important parameters to relate to the overall forces or stresses, the only thing that is lacking is the connecting practical experiment. McCafferty et al. have done such experiments, where the isoelectric point of an oxide film<sup>[56]</sup> is related to a peel energy and a pull-off force of a tape film with either an “acidic” or “alkaline” character. The relation is depicted for various oxides in figure 2.9. Summarizing, an alkaline coating (PMMA) adheres significantly better to an acidic surface oxide (e.g. Si, pH = 2) than to an alkaline oxide (e.g. Al, pH = 9). But, as can be seen for the PSA tape, adhesion energies from 140 to 380 J/m<sup>2</sup> are still two factors above the bonding energies that can be calculated for acid base

interactions. Changing to an alkaline oxide, with the same tape, the peel energy is more than doubled, leading to the conclusion that more (number of bonds) or better bonding (a stronger type) can significantly influence the outcome of a macroscopic experiment.

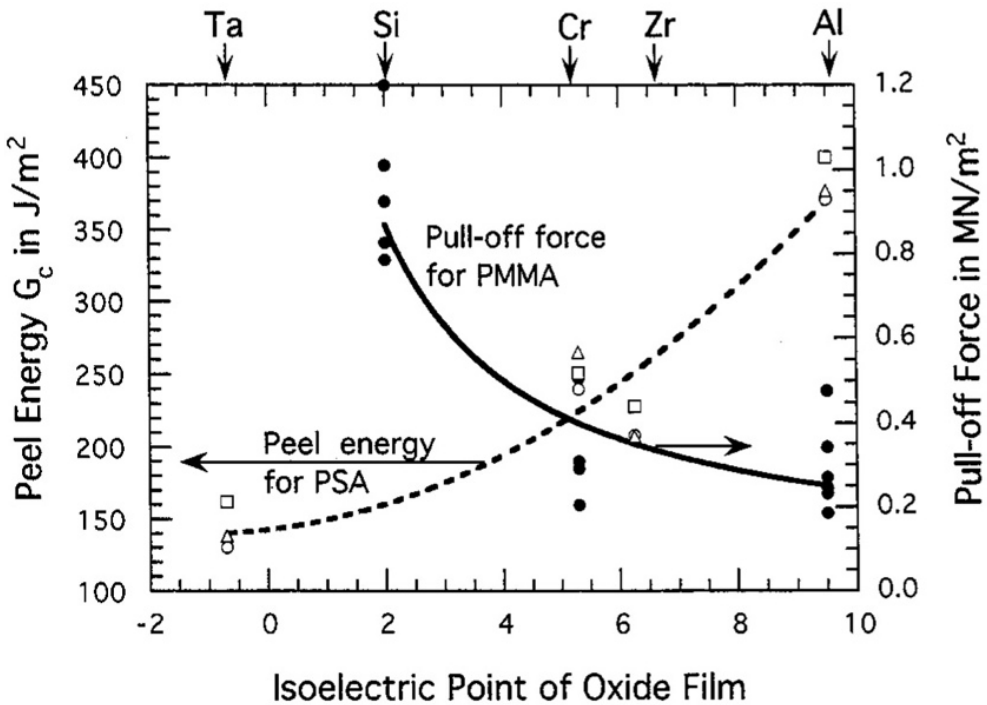


**Figure 2.9** Measured peel energy for a PSA or the measured pull-off force for PMMA vs. the IEP of the oxide film. The peel energy is shown for the various contact times prior to the peel measurement: 1 h, 10 h, and 24 h, McCafferty<sup>[57]</sup>.

It's expected, like shown in figure 2.9, that the choice of surface as well as the choice of polymer will give a large enough variation in results to be measurable by macroscopic adhesion testing. Best results possibly with "acid" coatings, because of higher compatibility with alkaline surfaces from aluminium (IEPS ~9.5) and magnesium (IEPS ~ 12).

In Chapter 8 it will be shown that for a well chosen mechanical test method for some coatings a qualitative agreement between bonding strength and mechanical testing results can be found.

**Table 2.6a.** Polar surface interactions with an organic acid, Bolger and Michaels<sup>[46]</sup>.

<i>Organic acid</i>	$pK_{A(A)}$	$\Delta_A \equiv \text{IEPS} - pK_{A(A)}$		
		<i>SiO<sub>2</sub></i>	<i>Al<sub>2</sub>O<sub>3</sub></i>	<i>MgO</i>
Dodecyl sulfonic acid	- 1	3	9	13
Trichloroacetic acid	0.7	1.3	7.3	11.3
Chloroacetic acid	2.4	- 0.4	5.6	9.6
Phthalic acid	3.0	- 1	5.0	9.0
Benzoic acid	4.2	- 2.2	3.8	7.8
Adipic acid	4.4	- 2.4	3.6	7.6
Acetic acid	4.7	- 2.7	3.3	7.3
Hydrogen cyanide	6.7	- 4.7	1.3	5.3
Phenol	9.9	- 7.9	- 1.9	2.1
Ethyl mercaptan	10.6	- 8.6	- 2.6	1.4
Water	15.7	- 13.7	- 7.7	- 3.7
Ethanol	16	- 14	- 8	- 4
Acetone	20	- 18	- 12	- 8
Ethyl acetate	26	- 24	- 18	- 14
Toluene	37	- 35	- 29	- 25

**Table 2.6b.** Polar surface interactions with an organic base, Bolger and Michaels<sup>[46]</sup>.

<i>Organic Base</i>	$pK_{A(B)}$	$\Delta_A \equiv \text{IEPS} - pK_{A(B)}$		
		<i>SiO<sub>2</sub></i>	<i>Al<sub>2</sub>O<sub>3</sub></i>	<i>MgO</i>
Trimethyl dodecyl ammonium hydroxide	12.5	10.5	4.5	0.5
Piperidine	11.2	9.2	3.2	- 0.8
Ethylamine	10.6	8.6	2.6	- 1.4
Triethylamine	10.6	8.6	2.6	- 1.4
Ethylenediamine	10	8	2.0	- 2
Ethanol amine	9.5	7.5	1.5	- 2.5
Benzylamine	9.4	7.4	1.4	- 2.6
Pyridine	5.3	3.3	- 2.7	- 6.7
Aniline	4.6	2.6	- 3.4	- 7.4
Urea	1.0	- 1.0	- 7	- 11
Acetamide	- 1	- 3	- 9	- 13
Water	- 1.7	- 3	- 9	- 13
Tetrahydrofuran	- 2.2	- 4.2	- 10.2	- 14.2
Ethyl ether	- 3.6	- 5.6	- 11.6	- 15.6
t-Butanol	- 3.6	- 5.6	- 11.6	- 15.6
n-Butanol	- 4.1	- 6.1	- 12.1	- 16.1
Acetic acid	- 6.1	- 8.1	- 14.1	- 18.1
Phenol	- 6.7	- 8.7	- 14.7	- 18.1
Acetone	- 7.2	- 9.2	- 15.2	- 19.2
Benzoic acid	- 7.2	- 9.2	- 15.2	- 19.2

**References**

- [1] J. van den Brand, PhD thesis, On the adhesion between aluminium and polymers Delft University of Technology (Delft), **2004**.
- [2] H. Wouters, D. Bol in *Material Scarcity An M2i study* **2009**
- [3] U.S. Geological Survey, **2007**
- [4] W.A. Dean, in *Aluminium properties and physical metallurgy*, 10th ed. (Ed.: J. E. Hatch), **1984**.
- [5] J. W.D. Callister, *Materials science and engineering an introduction*, 4th Edition ed., John Wiley & Sons, Inc., New York, **1997**.
- [6] J.E. Hatch, *Aluminum Properties and Physical Metallurgy*, American Society for Metals, Ohio, **1984**.
- [7] L. Lochte, K. Kuhnke, *Praktische Metallographie-Practical Metallography* **2008**, 45, 37.
- [8] J. Hartman, in *Case Studies in Manufacturing with Advanced Materials, Vol. Volume 1* (Eds.: J. H. W. de Wit, A. Demaid, M. Onillon), Elsevier Science Publishers B. V, Amsterdam, **1992**.
- [9] P.G. Sheasby, R. Pinner, *The surface treatment and finishing of aluminium and its alloys, Vol. 1*, Finishing publications LTD., Stevenage, **2001**.
- [10] F. Andreatta, Local electrochemical behaviour of 7xxx aluminium alloys, Delft University of Technology (Delft), **2004**.
- [11] J.R. Flores, The Role of Magnesium in the Electrochemical Behaviour of 5XXX Aluminium-Magnesium Alloys Delft University of Technology (Delft), **2006**.
- [12] Premendra, Investigation of surface layer on rolled recycled AA5050 in relation to Filiform Corrosion, Delft University of Technology (Delft), **2007**.
- [13] J.S. Zhang, X.H. Zhao, Y. Zuo, J.P. Xiong, *Surface & Coatings Technology* **2008**, 202, 3149.
- [14] Premendra, B.S. Tanem, J.M.C. Mol, H. Terryn, J.H.W. Dewit, L. Katgerman, *Surface and Interface Analysis* **2008**, 40, 1157.
- [15] S. Cottier, A. Feigenbaum, P. Mortreuil, A. Reynier, P. Dole, A.M. Riquet, *Journal of Agricultural and Food Chemistry* **1998**, 46, 5254.
- [16] T.S. Sun, J.M. Chen, J.D. Venables, R. Hopping, *Applied Surface Science* **1978**, 1, 202.
- [17] C.E. Moffitt, D.M. Wieliczka, H.K. Yasuda, *Surface & Coatings Technology* **2001**, 137, 188.
- [18] S. Feliu, M.J. Bartolome, *Surface and Interface Analysis* **2007**, 39, 304.

- 
- [19] G.E. Thompson, P. Skeldon, X. Zhou, K. Shimizu, H. Habazaki, C.F.E. Smith, *Aircraft Engineering and Aerospace Technology* **2003**, 75, 372.
- [20] W. Wen, Y.M. Zhao, J.G. Morris, *Materials Science and Engineering a-Structural Materials Properties Microstructure and Processing* **2005**, 392, 136.
- [21] S. Scotto-Sheriff, E. Darque-Ceretti, G. Plassart, M. Aucouturier, *Journal of Materials Science* **1999**, 34, 5081.
- [22] A.J. Kinloch, H.E. Bishop, N.R. Smart, *Journal of Adhesion* **1982**, 14, 105.
- [23] G.R. Wakefield, R.M. Sharp, *Applied Surface Science* **1991**, 51, 95.
- [24] K. Wefers, *Aluminium* **1981**, 57, 722.
- [25] D.J. Field, G.M. Scamans, E.P. Butler, *Metallurgical Transactions a-Physical Metallurgy and Materials Science* **1987**, 18, 463.
- [26] C. Lea, C. Molinari, *Journal of Materials Science* **1984**, 19, 2336.
- [27] J.H. Nordlien, K. Nisancioglu, S. Ono, N. Masuko, *Journal of the Electrochemical Society* **1996**, 143, 2564.
- [28] J.H. Nordlien, K. Nisancioglu, S. Ono, N. Masuko, *Journal of the Electrochemical Society* **1997**, 144, 461.
- [29] M. Pourbaix, *Atlas of Electrochemical Equilibria in Aqueous Solutions* **1966**, Pergamon Press, Oxford.
- [30] D.B. Blücher, J.E. Svensson, L.G. Johansson, M. Rohwerder, M. Stratmann, *Journal of the Electrochemical Society* **2004**, 151, B621.
- [31] G.L. Song, A. Atrens, *Advanced Engineering Materials* **2003**, 5, 837.
- [32] M. Koppers, K. Weber, V. Dehnke, J. Fuhrmann, *Materialwissenschaft Und Werkstofftechnik* **2001**, 32, 88.
- [33] R. Lindstrom, L.G. Johansson, G.E. Thompson, P. Skeldon, J.E. Svensson, *Corrosion Science* **2004**, 46, 1141.
- [34] D.B. Blucher, J.E. Svensson, L.G. Johansson, *Journal of the Electrochemical Society* **2003**, 150, B93.
- [35] C. Fotea, J. Callaway, M.R. Alexander, *Surface and Interface Analysis* **2006**, 38, 1363.
- [36] F.M. Reis, H.G. De Melo, I. Costa, *Electrochimica Acta* **2006**, 51, 1780.
- [37] G.T. Gregory, D.L. Nock, USA, **1988**.
- [38] A.J. Kinloch, N.R. Smart, *Journal of Adhesion* **1981**, 12, 23.
- [39] K.W. Allen, *International Journal of Adhesion and Adhesives* **1987**, 7, 213.
- [40] W.M. Bos, PhD thesis, Prediction of coating durability, Delft University of Technology (Delft), **2008**.

- [41] J.H.W. de Wit, J.M.C. Mol, W.M. Bos, G.M. Ferrari, in *High-performance organic coatings* (Ed.: A. S. Khanna), Woodhead Publishing Limited, Cambridge England, **2008**.
- [42] K.W. Allen, *Journal of Adhesion* **1987**, *21*, 261.
- [43] A.F. Harris, A. Beevers, *International Journal of Adhesion and Adhesives* **1999**, *19*, 445.
- [44] C.H. Hare, in *Paint film degradation - mechanisms and control* (Ed.: C. H. Hare), SSPC: The Society for Protective Coatings, **2002**.
- [45] F.M. Fowkes, D.O. Tischler, J.A. Wolfe, L.A. Lannigan, C.M. Ademujohn, M.J. Halliwell, *Journal of Polymer Science Part a-Polymer Chemistry* **1984**, *22*, 547.
- [46] J.C. Bolger, A. S Michaels, *Molecular structure and electrostatic interaction at polymer-solid interfaces*, Elsevier, New York, **1969**.
- [47] G.A. Parks, *Chemical Reviews* **1965**, *65*, 177.
- [48] P.A. Thiel, T.E. Madey, *Surface Science Reports* **1987**, *7*, 211.
- [49] E. McCafferty, J.P. Wightman, *Surface and Interface Analysis* **1998**, *26*, 549.
- [50] A.N. Rider, N. Brack, S. Andres, P.J. Pigram, *Journal of Adhesion Science and Technology* **2004**, *18*, 1123.
- [51] J. van den Brand, O. Blajiev, P.C.J. Beentjes, H. Terryn, J.H.W. de Wit, *Langmuir* **2004**, *20*, 6308.
- [52] D.G. Anderson, *Analytical Chemistry* **1999**, *71*, 21R.
- [53] K. Wapner, G. Grundmeier, *Advanced Engineering Materials* **2004**, *6*, 163.
- [54] R.B. Dupaix, M.C. Boyce, *Polymer* **2005**, *46*, 4827.
- [55] M.J. van den Bosch, P.J.G. Schreurs, M.G.D. Geers, *Journal of the Mechanics and Physics of Solids* **2008**, *56*, 3259.
- [56] E. McCafferty, J.P. Wightman, *Journal of Adhesion Science and Technology* **1999**, *13*, 1415.
- [57] E. McCafferty, *Journal of the Electrochemical Society* **2003**, *150*, B342.
- [58] *Coating Technology training programme*, Polymer Technology Netherlands foundation, Eindhoven, **2005**.

## **Chapter 3 - Experimental**





---

### 3.1 Introduction

In this chapter, the materials and experimental methods used throughout the thesis will be discussed in detail. I will refer back to the paragraphs of this chapter in the rest of the thesis, where applicable.

### 3.2 Materials

In general, sheet material of aluminium alloy and magnesium alloys was used as substrate. The exceptions were pure aluminium and magnesium vacuum evaporated onto glass slides. The following paragraphs give more details on the used samples.

#### 3.2.1 Substrates

##### *3.2.1.1 Aluminium alloy AA1050*

Samples were cut to dimensions of 80 × 25 mm out of 1 mm thick sheets of AA1050 aluminium alloy (see table 3.1) as specified by Hydro R&D Bonn. The long side of the substrates was taken in the rolling direction and this particular dimensions were chosen to fit into the grazing angle accessory of the FTIR apparatus.

##### *3.2.1.2 Aluminium alloy AA5182*

Al-Mg alloy AA5182 in 1 mm thick sheet “Innerlite” as supplied by Tata Steel Europe in IJmuiden, the Netherlands with magnesium as the main alloying element, was also cut to dimensions of 80 × 25 mm where the long side was always in the rolling direction. With X-ray fluorescence (XRF) was found that, except for 4.8% Mg, other elements were in amounts around the detection limits of the method and their presence was therefore not proved. Table 3.1 shows an overview of the AA5182 series composition as specified by Tata Steel.

**Table 3.1** Composition of AA1050, AA5182 and AZ31 in wt%

Element	AA1050	AA5182	AZ31
Al	99.5	Balance	3.13
Mg	-	4.8*	Balance
Fe	0.04	0.35	-
Si	0.25	0.2	-
Cu	-	0.15	-
Mn	-	0.2 - 0.5	0.49
Cr	-	0.1	-
Zn	-	0.25	0.98
Ti	-	0.1	-
Other	-	0.05 - 0.15	-

\*measured with XRF \*\*total content

### 3.2.1.3 Magnesium alloys

Magnesium alloys were obtained from extrusion samples, of 2.5 mm thickness. As the Light Metals group of the Materials Science and Engineering department from TU Delft produced it in strip form, only the length was cut to 80 mm, while the width was already around 30 mm. Since the samples were thicker than the aluminium ones, using a thinner slab of copper as support in the grazing angle accessory of the FTIR apparatus compensated for the height difference. The composition of the used AZ31 was measured by XRF. The results of that measurement are in table 3.2.

### 3.2.1.4 Vacuum evaporated metals

Thin aluminium and magnesium layers were obtained by using a Balzers BAE250 PVD machine to vacuum-evaporate pure metal onto cleaned glass sheets of 75 x 25 mm. For aluminium layers, about 10 cm of aluminium wire (supplied by Sigma-Aldrich) of 99.99% purity was cut and placed into the tungsten boat of the vacuum-evaporator. Magnesium turnings of 99.98% purity were also obtained from Sigma-Aldrich. Several turnings were put into a tungsten boat before vacuum pumping was started.

Each metal was then heated by electrically heating the tungsten boats in a vacuum around  $5 \cdot 10^{-6}$  bar. The thickness of the layers was monitored by a calibrated quartz-crystal thickness gauge inside the evaporation chamber. After reaching 200 nm thickness, the current was switched off and the vacuum chamber was slowly restored to room pressure with air. The samples were taken directly out of the vacuum chamber after cooling down and used immediately for further experiments.

### 3.2.2 Preparation

#### 3.2.2.1 Solvents and cleaning

All organic solvents mentioned were of analytical grade “Baker analysed” or better and were obtained from JT Baker, Deventer, The Netherlands, unless otherwise mentioned. When water is mentioned, triply distilled water with a conductivity of 18.2 MOhm·cm of 25°C was used from continuous distillation by a Millipore MilliQ installation.

The glassware was cleaned in a Miele Professional G7883 dishwasher where the last step consisted of rinsing with doubly de-ionized water.

#### 3.2.2.2 Grinding and polishing

The alloy samples were polished in several successive steps. Table 3.3 shows a detailed overview of the subsequent steps. The last polishing step of 0.025 µm was either done with a neutral (OP-AN) aluminum oxide based polishing slurry or an acidic one (OP-S). All materials were obtained from Struers GmbH Nederland, Maassluis, The Netherlands. The samples were cleaned in hot chloroform (99+ vol. % pure).

**Table 3.2.** Overview of grinding and polishing procedure for aluminium and magnesium alloys.

Step	Plane grinding	Fine grinding	Diamond polish 1	Diamond polish 2	Diamond polish 3	Oxide polish
Disc / Cloth	SiC-paper	MD-Largo	MD-Dur	MD-Mol	MD-Nap	MD-Chem
Abrasive and grain size	SiC 220 grit	DP-susp. 9 µm	DP-susp. 6 µm	DP-susp. 3 µm	DP-susp. 1 µm	OP-S/AN 0.025 µm
Lubricant	Water	Blue	Blue	Red	Red	Water
Disc speed (rpm)	300	150	150	150	150	150
Force (N)	40	50	50	40	40	30
Time (sec)	Until plane	180	150	150	120	60

### 3.2.3 Molecules

#### 3.2.2.1 Succinic acid

Succinic acid, or ethane-1,2- dicarboxylic acid, was used as the model molecule in the experiments. Figure 3.1 shows the chemical structure. It has two carboxylic acid

end groups connected to an ethane backbone. Sigma-Aldrich supplied the succinic acid, which was 99.5 +% pure and was used without further purification.

### 3.2.2.2 Dimethyl terephthalate (DMT)

Dimethylterephthalate was obtained from Sigma-Aldrich in tablet form and ground to a power. The purity was higher than 99%. Figure 3.2 shows the chemical structure.

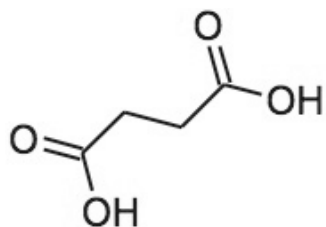


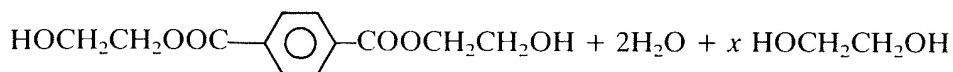
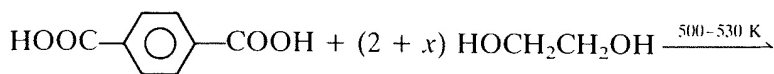
**Figure 3.1** Chemical structure of succinic acid



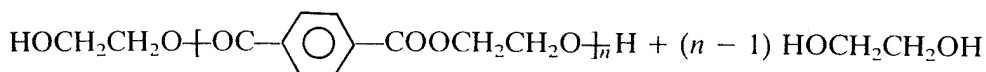
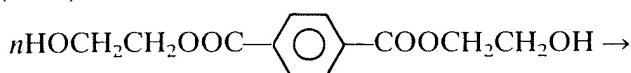
**Figure 3.2** Chemical structure of di-methyl terephthalate (DMT, left) and polyethylene terephthalate (PET, right)

### 3.2.4 PETG coatings

Glycol-modified polyethylene terephthalate (PETG) films (300  $\mu\text{m}$  Vivak, Bayer) were cut to 80 x 9 mm. To obtain adhesion, after leaving at 50°C for several days to dry, the PETG films were cleaned with alcohol and bonded at 150°C under a pressure of about 0.5 MPa for 300 s to the aluminium substrates. Pressure was exerted on the PETG via a glass slide covered with a spin-coated layer of methyl nonafluoro(iso)butyl ether to prevent sticking to the PETG. Subsequently the samples were left to cool. PET(G) can be made through a two step polymerizing reaction, which is as follows<sup>[1]</sup>:



After this reaction the temperature is raised to 550K so that the excess ethylene glycol and the ethylene glycol produced by further ester interchange reactions can be removed and so that the polymer is formed above its melting temperature (538K):



The resulting polymer has no free carboxylic acid groups, so the proper molecule to represent the bonding is dimethyl terephthalate.

### 3.3 Pre-treatments and application methods

#### 3.3.1 Pre-treatments of alloys

All alloys were polished and cleaned before they were given the following pre-treatments.

##### 3.3.1.1 Alkaline Pretreated Aluminum

Samples were mildly etched in a pH = 12.5 solution made of NaOH (97+ vol. % pure) in de-ionized water for a period of 30 seconds at room temperature. The substrates were then thoroughly rinsed for at least 3 minutes using de-ionized water and blown dry using nitrogen gas.

##### 3.3.1.2 Pseudoboehmite Oxide

Samples were immersed in boiling de-ionized water for a period of 15 seconds which resulted in the formation of a pseudoboehmite (AlOOH) layer [3]. The samples were then allowed to dry for a few minutes in an upright position.

### *3.3.1.3 Acid Pretreated Aluminum*

The substrates were immersed in a 33 vol. % HNO<sub>3</sub> solution (chemically pure) in deionized water for 30 seconds at room temperature. Finally, the substrates were thoroughly rinsed for at least 3 minutes using deionized water and blown dry using nitrogen gas.

### *3.3.1.4 Dehydroxylated Aluminum*

After being polished and cleaned, the samples were heated in air for 24 hours at a temperature of 275 °C in an Snijstaal/Nakertherm type N15-65A oven which was ventilated with surrounding air. This procedure removes the physically bound water molecules through condensation and subsequent desorption from the surface but leaves the hydroxide groups at the surface [4].

### *3.3.1.5 Temperature sensitization*

Subsequent to the chemical pre-treatments mentioned above, some samples were given a longer temperature pre-treatment. These samples were wrapped in aluminium foil and left in MMM Medcenter Ecocell autoclaves with air ventilation for 11 days at 100°C and 200°C. One sample was kept outside the oven in aluminium foil and kept at room temperature for 11 days.

## **3.3.2 Application of molecules**

### *3.3.2.1 Succinic acid*

The model compound was dissolved in THF(tetrahydrofuran, chemical grade) at a concentration of 0.02 g/l. After preparation of the substrates, a background infrared spectrum was recorded and immediately after this the substrates were immersed in the solvent/model compound mixture and allowed to interact for a period of 30 min. Longer immersion times (as tested up to 3 h) were found not to have a significant effect on the results [5, 6]. The substrates were then withdrawn from the solution and rinsed using clean solvent. Finally the samples were directly transferred into the infrared apparatus.

### *3.3.2.2 DMT*

DMT molecules were applied by dip-coating the substrates into a solution of 0.01M DMT in toluene and left for an hour. After taking out of solution, the substrates were rinsed with toluene to wash off the excess molecules with poor bonding. The samples were then immediately transferred into the FT-IR apparatus.

### 3.4 Experimental equipment and methods

#### 3.4.1 Auger Electron Spectroscopy (AES) depth profiling

All measurements were done on a PHI 650 scanning Auger microprobe (SAM) system with a relative energy resolution  $\Delta E/E$  of 0.25%. The primary electron energy and beam current were set to 5 keV and 20  $\mu\text{A}$ , respectively. The electron beam was set to a scan area of approximately 130  $\mu\text{m}$  by 130  $\mu\text{m}$ . The ion sputtering was performed with a beam of argon ions with a gun voltage of 3.5 kV and a gun current of 10  $\mu\text{A}$ . The sputtered area was approximately 3 mm x 3 mm. The system was calibrated with an average sputter rate of approximately 4 nm/min for  $\text{Al}_2\text{O}_3$ . Prior to each analysis, the surface of each sample was sputter cleaned for 20 seconds. This was done to eliminate possible surface contaminants that might influence the Auger spectra. The interpretation of Auger spectra and composition depth profiles was based on high energy  $\text{KL}_2\text{L}_2$  Auger lines at 1396 eV for aluminium and at 1378 eV for aluminium oxide. For magnesium, also the  $\text{KL}_2\text{L}_2$  Auger lines were evaluated, but at 1186 eV and 1174 eV. The elemental concentrations were calculated by taking into account the sensitivity factors for Al and Mg<sup>[7]</sup>.

#### 3.4.2 Fourier Transform Infrared - Reflection Absorbtion Spectroscopy (FTIR-RAS)

For investigating the nature of molecular bonds, FT-IR-RAS analysis was performed. This was done with a Thermo-Nicolet Nexus FT-IR apparatus equipped with a liquid-nitrogen-cooled mercury-cadmium-tellurium (MCT-A) detector and a nitrogen-purged measurement chamber. The measurements were performed using a Specac variable angle reflection accessory set at a near-grazing incident angle of 82°. The infrared radiation was p-polarized by employing a Specac grid-wire polarizer. 128 scans with a resolution of 4  $\text{cm}^{-1}$  were added together to obtain the final spectrum.

A strict measurement routine was followed for reproducibility and to obtain comparable results. After grinding and polishing, the samples were cleaned and pre-treated. The pre-treated samples were then measured as reference background spectrum in the FT-IR machine. They were then dipped in the THF solution of 0.02 g/l succinic acid and after this they were rinsed thoroughly with the pure solvent to make sure no loosely attached molecules had remained. Finally an FT-IR spectrum



was taken with respect to the previously taken background spectrum. For more details refer to earlier publications [5, 6].

### 3.4.3 Asymmetrical Double Cantilever Beam

Crack propagation was performed in an ADCB set-up mounted in a reflection optical microscope, see figures 3.3. and 3.4. For details on ADCB experiments and related issues reference is made to [10] and [11]. In ADCB the energy release rate  $G(a)$  is calculated with the most important input parameter the measured crack length  $a$ . This is done by using [11]:

$$G(a) = \frac{(3\Delta^2 E_1 E_2 h_1^3 h_2^3)(C_2^2 E_1 h_2^3 + C_1 E_2 h_2^3)}{8a^4 \Lambda^2} \quad (3.1)$$

with  $E_1 = 2$  GPa and  $E_2 = 70$  GPa, which are the Young's moduli of PETG and an aluminium alloy respectively,  $\Delta$  the fixed crack opening set by the thickness of a razor blade (100  $\mu\text{m}$ ).  $\Lambda = C_{13}E_2h_{23} + C_{23}E_1h_{13}$  and  $C_i = 1 + 0.64 h_i/a$  and  $i = 1, 2$ . In practice  $a \gg h_1, h_2$ , which are the thickness of the coating and the substrate, respectively.  $C_1$  and  $C_2$  are introduced due to the mixed mode of de-lamination of the two different materials. Taken into  $\Delta$  is a mathematical correction factor for the fact that the crack runs through the interface and not exactly through the centre of the total thickness of coating and substrate. Also at all times, for the remaining adhering portion of the beam  $L$ ,  $L \gg a$  should hold.

From the prepared samples, the PETG film was lifted by hand with a razor blade from the substrate to initiate a crack. Another razor blade (thickness 100  $\mu\text{m}$ ) was inserted at the interface. The crack front was observed through the PETG with a CCD camera of an Olympus microscope with macro objective. In the experiment the position of the knife is fixed, and the sample is clamped on one side of the stage. The stage with clamped sample is then pushed onto a fixed knife at the height of the interface between the PETG and aluminium at a speed of 20  $\mu\text{m/s}$ . The de-lamination is followed in real-time and at certain positions a still is taken.

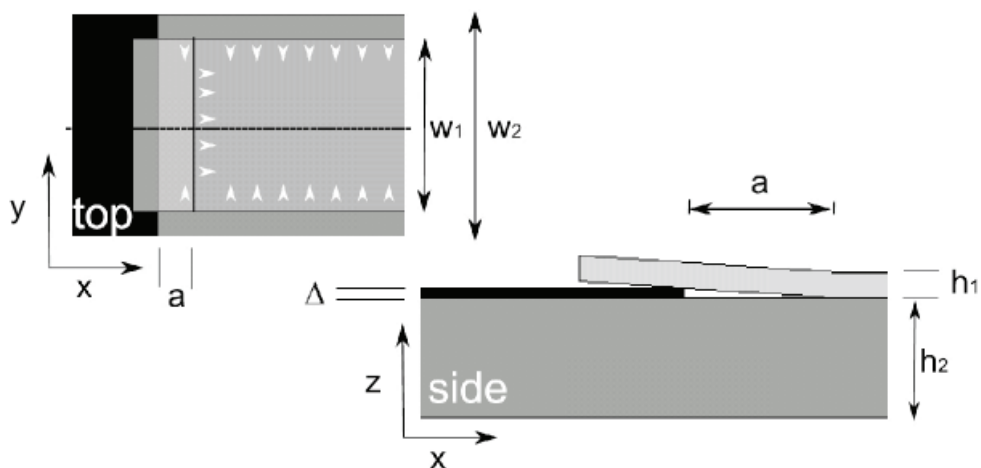


**Figure 3.3** Schematic representation of ADCB sample setup, top and side view

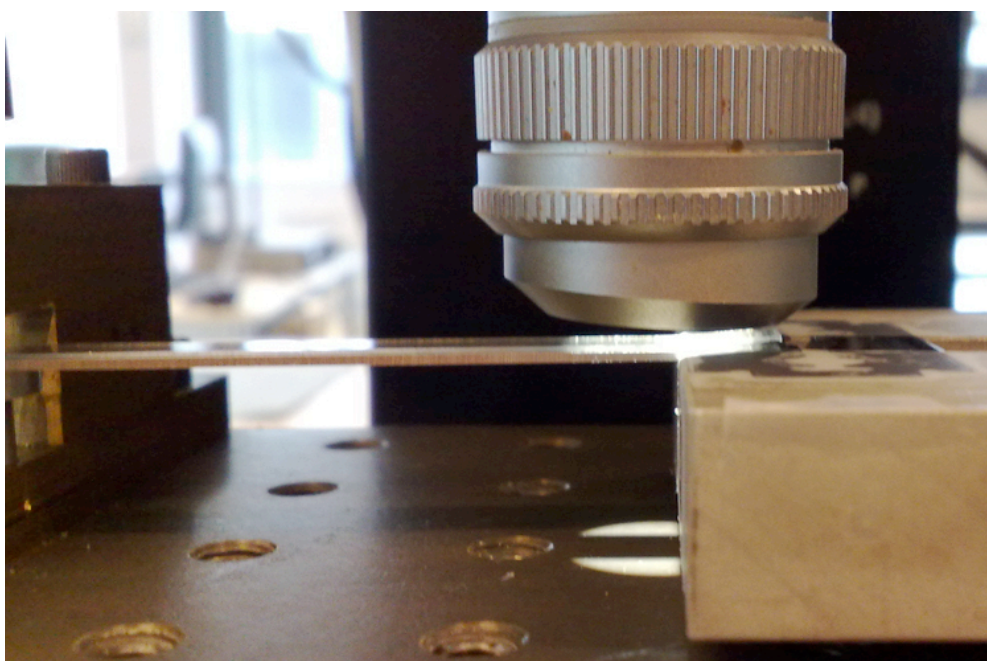


**Figure 3.4** ADCB setup side view with microscope placed above loaded sample

### 3.4.4 Potentiodynamic measurements

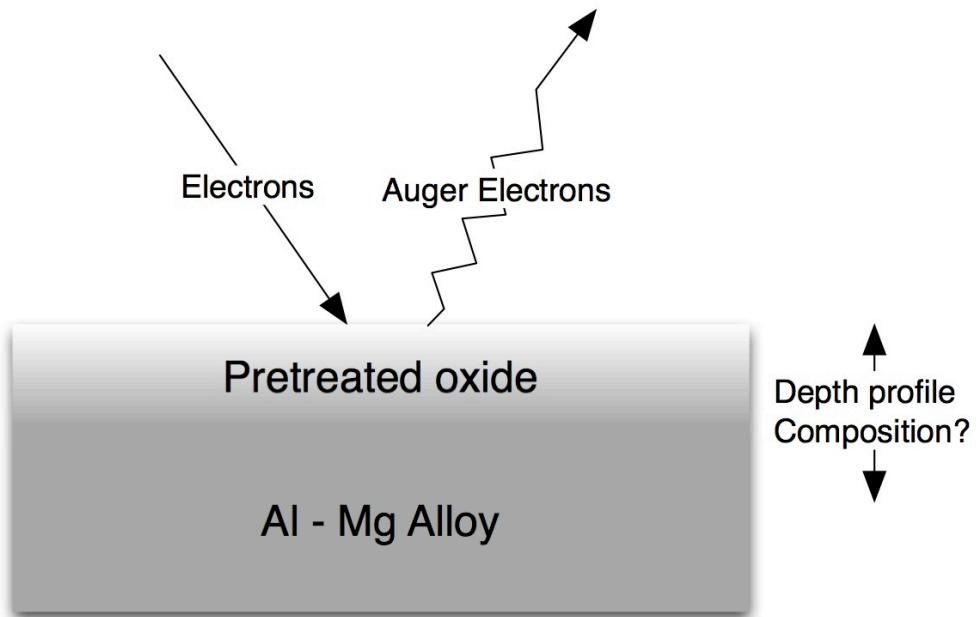
Open circuit measurements (OCP) were conducted with dual Solartron 1286/1287 potentiostats in custom-made upright cells. Two setups were used to exclude

systematic errors due to equipment. Temperature was kept at room temperature by means of air-conditioning and the cells were placed in Faraday cages to minimize electromagnetic interference. Standard saturated calomel electrodes (SCE) were used as reference electrodes. All solutions were made with chemically pure  $K_2SO_4$  or chemically pure NaCl and acidified to pH = 3 (measured with a calibrated pH-meter) with drops of 37 vol. % HCl solution (reagent grade).

## References

- [1] R. J. Young, P. A. Lovell, *Introduction to polymers - Second Edition*, Second Edition ed., Chapman & Hall, London, **1991**.
- [2] E. McCafferty, J. P. Wightman, *Journal of Adhesion Science and Technology* **1999**, *13*, 1415.
- [3] A. B. Kiss, G. Keresztury, L. Farkas, *Spectrochimica Acta Part a-Molecular and Biomolecular Spectroscopy* **1980**, *36*, 653.
- [4] L. Vlaev, D. Damyanov, M. M. Mohamed, *Colloids and Surfaces* **1989**, *36*, 427.
- [5] J. van den Brand, O. Blajiev, P. C. J. Beentjes, H. Terryn, J. H. W. de Wit, *Langmuir* **2004**, *20*, 6318.
- [6] J. van den Brand, O. Blajiev, P. C. J. Beentjes, H. Terryn, J. H. W. de Wit, *Langmuir* **2004**, *20*, 6308.
- [7] N. C. M. L.E. Davis, P.W. Palmberg, G.E. Riach, R.E. Weber, *Handbook of Auger Electron Spectroscopy, 2nd Edition* **1976**, Perkin-Elmer Corp.
- [8] W. P. Vellinga, A. Fedorov, J. T. De Hosson, *Journal of Computer-Aided Materials Design* **2007**, *14*, 37.
- [9] F. M. d. Wit, G. Eising, T. Hauffman, W.-P. Vellinga, J. T. M. D. Hosson, J. M. C. Mol, H. Terryn, J. H. W. d. Wit, in *EuroCorr 2008*, Edinburgh, United Kingdom, **2008**, p. 1306.
- [10] J. W. Hutchinson, Z. Suo, *Advances in Applied Mechanics, Vol 29* **1992**, *29*, 63.
- [11] B. Bernard, H. R. Brown, C. J. Hawker, A. J. Kellock, T. P. Russell, *Macromolecules* **1999**, *32*, 6254.

# Chapter 4 - Analysis of the surface composition of pre-treated aluminium alloys



This chapter is based on (parts of): "The influence of Chemical Pretreatment and Magnesium Surface Enrichment on Bonding of Succinic Acid Molecules to aluminium alloy" by F.M. de Wit, J.M.C. Mol, H. Terryn and J.H.W. de Wit, published in Journal of Adhesion Science and Technology 22 : 1089 2008

## **Synopsis**

The composition of oxides on metal surfaces is one of the parameters which influences the total coating system. In this chapter the determination of the composition of oxides on selected aluminium-magnesium alloys through AES is reported. The influence of chemical as well as heat treatments is explored. The detailed results will serve as reference for the following chapters.

## 4.1 Introduction

Oxide surfaces of commercial alloys (e.g. AA2024<sup>[1, 2]</sup>, AA7075<sup>[2]</sup> and AA5754<sup>[3]</sup>) have different compositions due to incorporation of alloying elements, like copper, zinc and magnesium. Preferential dissolution or enrichment of alloying elements can be induced by chemically pre-treating the surfaces or by anodizing<sup>[1, 4]</sup> in acid and alkaline solutions. Preferential (unwanted) surface enrichment can also be achieved with heat treatments<sup>[1]</sup>.

In this chapter, the focus will be on surface enrichment of magnesium, which is, present at 4.8 wt% in the bulk, the most important alloying element in AA5182. Magnesium from the bulk structure can not only segregate on grain boundaries and form precipitates ( $Mg_2Al_3$ )<sup>[5]</sup> but it can also diffuse into the oxide at elevated temperatures<sup>[6]</sup>, which either occurs after casting or during the tempering step to influence mechanical properties. Several authors<sup>[7, 8]</sup> have shown by means of AES and XPS that the oxide layer of an Al-Mg alloy can be enriched in Mg by subjecting the material to a prolonged heat treatment at temperatures below 200°C if the alloy contains more than 4.5 wt% magnesium. Lea and Molinari<sup>[9]</sup> have extensively studied the diffusion of magnesium in aluminium AA5657 and AA5252 alloys (lower alloyed 0.8 and 2.5 wt% magnesium) and have found that considerably higher temperatures (up to 600°C) are needed for magnesium surface enrichment of these alloys. The rationale for this enrichment is the solid-solubility of 4.5 wt% magnesium in aluminium (at 200°C, less than 1 wt% at room temperature). Above this limit, the diffusion of magnesium to the surface is energetically more favorable than additional precipitation. The higher temperatures are needed to dissolve the  $Al_3Mg_2$  phase at lower concentrations of Mg.

The enrichment of the surface by magnesium leads thus to the formation of a mixed (hydr)oxide in normal air, since magnesium is more reactive than aluminium<sup>[6]</sup>. Aluminium-magnesium alloys are known to form different oxides and hydroxides at the surface as a function of time and depending on the environment. Magnesium carbonates can also form from the hydroxides on the surface in the presence of  $CO_2$  <sup>[10, 11]</sup>.

For the purpose of defining the surfaces of the samples to be studied, also in further chapters, AES depth profiling was performed on AA5182 samples. The AA5182 samples were given temperature treatments at room temperature (RT), 100°C and 200°C for 11 days to ensure enrichment. The results were analyzed with AES depth profiling of the enrichment in magnesium in addition to the overall composition.

Also, four different chemical ways to influence the OH-fraction and the composition of the surface oxides in AA5182 were selected; acid, alkaline and boiling treatments

as simplified industrial treatments and dehydroxylation treatment to remove the physically bound water.

## 4.2 Results

The Auger peaks of Al (1396 eV), Al-O (1378 eV), Mg (1186 eV), Mg-O (1174 eV), O (505 eV) and C (260 eV) were evaluated at their energy positions as determined by the Multi-Pak software package<sup>[12]</sup>. Please refer to chapters 2 and 3 for more details on AES.

As explained in chapter 3, before each depth-profile, the samples were sputter-cleaned. To illustrate this, as an exception figure 4.1 shows the AES survey spectrum of a AA5182 sample after 11 days at 200°C before sputter-cleaning. This figure shows clearly that sputter-cleaning is necessary to clean the sample of contamination, to which the large C 1s is attributed.

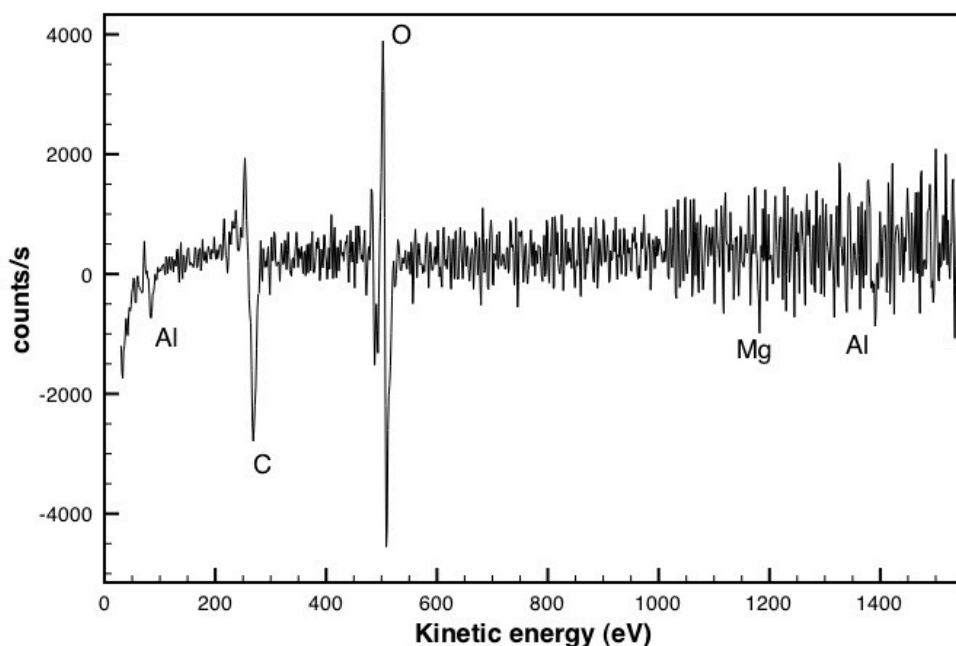


**Figure 4.1.** Complete AES survey spectrum of AA5182 sample after 11 days at 200°C.

#### 4.2.1 AES analysis of chemically pre-treated samples

From the AES measurements, chemical information was obtained using Principal Component Analysis (PCA). In a PCA the number of component spectra that is required to reproduce the original spectral data within the experimental error is determined. The basic principle of PCA and its application to Auger spectra is explained<sup>[12]</sup> and was applied recently<sup>[13]</sup> elsewhere. In spectra that are expected to have several components, a Target Factor Analysis (TFA) compares internal standards with the component spectra found by PCA. TFA produces the component profiles automatically after the component spectra are identified. This technique was used on the Al and Mg spectra, which are suspected to contain metallic as well as oxide peaks. Further details were discussed in paragraph 3.4.1. Please note that when the peaks of the metallic components and oxides are too small and the components are not distinguishable.

By combining Auger analysis with sputtering of the surface, an image of the buildup of surface (oxide) layers can be obtained. The C 1s, O 1s and Mg 2p and Al 2p peaks were used for further interpretation of the surface concentrations. In figure 4.2, the depth profiles for the chemically pre-treated samples are shown after alkaline (a), boiling (b), acid (c) and dehydroxylating (d) pre-treatments.

The oxygen concentration shows a direct and constant decrease for alkaline and acid pre-treated samples. After boiling there is no oxygen decrease. And only after 2 minutes sputtering does the oxygen signal decrease for dehydroxylating. The sputtering was calibrated at 4 nm per minute, as discussed in chapter 3. Therefore, the thickness of the oxide  $Z_0$ , the sputter depth, where the Al signal reaches 50%<sup>[14]</sup>, can be determined and is at around 7.5 minutes sputter time for the alkaline, at 1.5 minutes for acid (indicated as example) and at 3 minutes for dehydroxylated. Therefore, the alkaline pre-treated sample has a thicker oxide (30 nm), while the acid oxides are 6 nm and dehydroxylated 12 nm respectively. The thickness of the boiled sample's oxide could not be determined from these measurement, but is more than 40 nm. Table 4.1 summarizes these results.

On the alkaline sample, in figure 4.2a, the magnesium oxide component decreases from 30 wt% at the surface to bulk level after 6 minutes sputtering, where it crosses the magnesium metal component. After this, the magnesium metal signal increases to 10 wt%, which is more than bulk. The aluminium oxide component starts around 22 wt% at the surface, which is significantly less than the magnesium oxide.

The boiled sample (figure 4.2b) shows a bulk composition for magnesium and predominantly a layer composed of aluminium and oxygen. No separate components neither aluminium nor magnesium oxide were found.



After acid pre-treatment (figure 4.2c), the samples show a thin aluminium oxide, but again only a bulk magnesium signal and no distinguishable magnesium oxide component, because of the low total magnesium signal.

Finally, the dehydroxylated samples (figure 4.2d) show an increase in magnesium metal at the surface, while the aluminium metal is almost all missing for the first 2 minutes (8 nm) sputtering. Again, no oxide components could be distinguished.

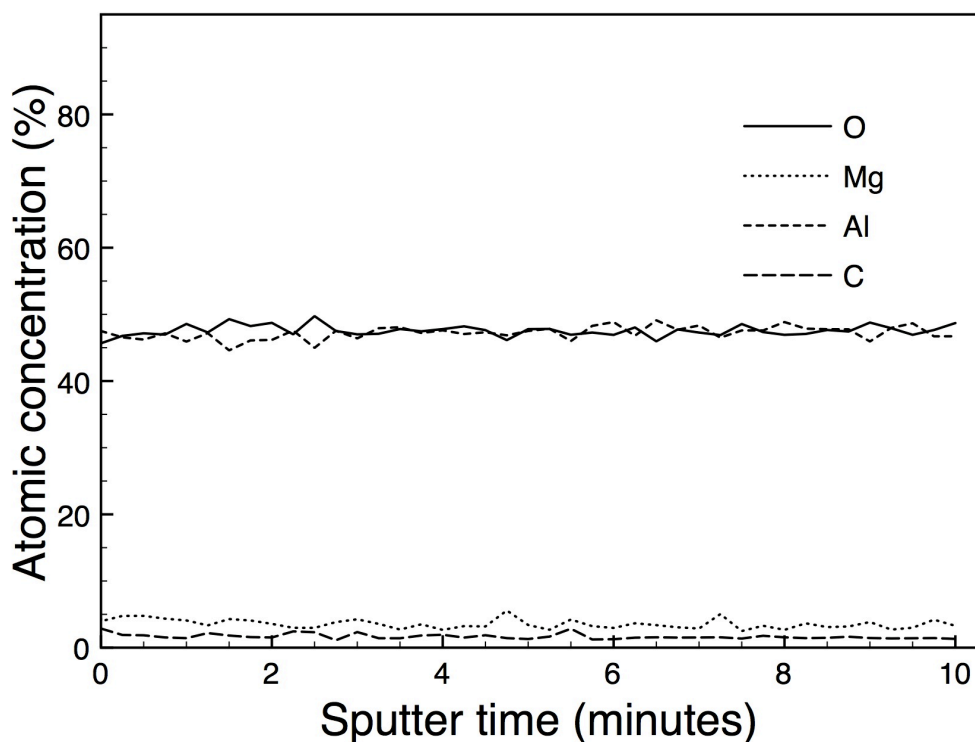


**Figure 4.2b.** AA5182 AES depth-profile for boiling pre-treatment

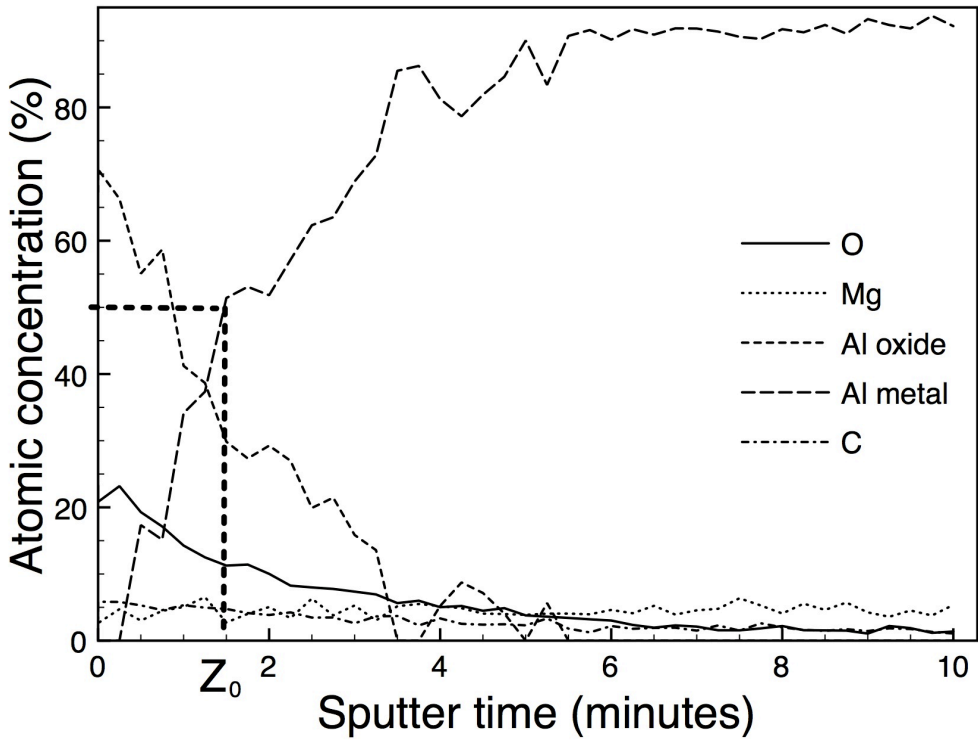
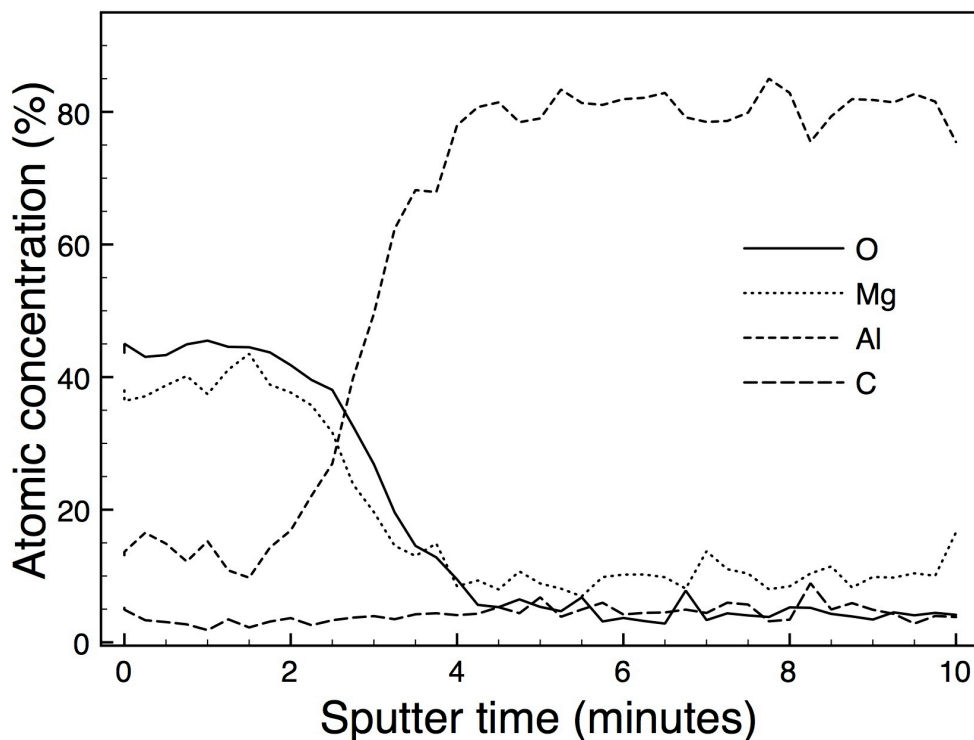


Figure 4.2c. AA5182 AES depth-profile for acid pre-treatment



**Figure 4.2d.** AA5182 AES depth-profile for dehydroxylated pre-treatment.

**Table 4.1.** Summary of pre-treatments and resulting oxide thickness as determined by AES depth-profiling on AA5182 samples.

Pre-treatment	Alkaline	Boiling	Acid	Dehydr-oxylated	RT	100°C	200°C
Z <sub>0</sub> time (min)	7.5	> 10	1.5	3.5	0.75	0.75	1
Thickness (nm)	30	> 40	6	12	3	3	4

#### 4.2.2 AES analysis of heat pre-treated samples

The results of the previously mentioned fitting procedure and concentration determination are shown in figure 4.3 for the heat pre-treated samples. The atomic concentration profiles of Al, Mg, O and C of the AA5182 samples that were heat-treated at room temperature, 100°C and 200°C with Auger sputtering measurements are given in parts a, b and c of figure 4.3, respectively.

For all heat pre-treatments, the oxygen concentration levels off at 1 minute sputter time, disappearing into the background noise at 1.5 minutes. The thickness of the oxide  $Z_0$ , the sputter depth, where the Al signal reaches 50%<sup>[14]</sup>, is indicated as an example from the Auger spectra in figure 4.3a.  $Z_0$  is at around 0.75 minutes sputter time for the RT and 100°C samples, while for the 200 °C pretreated sample this is at 1 minute. Therefore, the 200°C sample has a slightly thicker oxide (4 nm), while the other oxides are 3 nm thick. Again, table 4.1 summarizes these results.

The major difference between the three spectra, is the presence and increase in magnesium oxide component signal. This signal is not present at room temperature, therefore, there is a negligible amount of magnesium oxide at the surface. After 11 days at 100°C, there is a presence, which increases to about 10 wt %. After 11 days at 200°C, this has increased to a similar level as the aluminium oxide, i.e. around 20 wt%. Note that the aluminium oxide component has decreased from 27 wt% at room temperature to 20 wt% after the 200°C treatment.

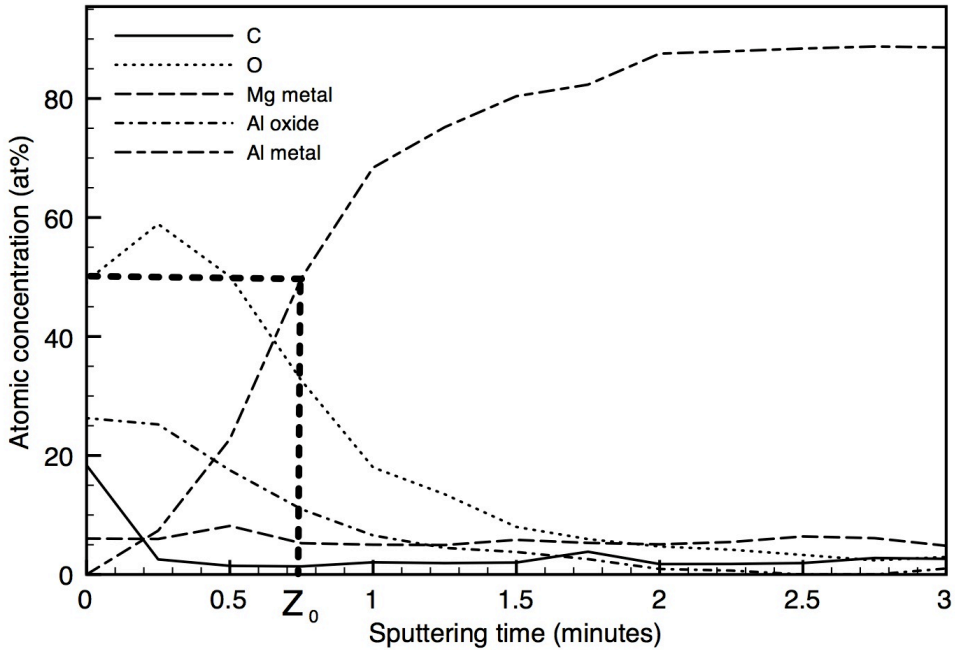


Figure 4.3 a. AA5182 AES depth-profile after 11 days at room temperature.

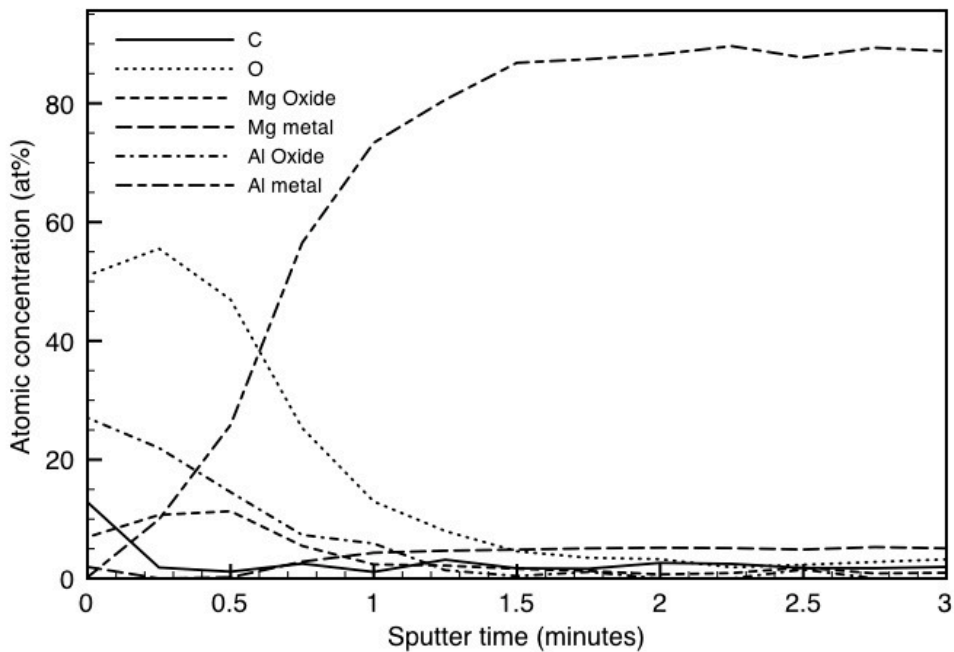


Figure 4.3 b. AA5182 AES depth-profile after 11 days at 100°C.

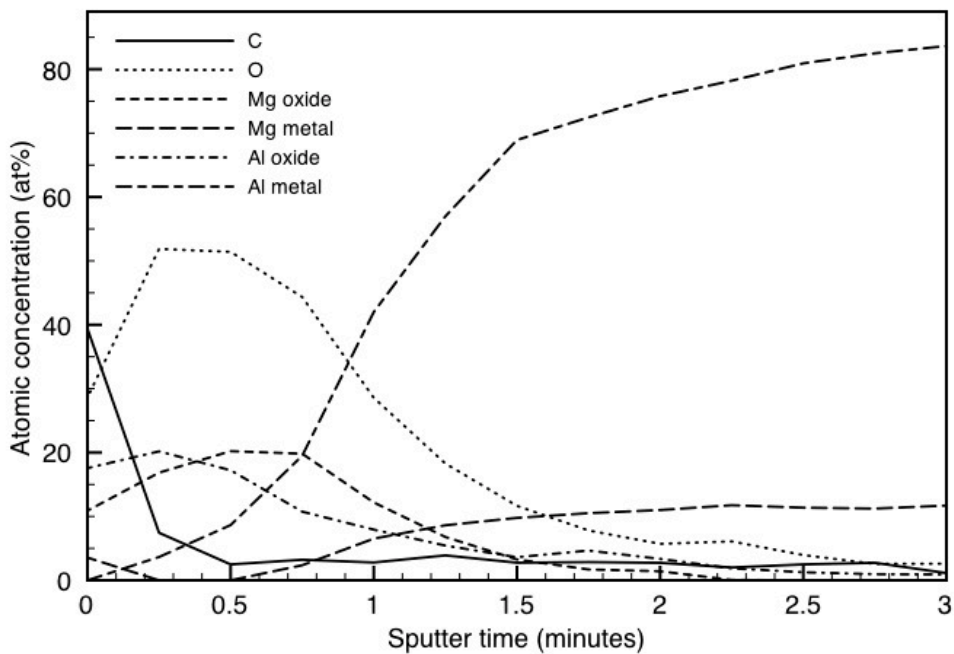


Figure 4.3 c. AA5182 AES depth-profile after 11 days at 200°C.

## 4.3 Discussion

### 4.3.1 AES analysis of chemically pre-treated samples

The thickness of the oxides, except for the alkaline pre-treatment, is in line with results found in previous research<sup>[3, 15, 16]</sup>. After alkaline etching of aluminium, commonly an acid de-smutting treatment is given<sup>[17]</sup>. The only slowly declining oxygen signal in figure 4.3a would indicate the presence of thick overlayer containing oxide species. Looking at the composition of this layer, the magnesium oxide concentration is of a similar level as the aluminium oxide. This can be explained by the fact that magnesium-hydroxides are stable only above  $\text{pH} = 12$ <sup>[18]</sup>. Therefore, during the pre-treating, the aluminium-oxide, which is unstable above  $\text{pH} \sim 8$ , is etched away, leaving the magnesium-(hydr)oxides.

Boiling the samples resulted in a complete lack of magnesium at the surface. This is probably due to the fact that magnesium is completely dissolved environment of boiling water, since the corrosion takes place below  $\text{pH} = 12$  (see Pourbaix diagram chapter 2). The combination of high temperature, bubbling and relatively low  $\text{pH}$  results in the growing of a pseudoboehmite layer, as found extensively in literature<sup>[16]</sup>. This pseudoboehmite layer does not incorporate magnesium.

The acid pre-treatments showed to be another way of removing magnesium from the surface, due to the instability of  $\text{Mg}(\text{OH})_2$  in acid environments, of which the  $\text{HNO}_3$  solution is an extreme example. Since it is usual to combine an acid treatment with an alkaline (first alkaline etching and then de-smutting with an acid solution), in literature it was also found that after acid etching no magnesium remained in AA2024<sup>[2]</sup>.

The concentration of Mg metal (no oxide component could be found) in the dehydroxylated samples is as high as the Al content. This was previously found by Textor et al.<sup>[15]</sup> after similar times and temperatures. The fact that there is no magnesium oxide component found could be due to the relatively quick growth of the layer and the distinct lack of free water molecules at the surface.

There is no Mg oxide signal distinguishable in the boiled and in the dehydroxylated sample. These results are summarized in table 4.2.

**Table 4.2.** Summary of pre-treatments and resulting aluminium and magnesium surface states and concentrations as determined by AES depth-profiling on AA5182 samples.

Pre-treatment	Alka-line	Boiling	Acid	Dehydr-oxylated	RT	100°C	200°C
Aluminium	Al <sub>2</sub> O <sub>3</sub>	Al-O*	Al <sub>2</sub> O <sub>3</sub>	Metallic at surface**	Al <sub>2</sub> O <sub>3</sub>	Al <sub>2</sub> O <sub>3</sub>	Al <sub>2</sub> O <sub>3</sub>
Magnesium	MgOH <sub>2</sub>	solid state**	solid state**	Metallic at surface**	solid state**	MgOH <sub>2</sub>	MgOH <sub>2</sub>
[Mg(OH) <sub>2</sub> ]: [Al <sub>2</sub> O <sub>3</sub> ]	3:2	n/a	n/a	n/a	n/a	1:2	1:1

\* Pseudoboehmite

\*\* oxides not distinguishable

A distinction between magnesium oxide and hydroxide could in principle be made with either the magnesium Mg 2p signal or the O 1s signal. The intensity of the magnesium signal, however, was too low to be able to confidently separate into oxide or hydroxide components. The intensity of the oxygen signal was dominated by the aluminium oxides, which complicated the deconvolution of that peak into both aluminium and magnesium oxides and hydroxides impossible. Furthermore, for a proper AES concentration profile, a series of calibration specimens would have had to been prepared, their composition determined by another analytical technique, e.g. XRF or SIMS. We assume however, that when magnesium oxides reach the surface, due to the high reactivity, MgO will be reacted with water from the air to Mg(OH)<sub>2</sub> or more complicated hydroxy-carbonate species<sup>[11]</sup>.

#### 4.3.2 AES analysis of heat pre-treated samples

The thickness of the oxides determined in this study is in reasonable agreement with Lea and Molinari<sup>[9]</sup>, who also found relatively small oxide thicknesses at temperatures lower than 300°C, although after only 1 hour heat-treatment.

Furthermore the oxygen peaks show a maximum at less than 0.5 minutes. At the surface the carbon peaks also show their maximum, which could indicate some carbon incorporated into MgCO<sub>3</sub>, although this cannot be elucidated by the present

measurements. However, magnesium shows the highest concentration at the surface, while the Al signal increase less rapidly. This suggests that the outer surface is rich in Mg and O species, be it  $\text{Mg}(\text{OH})_2$  or  $\text{MgCO}_3$ , which is consistent with literature<sup>[10, 11]</sup>.

Both room temperature samples as well as the samples heat-treated at 100°C show a bulk composition of magnesium around 5 wt%, which is in accordance with the composition determined for this alloy. The sample aged at 200°C however, shows for the first few nanometers a higher concentration of about 10 wt% magnesium. This could be due to diffusion to the surface from the bulk at a higher rate, or the formation of higher extent of precipitates at the surface, since solid solubility of magnesium in aluminium is around 5 wt%.

At the surface, all oxides are enriched in magnesium from non-detectable magnesium oxide at room temperature to 1:2 Mg:Al after heat-treating at 100°C to 1:1 ratio for 200°C. These results are graphically shown in figure 4.4 and are summarized in table 4.2 as well.



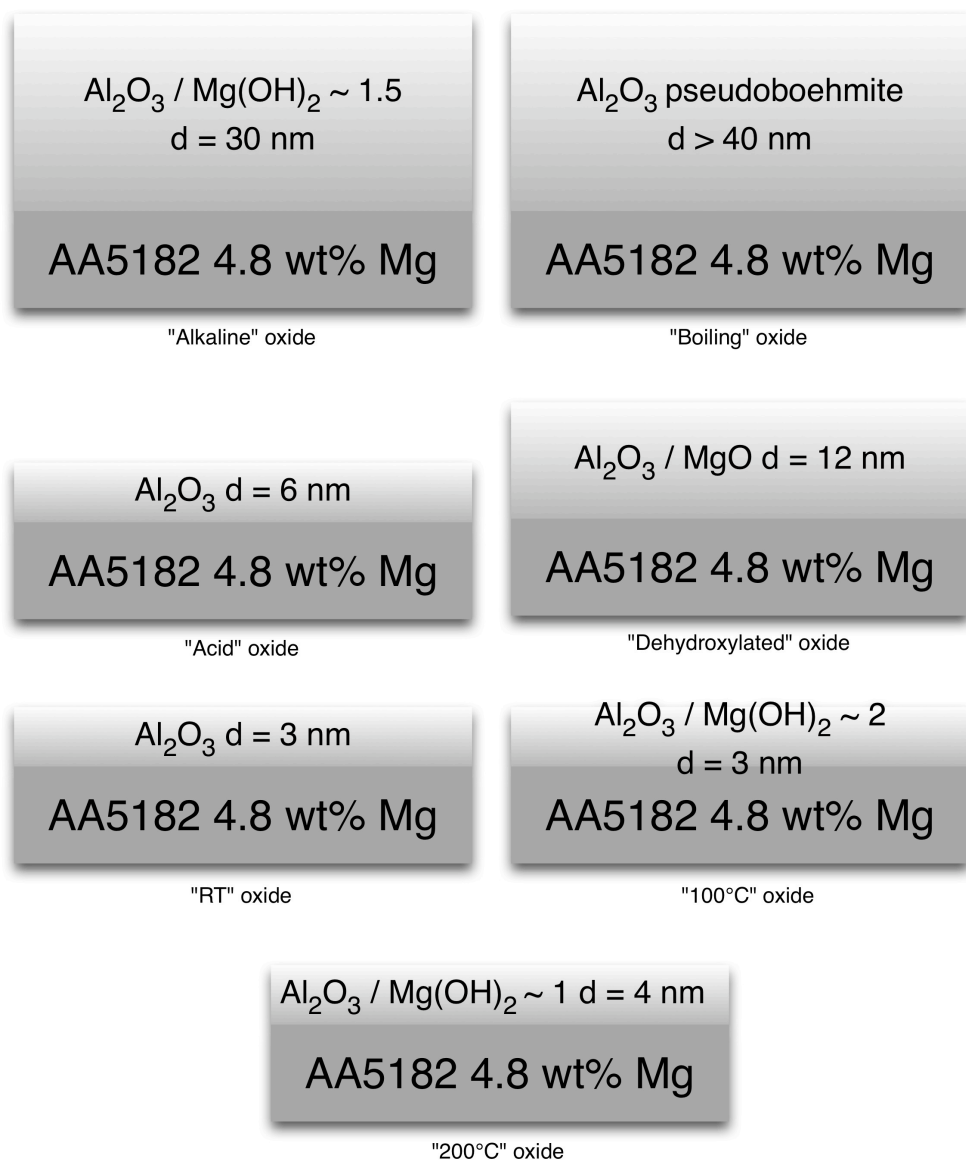


**Figure 4.4** Graphical overview of composition after pre-treatments.

#### 4.4 Conclusions

The concentration of magnesium in the oxide surface of aluminium-magnesium alloy AA5182 can be changed by different pre-treatments. As already reported in literature, both heat pre-treatments as well as chemical pre-treatments change the composition of oxides of aluminium alloys. For AA5182, heat pre-treatments,

especially if carried out for long times, increase the concentration of magnesium at the surface most at elevated temperatures. After 11 days at 200°C, the ratio Mg:Al reaches 1:1 at the surface. The AES results show that the oxide film composition can vary considerably with temperature treatment. Although at the outer surface of the alloy there is still Al<sub>2</sub>O<sub>3</sub> present, but in the 4 nm thick oxide, magnesium is dominantly present. After the 200°C treatment, magnesium (hydro)oxide is present almost exclusively, probably in the form of Mg(OH)<sub>2</sub> due to reaction with the atmospheric water.

Chemical pre-treatments also alter the surface, by favorably removing either aluminium or magnesium. Alkaline pre-treatment enriches the surface considerably in magnesium (hydr)oxide, higher than the level of aluminium oxide. However, this is probably present in a thick smut. Boiling completely removes the magnesium and leaves a thick pseudoboehmite layer. Acid pre-treatment mostly removes the magnesium, resulting in a thin Al<sub>2</sub>O<sub>3</sub> oxide. And finally, dehydroxylating results in the forming of a magnesium metal surface, where neither magnesium nor aluminium oxides are present.

### **Acknowledgments**

Many thanks go to Tom Hauffmann and Oscar Steenhaut for performing the AES measurements at VUB, Belgium.

**References**

- [1] T. S. Sun, J. M. Chen, J. D. Venables, R. Hopping, *Applied Surface Science* **1978**, *1*, 202.
- [2] C. E. Moffitt, D. M. Wieliczka, H. K. Yasuda, *Surface & Coatings Technology* **2001**, *137*, 188.
- [3] S. Feliu, M. J. Bartolome, *Surface and Interface Analysis* **2007**, *39*, 304.
- [4] G. E. Thompson, P. Skeldon, X. Zhou, K. Shimizu, H. Habazaki, C. F. E. Smith, *Aircraft Engineering and Aerospace Technology* **2003**, *75*, 372.
- [5] W. Wen, Y. M. Zhao, J. G. Morris, *Materials Science and Engineering a-Structural Materials Properties Microstructure and Processing* **2005**, *392*, 136.
- [6] S. Scotto-Sheriff, E. Darque-Ceretti, G. Plassart, M. Aucouturier, *Journal of Materials Science* **1999**, *34*, 5081.
- [7] A. J. Kinloch, H. E. Bishop, N. R. Smart, *Journal of Adhesion* **1982**, *14*, 105.
- [8] G. R. Wakefield, R. M. Sharp, *Applied Surface Science* **1991**, *51*, 95.
- [9] C. Lea, C. Molinari, *Journal of Materials Science* **1984**, *19*, 2336.
- [10] D. B. Blucher, J. E. Svensson, L. G. Johansson, M. Rohwerder, M. Stratmann, *Journal of the Electrochemical Society* **2004**, *151*, B621.
- [11] C. Fotea, J. Callaway, M. R. Alexander, *Surface and Interface Analysis* **2006**, *38*, 1363.
- [12] P. Electronics, *Operator's Multipak Software Manual — Version 6.0*, Chanhassen, MN, **1998**.
- [13] I. Vandendael, O. Steenhaut, A. Hubin, J. Vereecken, P. Prince, F. Reniers, T. Segato, *Surface and Interface Analysis* **2004**, *36*, 1093.
- [14] J. Delaet, K. Deboecik, H. Terryn, J. Vereecken, *Surface and Interface Analysis* **1994**, *22*, 175.
- [15] M. Textor, R. Grauer, *Corrosion Science* **1983**, *23*, 41.
- [16] M. R. Alexander, G. E. Thompson, G. Beamson, *Surface and Interface Analysis* **2000**, *29*, 468.
- [17] Y. Liu, F. Colin, P. Skeldon, G. E. Thompson, X. Zhou, H. Habazaki, K. Shimizu, *Corrosion Science* **2003**, *45*, 1539.
- [18] M. Pourbaix, *Atlas of Electrochemical Equilibria in Aqueous Solutions* **1966**, Pergamon Press, Oxford.

**Chapter 5 - Electrochemical behavior of  
pre-treated aluminium and aluminium-  
magnesium alloy in neutral and acidified  
saline environments**

## Synopsis

Oxide - polymer interactions are important for adhesion of coatings. The composition of oxides on metal surfaces is then one of the parameters which influences the total system. In this chapter the determination of the composition of oxides through the related iso-electric point of the surface (IEPS) of several pre-treated aluminium alloys is reported. A faster way than using contact angle measurements, as described in literature, is explored. The composition of the oxides on the used alloys was already experimentally determined by AES as reported earlier in chapter 4. This data is used as a reference for the composition of the oxides present at the surface. Electrochemical measurements, more specifically open circuit potential (OCP), were chosen because these are relatively simple and can be conducted fairly fast and at low cost. The electrochemical behavior of previously described pre-treated aluminium alloy AA5182 and AA1050 surfaces exposed to a neutral conducting and to an acidified saline aqueous solution was studied. The relevant literature that described the relation between flat-band potentials,  $E_{FB}$ , band gaps,  $E_g$  and the iso-electric point of the surface, IEPS, is discussed. Experimentally found open circuit potentials in saline and acidified solution, are then compared to literature. The IEPS of the samples was subsequently calculated from these OCP values, taking into account the composition determined by AES.

## 5.1 Introduction and background

Surfaces of aluminium alloys can be characterized in many ways, as was discussed in chapter 2.

Local techniques like SKPFM, SVET and droplet cell techniques have become available and are used extensively to study the electrochemical behavior of precipitates and other impurities in the matrix locally, both on aluminium alloys and recently also on steels. These techniques only work well on bare metals, exposed to the environment, where in practice mostly coated metals are used. Before coating, it is of crucial importance to evaluate both composition as well as cleanliness of a surface, as many coatings show decreased adhesion on contaminated surfaces. There is evidence that if oxides and polymers can be tailored to “fit” together before application, much higher durability can be achieved<sup>[1]</sup>.

While local phenomena may also determine coating adhesion on longer time scales (e.g. in filiform corrosion), as will be discussed in chapter 8, the average electrochemical behavior might nevertheless provide a fast way to determine the bonding capabilities of a macroscopic coating by comparison of the IEPS of the substrate with the (known) coatings' pH/pK<sub>a</sub>.

Unfortunately, limited methods are available to determine the iso-electric point of a surface (IEPS). An effective way for several metallic surfaces reported in literature was a method used by McCafferty and co-workers<sup>[2]</sup>. This method requires the immediate measurement of contact angles of several metallic surfaces after cleaning by plasma. A range of aqueous solutions with increasing pH value under an organic solvent was evaluated; the point where a deviation from the otherwise straight slope of surface energy versus pH was detected, was identified as the IEPS. These were close to stability lines in the Pourbaix diagrams<sup>[3]</sup> for solution of the oxides (e.g. pH = 9 for aluminium), which was actually not reported in their publications. Since this method is labor-intensive, in this chapter an easier way to determine the IEPS of the previously used surfaces is explored based on open circuit potential (OCP) measurements.

The relation between  $E_{\text{pit}}$  and IEPS first has to be established, which was done in literature before<sup>[4-6]</sup>.  $E_{\text{pit}}$  is defined by McCafferty<sup>[2]</sup> as “any small value of  $i_a$  above the background value for the passive film current ( $i_a = i_{\text{crit}}$ ) to consistently mark the start of pitting. Thus, when  $i_a = i_{\text{crit}}$ ,  $E = E_{\text{pit}}$ , the critical pitting potential. The value of  $E_{\text{pit}}$  can be determined by several electrochemical (of which anodic polarization is the most common) and analytical methods, which are discussed extensively by Szklarska-Smialowska<sup>[7]</sup>.

The open circuit potential (OCP) is defined more generally as “the corrosion potential ( $E_{\text{corr}}$ ) in the absence of an externally applied potential”<sup>[8]</sup>. It is argued here that  $E_{\text{pit}}$  can be determined by OCP measurement for the materials where an aqueous electrolyte is used which contains NaCl and  $E_{\text{corr}}$  is measured; essentially  $E_{\text{corr}} = E_{\text{pit}}$ . Several authors have shown, e.g. Afseth et al.<sup>[9]</sup>, that local phenomena related to precipitates in aluminium alloys do in fact largely determine the behavior of active surfaces in OCP measurements.

It is expected that after a chemical surface pre-treatment OCP changes because of preferential etching. This would still lead to an average surface IEPS, as was already theoretically explored in the 1960s<sup>[10]</sup>.

As mentioned before, IEPS, also referred to as point of zero charge (PZC)<sup>[10]</sup>, can be expressed by a pH on the surface. In previous work, Flores<sup>[5]</sup> has derived, using the data, definitions and equations by Bockris<sup>[11]</sup>, McCafferty<sup>[12]</sup> and Butler<sup>[13]</sup> on electronegativity, electron affinity,  $E_g$  and IEPS, an equation which relates  $E_{\text{pit}}$  (V vs. NHE) ) with IEPS and  $E_g$  via equation 5.1:

$$E_{\text{pit}} = 4.683 - 0.236 \text{ pH}_{\text{PZC}}(\text{oxide}) - 1.122 E_g \quad (5.1)$$

The  $\text{pH}_{\text{PZC}}$  of a complex oxide has been reported to be approximately the weighted average of its components<sup>[4]</sup>. For a mixed oxide layer the  $\text{pH}_{\text{PZC}} = \text{IEPS}$  is calculated with equation 5.2:

$$\text{pH}_{\text{PZC}}(\text{alloy}) = f_{\text{MgO}} \cdot \text{pH}_{\text{PZC}}(\text{MgO}) + (1 - f_{\text{MgO}}) \cdot \text{pH}_{\text{PZC}}(\text{Al}_2\text{O}_3) \quad (5.2)$$

Equation 5.2 can of course be extended if more than 2 species are present.

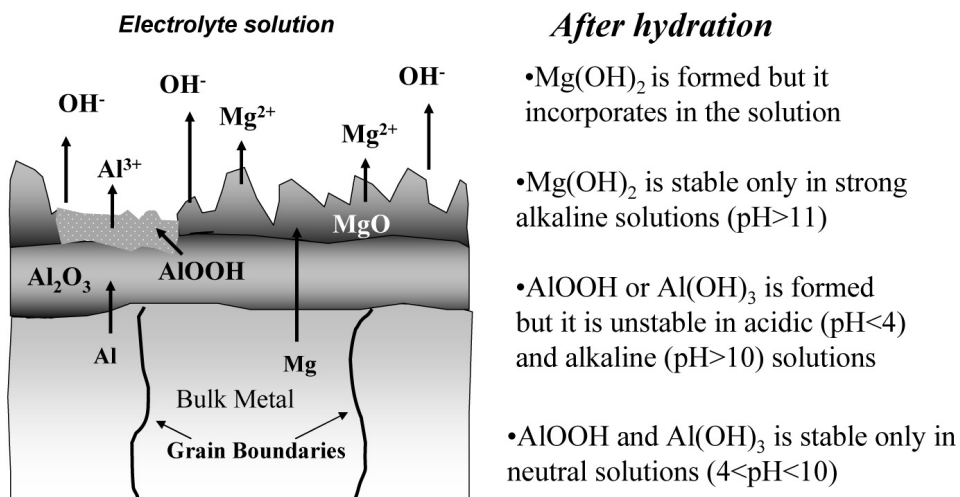


**Figure 5.1.** Surface dissolution of the enriched oxide layer in Al-Mg alloys, Flores<sup>[5]</sup>, page 59.

For the specific systems studied here, in figure 5.1, a model was proposed earlier by Flores<sup>[5]</sup> of the dissolution of a Al-Mg alloy surface. As can be seen, there are several variations of magnesium and aluminium (hydr)oxides. The omission in this model is that the presence of  $\text{Mg}(\text{OH})_2$  is not taken into account and neither was  $\text{MgCO}_3$ . The latter was shown before to exist in non-deaerated electrolytes on magnesium alloys. Blücher and coworkers<sup>[14]</sup> have shown that the corrosion of magnesium-aluminium alloys is dependent on the  $\text{CO}_2$  concentrations in the solutions.

Using the information just described on surface composition, the  $E_{\text{pit}}$  was calculated with formula 1. The results of these calculations are given in table 5.1. In this table the first column contains the oxide surface species. The  $\text{pH}_{\text{PZC}}$ , the pH at the point of zero charge (PZC) and  $E_g$  are given as obtained from the mentioned references in literature. An important assumption is that for all samples some  $\text{Al}_2\text{O}_3$  is present at the surface. Therefore, for all calculations the  $E_g$  of  $\text{Al}_2\text{O}_3$  was used because this is the species with the lowest bandgap, which is responsible for the conduction of electrons. The  $\text{pH}_{\text{PZC}}$  according to equation 2 is not sensitive to variations of low amounts of  $\text{Al}_2\text{O}_3$ , which are assumed to be sufficient for a conductive surface. As an example, 5%  $\text{Al}_2\text{O}_3$  would result for  $\text{Mg}(\text{OH})_2$  in a  $\text{pH}_{\text{PZC}}$  of 11.85 instead of 12, the value given in the table.



**Table 5.1** Overview of expected  $E_{\text{pit}}$  potentials on a mixed Al/Mg oxide as can be supposed on AA5182, calculated by equations (5.1) and (5.2).

Species	pH <sub>PZC</sub>	$E_g$	References	Calculated $E_{\text{pit}}$ (V vs. SCE)
$\alpha\text{-Al}_2\text{O}_3$	~ 9	2.9 eV	[10]	-0.94
$\alpha/\delta\text{-AlOOH}$ (boehmite)	~ 8	~ 6 eV*	[10, 18, 19]	-0.70
$\text{MgCO}_3$	~ 8.7	5.0 eV* (DFT) 6.0 eV* (experimental)	[20, 21]	-0.87
$\text{Mg}(\text{OH})_2$	~ 12	5.7 eV*	[10]	-1.65
$\text{MgO}^{**}$	12.4	7.7 eV*	[10]	-1.74

\*  $E_g = 2.9$  eV used for calculation of  $E_{\text{pit}}$  because of presence of aluminium oxide

\*\*unlikely to exist in an oxygen containing aqueous solution, referring to Pourbaix diagram of magnesium and [14].

In the experimental part of this chapter OCP data is shown that will be compared to the calculated  $E_{\text{pit}}$  (table 5.1). Flores<sup>[5]</sup> did similar measurements with two alloys which are similar to the ones used in this chapter, as given in figure 5.2. Please note that the solution used is acidified and contains NaCl. From this figure it can be seen that the potential of a nearly pure aluminium (AA1050) drops to a stable value of around -0.9 V vs. SCE after 17 hours. The non-sensitized AA5083 shows different initial behavior, but a slightly lower end value. Both lines for the sensitized samples (100°C and 200°C) have a similar shape but reach a slightly lower OCP value after 24 hours immersion, around -0.95 V vs. SCE. This behavior is explained in figure 5.1, where Flores<sup>[5]</sup> proposed a model for the dissolution of magnesium and aluminium from the aluminium-magnesium alloy. In our evaluation of the experimental data we will incorporate the possible presence of hydroxy-carbonates.

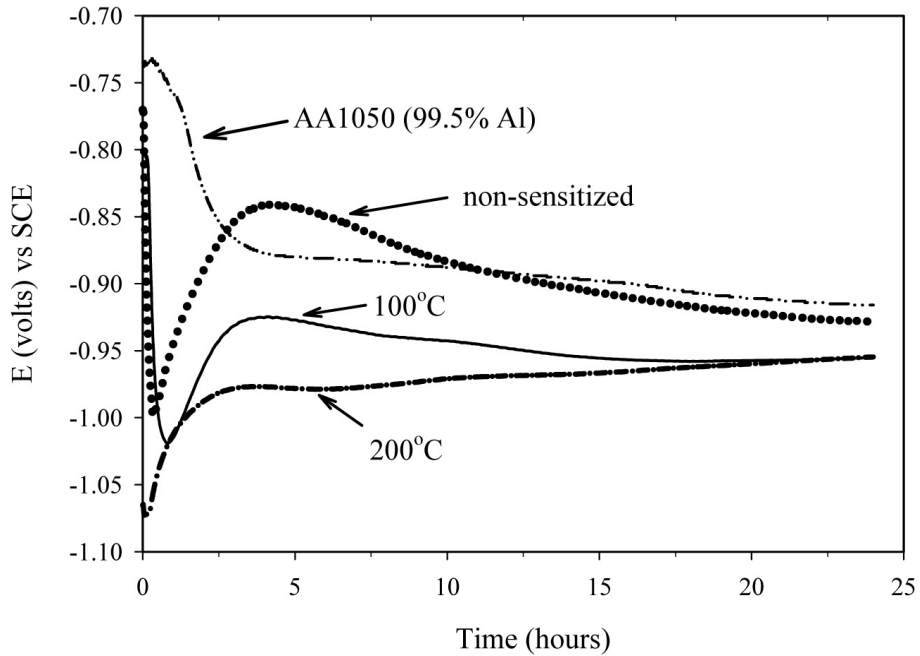


**Figure 5.2** Electrochemical open circuit potential (OCP) curves of AA5083 (4.5 wt% Mg) (in non-sensitized and sensitized conditions) and AA1050 immersed in 0.6 M NaCl pH = 3 electrolyte solution, Flores<sup>[5]</sup>, page 51).

Next to an aqueous, acidified (pH = 3), 0.6M NaCl solution as was used by Flores<sup>[5]</sup>, a neutral solution was also used for the experiments in this chapter, with 0.1M K<sub>2</sub>SO<sub>4</sub> added for conductivity. Please refer to chapter 3 for further experimental details. This neutral electrolyte will only result in dissolution of the oxide if these are intrinsically unstable. This would only be the case for surfaces which consist of Mg(OH)<sub>2</sub>, as expected from the Pourbaix diagram<sup>[3]</sup>.

## 5.2 Results

Figure 5.3 shows examples of typical results of OCP measurements. From this figure can be seen that initially, all samples have an OCP ranging from -0.6 V to -0.8 V vs. SCE. The potentials then reach their final states over the course of one to two days.

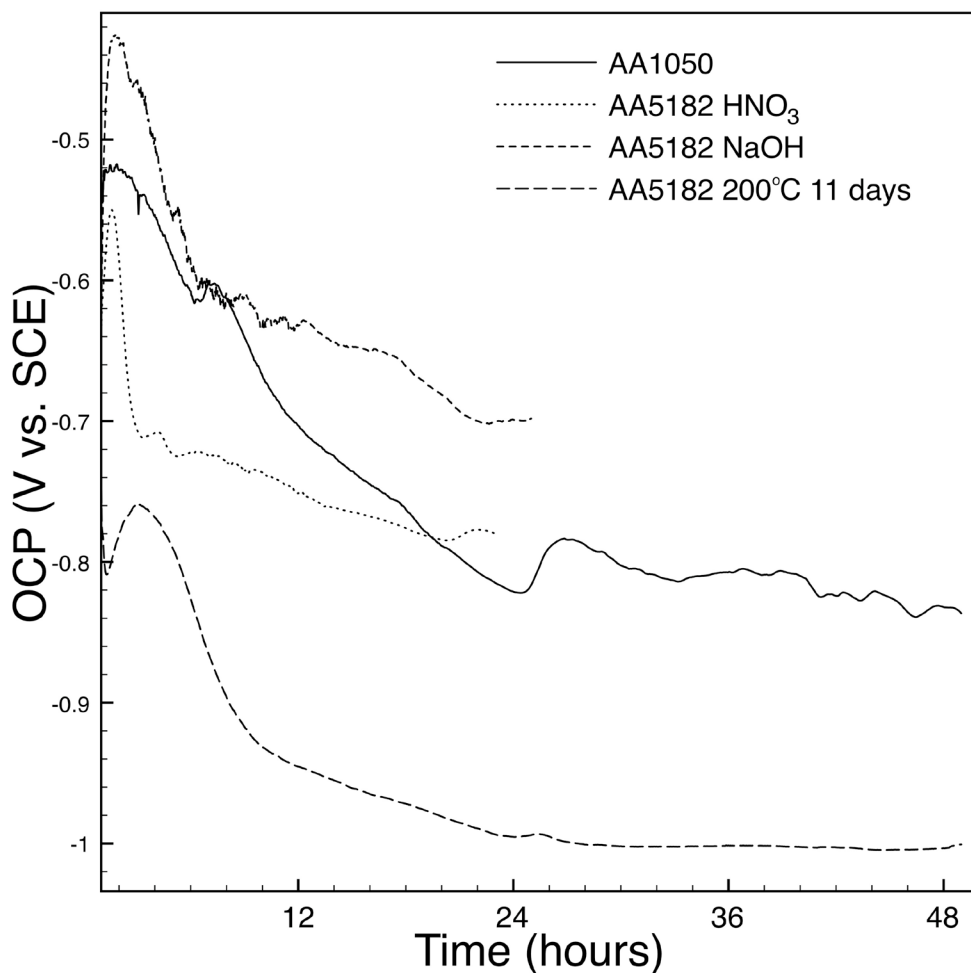


**Figure 5.3** OCP in V vs. SCE for several samples measured in aqueous solution of 0.1M  $K_2SO_4$ .

The aluminium oxide surface of AA1050 shows a declining slope towards -0.8 V vs. SCE. This behavior is similar for the  $HNO_3$  pretreated AA5182. The alkaline pretreated AA5182 however starts at a similar value, but stays approximately 100 mV vs. SCE higher in this solution. Finally, AA5182 aged at 200°C for 11 days resulting in a surface enriched in magnesium, shows a lower starting value of OCP and a 300-400 mV vs. SCE lower end value.

Table 5.2 contains the results of typical OCP measurements in 0.1M  $K_2SO_4$  aqueous solution. Also this data from the AES results from chapter 4 are added. The presence of magnesium at the surface (enriched oxide layer) and the oxide thickness are given using the AES results. Furthermore the  $pH_{PZC}$  is calculated using equation 5.2.

**Table 5.2** Substrate/pretreatment, equilibrated OCP and IEPS in 0.1M K<sub>2</sub>SO<sub>4</sub> aqueous solution, all samples after 550 grit grinding.

Substrate/ pretreatment	Initial OCP (V vs. SCE)	Eq. OCP (V vs. SCE)	Original Mg/Al (AES) concentration	Original oxide thickness (nm, AES)	pH <sub>PZC</sub> calculated with eq. 5.2
AA1050	-0.54	-0.82	0	2*	9
AA5182 HNO <sub>3</sub>	-0.58	-0.78	0	6	9
AA5182 NaOH	-0.60	-0.70	1.2	30	10
AA5182 11 days 200°C	-0.74	-1.0	1	4	10.5

\*estimated

Table 5.3 shows the results of OCP measurements for the given samples with the same pretreatments as in table 5.2, but now exposed to acidified saline solution. The number in brackets is the grit size of the grinding paper used before the chemical pretreatments.

AA1050 starts at a higher potential than in the K<sub>2</sub>SO<sub>4</sub> solution: the OCP (-0.73 V) is higher and settles around -0.8 V vs. SCE. This is explained by the fact that there are very few precipitates in the AA1050 and therefore there is not much active surface where pitting can start even in this acidic, chloride containing electrolyte.

The AA5182 HNO<sub>3</sub> pretreated samples start at the same potential as in K<sub>2</sub>SO<sub>4</sub> but finally reach a lower potential (-1.06 V vs. -0.78 V). The AA5182 NaOH pretreated samples start at a slightly lower potential (-0.74 V) and finally end at the same potential as the acid pretreated and much lower again than in K<sub>2</sub>SO<sub>4</sub> solution (-0.70V). The at 200°C aged AA5182 samples behave exactly the same as in K<sub>2</sub>SO<sub>4</sub>. Extra samples of AA5182 were pretreated in boiling water and showed the same initial and final OCP values as AA1050. For comparison, non-pretreated AA5182 samples were introduced in the table, which had comparable values as for the acid and alkaline pretreated samples.

**Table 5.3** Results of OCP measurements in 0.6 M NaCl aqueous solution acidified to pH = 3 by HCl initial and final combined with previous AES results

Substrate/ pretreatment (grit #)	Initial OCP (V vs. SCE)	Final OCP (V vs. SCE)	Original Mg/Al (AES) concentration	Original oxide thickness (nm, AES)
AA1050 (550)	-0.73	-0.81	0	2*
AA5182 HNO <sub>3</sub> (800)	-0.58	-1.06	0	6
AA5182 NaOH (550)	-0.74	-1.01	1.2	30
AA5182 11 days 200°C (550)	-0.74	-0.99	1	4
AA5182 boiling water	-0.75	-0.82	0	>40
AA5182 none (800)	-0.76	-1.05	0.05	3*
AA5182 NaOH (800)	-0.76	-0.99	1.2	30

\*estimated based on the AES measurements

In table 5.4, the final OCP values from table 5.3 are taken as “virtual”  $E_{pit}$ . Using equation (1) and (2), the IEPS value was calculated using various values for the surface composition to achieve the right  $E_{pit}$  value. This resulted in the given surface composition in table 5.4..

**Table 5.4** Calculated  $E_{pit}$  from equation 5.1, based on tentative composition to match OCP values from table 5.3

Substrate/ pretreatment (grit #)	Original Mg/Al (AES) concentration	Assumed composition from eq. 5.2	IEPS calculated from eq. 5.2	“Virtual” $E_{pit}$ (V vs. SCE) Calc. with 5.1
AA1050 (550)	0	45% $Al_2O_3$ 55% $AlOOH$	8.5	-0.81
AA5182 $HNO_3$ (800)	0	83% $Al_2O_3$ 17% $Mg(OH)_2$	9.5	-1.06
AA5182 NaOH (550)	1.2	45% $Al_2O_3$ 14% $Mg(OH)_2$ 41% $MgCO_3$	9.3	-1.01
AA5182 11 days 200°C (550)	1	50% $Al_2O_3$ 11% $Mg(OH)_2$ 39% $MgCO_3$	9.2	-0.99
AA5182 boiling water	0	45% $Al_2O_3$ 55% $AlOOH$	8.5	-0.82
AA5182 none (800)	0.05	85% $Al_2O_3$ 15% $Mg(OH)_2$	9.5	-1.05
AA5182 NaOH (800)	1.2	45% $Al_2O_3$ 12% $Mg(OH)_2$ 43% $MgCO_3$	9.2	-0.99

### 5.3 Discussion

All OCP measurements are macroscopical averages of the electrochemical processes on various phases at the surface. Therefore it can be expected that the found potentials are mixed potentials, resulting from a complex combined action of different oxides on the surface. It is furthermore assumed that grinding the samples has removed sufficient material from the contaminated layer of oxides produced at rolling. These surface layers were shown to have a thickness of less than 1  $\mu m$  previously by Premendra et al.<sup>[16]</sup>.

From table 5.2, which summarizes OCP measurements in neutral  $K_2SO_4$  solutions, it can be seen that the OCP for the acid pretreated AA5182 eventually approaches the one for AA1050, of which the surface consists of aluminium oxides fully. This is in line with previous AES measurements, where also the thickness of the oxides was found to be in a similar range. The alkaline pretreated samples however eventually have a slightly higher potential. Although AES measurements have shown that there is a strong presence of magnesium, the higher potential might be explained by the significantly thicker oxide layer, which forms a barrier and consists of insoluble species in aqueous environments from the alkaline etching step. It is a well-established fact that these steps leave an insoluble “smut” layer. Because of the short time (30 seconds) of the pre-treatment however, the thickness is still low (tens of nm), but is thick enough to influence the OCP to more passive values in this non-aggressive solution. This can be compared to boehmite surfaces which have a predicted higher OCP also (-0.70 V vs. SCE, table 5.1). Finally, the AA5182 sample of which the surface was enriched in magnesium (11 days at 200°C), shows a significantly lower OCP, indicating the presence of magnesium hydroxides (table 5.1). Also, the original thickness of the oxide as measured with AES was comparable to the acid pretreated sample. This was studied before<sup>[17]</sup>, where it was found that the presence of small amounts of Mg does not appear to significantly change the thickness of layers that form in the saline solution under open circuit conditions.

In table 5.3, the results of OCP measurements in acidified saline solution are shown. Only the AA5182 sample that was given a boiling water pretreatment shows a similar final potential, i.e. - 0.8 V vs. SCE, as the AA1050. This is to be expected, since the pseudoboehmite layer that results from this pretreatment is a relatively thick layer of  $AlOOH/Al_2O_3$ . The other final OCP values are found to be around -1.0 V vs. SCE. From literature it is known that in air-formed oxides pitting potential increases when  $pH_{PZC}$  decreases<sup>[4]</sup>, see table 5.1 and equation 5.1. However, the experimentally determined  $E_{pit}$  depend in a complex way on the surface composition of the used alloys. That is why, based on the measured OCP values, a calculation was made using equations 5.1 and 5.2 to determine the composition of the oxide layers present after the timeframe of 24 hours. The calculations were described under Results and the final composition is given in table 5.4.

For pure aluminium AA1050, the IEPS ( $pH = 8.5$ ) as calculated from the measured OCP is lower than the standard  $Al_2O_3$  IEPS ( $pH = 9$ ). Calculation showed that this can be explained by the presence of  $AlOOH$  (%55%), which is not unreasonable. For the acid pretreated AA5182, the OCP can only be explained by the presence of

Mg(OH)<sub>2</sub>, which seems to be in contrast to the AES results. However since these were taken before the exposition, it is very probable that due to corrosion, a part of the Al<sub>2</sub>O<sub>3</sub> oxides has dissolved, allowing for the presence of magnesium at the surface eventually.

Both alkaline pretreated AA5182 samples show a mixed presence of both magnesium hydroxides, carbonates and aluminium oxide. As AES measurements still showed an elemental magnesium enrichment of more than 50%, the presence of MgCO<sub>3</sub> is probable; if only magnesium hydroxides would have been present, OCP values would have been much lower (since Mg(OH)<sub>2</sub> has an E<sub>pit</sub> of - 1.65V). This consideration was also taken account for the AA5182 magnesium enriched surface (200°C, 11 days). Boiling water leads to an aluminium oxide/hydroxide surface, with a conforming high OCP (- 0.82V). No pretreatment resulted in a lower OCP (- 1.05V), comparable to that of the acid pretreated sample. This is in accordance with the fact that the acid pretreatment would be too short to dissolve any more aluminium than would be present naturally on the bulk material.

## 5.4 Conclusions

Open circuit potential (OCP) measurements were used to determine the IEPS of various pretreated surfaces of AA1050 and AA5182. First, the relation between E<sub>pit</sub> and IEPS and was established from revisiting the literature. Working under the assumption that in a chloride containing electrolyte, E<sub>corr</sub> as determined in OCP measurements equals E<sub>pit</sub>, results of OCP measurements on several pre-treated substrates were discussed. Determining initial and final OCP after 24/48 hours in K<sub>2</sub>SO<sub>4</sub> electrolyte showed the presence of Mg (enrichment) in AA5182 samples by lower OCP values as predicted by theory.

A clear relation between measured final OCP values (E<sub>corr</sub> = E<sub>pit</sub>) and IEPS however was established in acidified chloride containing electrolytes. Calculations using AES information on initial surface elemental concentrations (chapter 4), based on E<sub>pit</sub> resulted in reasonable oxide compositions. The presence of Mg(OH)<sub>2</sub> and MgCO<sub>3</sub> was quantified for all pretreated samples, in good agreement with the tentative presence of these species as discussed in chapter 4.

Prediction of E<sub>pit</sub> from E<sub>g</sub> and IEPS or pH<sub>pzc</sub> was shown to be possible only if one does take into account the mixed nature of the oxides and carbonates on the surface based on preexisting knowledge from other sources. When this however is taken into account fast and simple OCP measurements, can show to some extent quantitatively the composition of mixed Al/Mg surfaces.



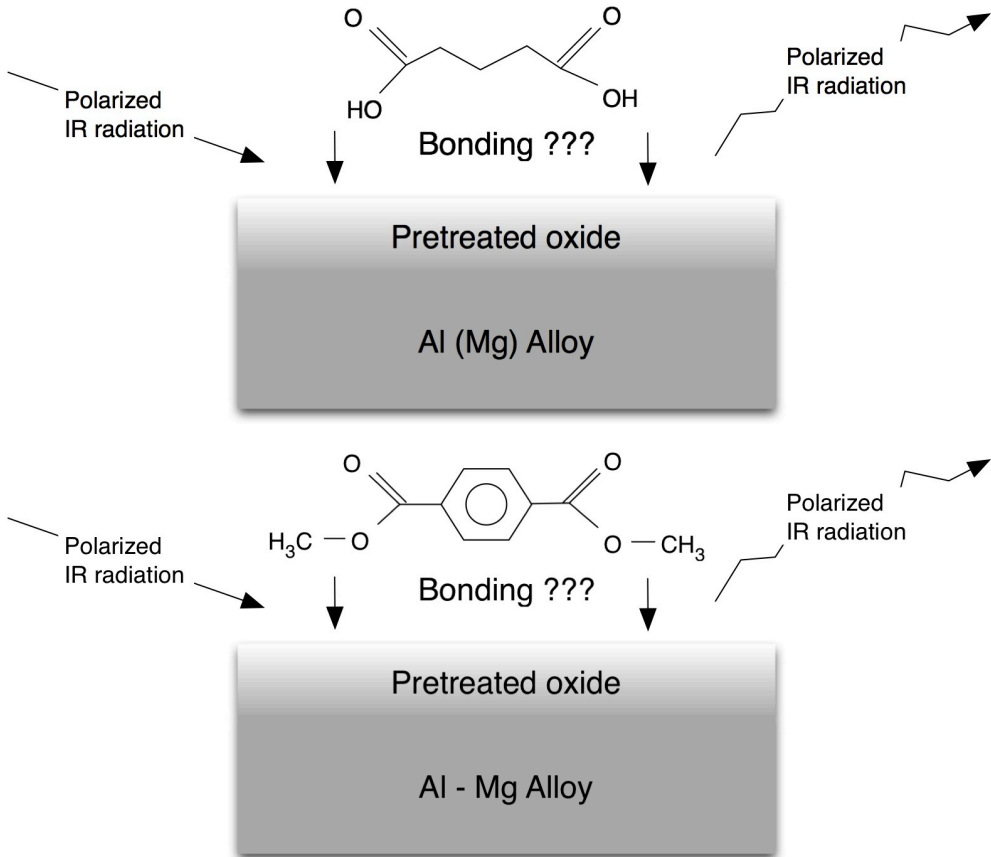
**References**

- [1] R. Hausbrand, M. Stratmann, M. Rohwerder, *Journal of the Electrochemical Society* **2008**, *155*, C369.
- [2] E. McCafferty, J.P. Wightman, *Journal of Adhesion Science and Technology* **1999**, *13*, 1415.
- [3] M. Pourbaix, *Atlas of Electrochemical Equilibria in Aqueous Solutions* **1966**, Pergamon Press, Oxford.
- [4] P.M. Natishan, E. Mccafferty, G.K. Hubler, *Journal of the Electrochemical Society* **1988**, *135*, 321.
- [5] J.R. Flores, The role of magnesium in the electrochemical behaviour of 5XXX aluminium-magnesium alloys, Delft University of Technology (Delft), **2006**.
- [6] M. Casamassima, E. Darqueceretti, A. Etcheberry, M. Aucouturier, *Applied Surface Science* **1991**, *52*, 205.
- [7] Z. Szklarska-Smialowska, *Pitting and Crevice Corrosion*, NACE International, Houston, **2005**.
- [8] N. Perez, *Electrochemistry and corrosion science*, Kluwer Academic Publishers, NewYork, **2004**.
- [9] A. Afseth, J.H. Nordlien, G.M. Scamans, K. Nisancioglu, *Corrosion Science* **2001**, *43*, 2359.
- [10] G.A. Parks, *Chemical Reviews* **1965**, *65*, 177.
- [11] J.O. Bockris, Y.K. Kang, *Journal of Solid State Electrochemistry* **1997**, *1*, 17.
- [12] E. McCafferty, J.P. Wightman, *Journal of Colloid and Interface Science* **1997**, *194*, 344.
- [13] M.A. Butler, D.S. Ginley, *Journal of the Electrochemical Society* **1978**, *125*, 228.
- [14] D.B. Blücher, J.E. Svensson, L.G. Johansson, M. Rohwerder, M. Stratmann, *Journal of the Electrochemical Society* **2004**, *151*, B621.
- [15] G. Song, A. Atrens, D. Stjohm, J. Nairn, Y. Li, *Corrosion Science* **1997**, *39*, 855.
- [16] Premendra, B.S. Tanem, J.M.C. Mol, H. Terry, J.H.W. de Wit, L. Katgerman, *Surface and Interface Analysis* **2008**, *40*, 1157.
- [17] D.R. Baer, C.F. Windisch, M.H. Engelhard, M.J. Danielson, R.H. Jones, J.S. Vetrano, *Journal of Vacuum Science & Technology a-Vacuum Surfaces and Films* **2000**, *18*, 131.

- [18] Z.Q. Yu, C.X. Wang, X.T. Gu, C. Li, *Journal of Luminescence* **2004**, *106*, 153.
- [19] S. Li, R. Ahuja, B. Johansson, *Solid State Communications* **2006**, *137*, 101.
- [20] O.S. Pokrovsky, J. Schott, F. Thomas, *Geochimica Et Cosmochimica Acta* **1999**, *63*, 863.
- [21] F.M. Hossain, B.Z. Dlugogorski, E.M. Kennedy, I.V. Belova, G.E. Murch, *Solid State Communications* **2010**, *150*, 848.



# Chapter 6 - Bonding of succinic acid and di-methyl terephthalate



This chapter is based on (parts of) “The influence of Chemical Pretreatment and Magnesium Surface Enrichment on Bonding of Succinic Acid Molecules to aluminium alloy” by F.M. de Wit, J.M.C. Mol, H. Terryn and J.H.W. de Wit, published in *Journal of Adhesion Science and Technology* 22 : 1089 2008 and “The influence of pre-treatments of aluminium alloys on bonding of PET coatings” by F.M. de Wit, Ö. Özkanat, J.M.C. Mol, H. Terryn and J. H.W. de Wit, published in *Surface and Interface Analysis* 42, 316–320, 2010

## **Synopsis**

In this chapter, bonding of succinic acid and a model molecule for a polyethylene terephthalate (PET) type coating is investigated. Di-methyl terephthalate (DMT) was chosen and bonded to the previously discussed differently pre-treated samples of AA1050 and AA5182 alloys. Succinic acid was also bonded to aged AA5182 alloy, AZ31 and vacuum-evaporated pure aluminium and magnesium on glass slides. The bonding was studied by means of Fourier Transform Infrared Reflection Absorption spectroscopy (FTIR-RAS). Bonding is expected to give a direction for the adhesion of the coating system, which will be discussed in chapter 8, where PET coating adhesion is tested macroscopically.

## 6.1 Introduction

As discussed in chapter 2, the use of coatings to protect aluminium from corrosion is necessary as the native oxide offers limited protection only in neutral environments (pH 4-8)<sup>[1]</sup> where no chlorides are present. One way of protecting aluminium alloys is by using an organic coating. To obtain good protection, next to being a good barrier to water and gasses and additional (self-healing) properties, it is of high importance that coatings adhere well to the substrates. The adhesion and potential delamination of organic coatings on aluminium are therefore important topics in the food and beverage industry<sup>[2]</sup> and where adhesives are concerned, e.g. in transport<sup>[3]</sup>.

One of the reasons organic coatings are used extensively is to protect aluminium against corrosion. The efficacy of this protection depends largely on the interfacial bonding of the coating. Ideally, one would want to study thicker polymer coatings, which are used in practice. It is, however, experimentally difficult to obtain detailed information about the polymer/oxide interface. One method is to peel off a coating and then examine the surface with, for instance, XPS<sup>[4]</sup>. Another method is to use positron annihilation<sup>[5]</sup>, which can show molecular changes but only in the coating, and is not sensitive on the interface.

When studying adhesion properties, the surface composition and chemical properties of the oxides on aluminium alloys need to be determined by using surface sensitive techniques like XPS<sup>[4, 6]</sup>. In the recent past it was found that the OH-fraction in the oxides changes after chemical pre-treatments<sup>[7]</sup>. It is also possible to tailor the composition of the oxide at the surfaces by temperature or chemical pre-treatments as was shown in chapter 4.

Some studies have combined analysis of surface composition and mechanical tests, with various pre-treatments<sup>[8, 9]</sup> and used the theory of acid-base characteristics of both substrate (in the reference: steel) and several polymers<sup>[10]</sup>. Brogly et al.<sup>[11]</sup> have studied the relationship between bonding thin layers of poly(ethylene-co-vinyl acetate) (EVA) and the mechanical adhesion of EVA coatings on pure aluminium.

Organic coatings and adhesives often contain carboxylic acid groups<sup>[12]</sup>. Some self-assembling monolayers (SAMs) also contain carboxylic acids as end-groups<sup>[13]</sup>. These carboxylic acid groups can coordinate well to aluminium oxide surfaces. In industry, prior to application of SAMs or organic coatings, aluminium alloys are given an aqueous pretreatment to alter the surface chemistry and composition in a way that is favorable to the adhesion of the organic coating. It is, therefore,

important to understand the influence these pre-treatments have on the bonding behavior.

There are some studies done on buried interfaces with Fourier Transform Infrared (FTIR) Attenuated Total Reflection (ATR) experiments on polymer coated ATR-crystals<sup>[14]</sup>. However, this does not allow to examine the individual groups that bond, since the infrared radiation is scattered by the surrounding polymer groups and is, therefore, not surface sensitive. For coatings on metallic substrates, such a study is even more difficult, because a thin metallic layer needs to be deposited on an ATR crystal and subsequently coated with an organic coating<sup>[15]</sup>. For alloys the use of the ATR crystal method is impossible due to the alloying elements, which cannot be vacuum-evaporated onto the crystal in an as-cast or rolled structure.

Research by Van den Brand and coworkers<sup>[8, 16, 17]</sup> focused on the bonding of thin layers of succinic acid and anhydrides to pretreated aluminium (AA1050, 99.5% Al) surface with infrared techniques. The nature of the bonds was determined on AA1050 by Van den Brand et al.<sup>[17]</sup>, who showed that the distance between the symmetrical and asymmetrical stretching vibration peaks of carboxylic acid groups could be used to determine the bonding configuration of succinic acid groups to aluminium. They showed that this bonding was in bidentate mode, where the oxygen groups of the carboxylic acid were deprotonated and bonded to hydroxyl groups present at the aluminium surface, releasing water. More specifically, the density of OH-groups, the hydroxide fraction of the oxide layer, was determined as the most important factor in the extent of bonding.

The main goal was to investigate a range of materials varying from pure aluminium to Al-Mg, Mg-Al and finally pure magnesium. The AA5182 samples were therefore enriched in magnesium with temperature treatments at room temperature (RT), 100°C and 200°C for 11 days to ensure enrichment. The bonding of succinic acid to these enriched samples was then compared to an alkaline pretreated AZ31 magnesium-aluminium alloy and a pure Mg evaporated onto glass slides with FTIR-RAS.

To extend the previous work, in this chapter the bonding of two model molecules is studied. Succinic acid (the structural formula is shown in the cover page for the chapter) was chosen as the model molecule with two carboxylic acid groups, which can represent the bonding molecules that are grafted to the backbone of non-polar polymers. Succinic acid is formed from succinic anhydride and water.

As the other model molecule we have chosen di-methylterephthalate (DMT), since this represents the most likely and abundant bonds in a PET(G) coating (see figure 6.1). The quantitative macroscopic adhesion testing in combination with similar pre-treatments that are used in this chapter, is discussed in chapter 8.

The substrates were studied before in chapter 4 and in literature<sup>[16, 18]</sup>: AA1050 (99.5 wt% pure Al), AA5182 (4.8 wt% Mg). Glycol-modified polyethylene terephthalate (PETG) was also studied before<sup>[19]</sup> extensively.

In this study the AA5182 was selected because of the controllable surface content of magnesium. The surface content of magnesium of this alloy was already shown to depend on certain heat pre-treatments by Auger Electron Spectroscopy (AES)<sup>[18]</sup>. After chemical pre-treatments the magnesium contents also vary (see chapter 4), which was predicted by the Pourbaix diagrams of Al and Mg ( $\text{Mg}(\text{OH})_2$  stable only above  $\text{pH} = 12$ )<sup>[1]</sup>. In both cases depth profiling Auger Electron Spectroscopy was used (chapter 4) to gain insight into the chemical properties of the oxide surfaces.



**Figure 6.1** Chemical structure of di-methyl terephthalate (DMT, left) and polyethylene terephthalate (PET, right).

## 6.2 Results

### 6.2.1 FTIR-RAS analysis of bonding of succinic acid to chemically pretreated aluminium alloy surfaces

Figure 6.2 shows an overview spectrum of the full wavenumber range of an alkaline pretreated and succinic acid covered AA5182 sample. The vertical axis gives the intensity of the peaks or absorbance, in arbitrary units and the horizontal axis shows the wavenumbers (in  $\text{cm}^{-1}$ ) range. There are four regions of interest indicated, namely the areas under  $3500\text{-}3000\text{ cm}^{-1}$ ,  $3000\text{ - }2700\text{ cm}^{-1}$ ,  $2000\text{ - }1200\text{ cm}^{-1}$  and  $1200\text{ - }1000\text{ cm}^{-1}$  regions. The  $3500\text{ - }3000\text{ cm}^{-1}$  region is related to the loss of hydroxyl groups with respect to the pre-treated sample, be it from the bonding of the succinic acid molecules or the desorption of water in the solvent. The  $3000\text{ - }2700\text{ cm}^{-1}$  region contains some  $\text{CH}_2/\text{CH}_3$  peaks of either the succinic acid molecules or the desorption of some aliphatic chains still present after pre-treatment. The focus of the discussion will be on the  $2000\text{ - }1200\text{ cm}^{-1}$  region, which contains the carboxylic acid stretching vibrations. Finally, the  $1200\text{ - }1000\text{ cm}^{-1}$  regions contains some aliphatic chains which are due to the presence of the succinic acid molecules.



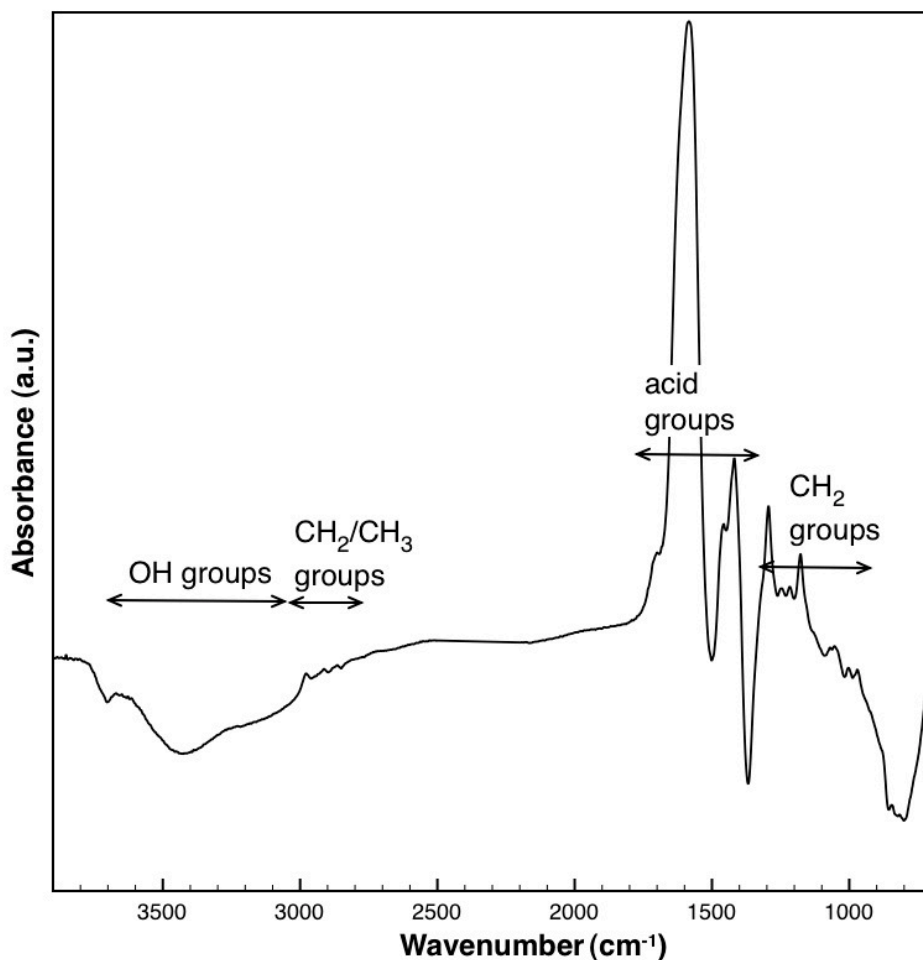


**Figure 6.2** FTIR spectrum (2000-1200 cm<sup>-1</sup> range) of AA5182 after NaOH pretreatment and succinic acid molecules deposition from THF.

Figure 6.3 zooms in on the 2000 - 1200 cm<sup>-1</sup> region from figure 6.2. In this figure, spectra of all four pre-treatments and the vacuum evaporated aluminium are shown. The vertical axis gives the intensity of the peaks or absorbance, in arbitrary units and the horizontal axis shows the relevant wavenumber (cm<sup>-1</sup>) range. The order of magnitude of all spectra is scaled to  $2 \times 10^{-2}$  -  $5 \times 10^{-2}$  arbitrary units on the vertical axis, which means approximately a factor 4 or 8 larger than the alkaline and boiling pretreated samples, which are displayed at their true size. Most noticeable in this figure are four peaks: a shoulder at 1720 cm<sup>-1</sup>, peaks between 1610 - 1570 cm<sup>-1</sup>, between 1460 - 1418 cm<sup>-1</sup> and around 1300 cm<sup>-1</sup>.

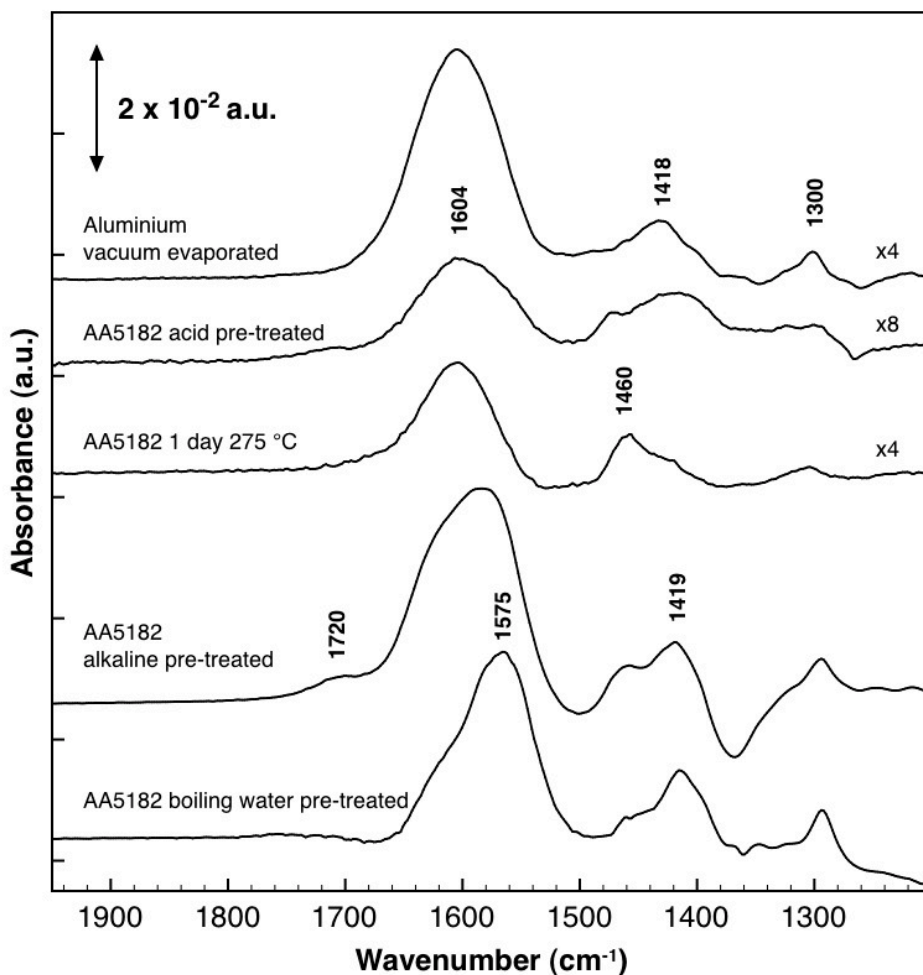


**Figure 6.3** FTIR spectrum (2000-1200 cm<sup>-1</sup> range) for the differently pretreated substrates. Note the differences in scale, indicated by the multiplication factor.

Table 6.1 summarizes the infrared peaks from figure 6.3 with assignments from the previous literature<sup>[17]</sup>. For the alkaline and somewhat weaker for acid pretreated samples a shoulder can be distinguished around 1720 cm<sup>-1</sup>, which was assigned by Van den Brand et al.<sup>[17]</sup> to a small amount of singly coordinatively bonded carboxylic acid groups (C=O) of the succinic acid molecules while the second carboxylic group is only weakly bonded through a hydrogen bond.

The principal peaks that can be attributed to the asymmetric and symmetric stretch vibrations,  $\nu_{as}$  and  $\nu_s$  of the COO<sup>-</sup> bonds are found at around 1610-1570 cm<sup>-1</sup> and 1460-1418 cm<sup>-1</sup> in all cases for bridging bidentate on aluminium oxide. The other main peak position around 1300 cm<sup>-1</sup> is attributed to the  $\nu_s$  of the COO<sup>-</sup> bonds in unidentate bonding on aluminium oxide. The asymmetrical stretching of this peak

cannot be distinguished, as it is in the shoulder of the  $1600\text{ cm}^{-1}$  peak around  $1570\text{ cm}^{-1}$ . The other possibility is that this is the  $\text{CH}_2$  bond wagging described by several authors e.g. Tao et al.<sup>[20]</sup>.

**Table 6.1** FTIR peak positions ( $\text{cm}^{-1}$ ) as measured after various pre-treatments and succinic acid deposition from THF and rinsing in THF after chemical pre-treatments.

Alkaline pre-treated AA5182	Vacuum Evaporated Aluminium	Dehydroxylated AA5182	Pseudo-boehmite AA5182	Acid pre-treated AA5182	Assignment*
1720	-	-	-	1720	Singly bonded succinic $\text{COO}^-$
1585	1606	1606	1583	1601	$\nu_{\text{as}} (\text{COO}^-)$
1462(m) 1419	1460 (m) 1431	1462 1423(m)	1470(m) 1416	1472 (m) 1419	$\nu_{\text{s}} (\text{COO}^-)$
1295	1302	1305	1295	1305	$\nu_{\text{s}} (\text{COO}^-)$ or $\text{CH}_2$ wagging

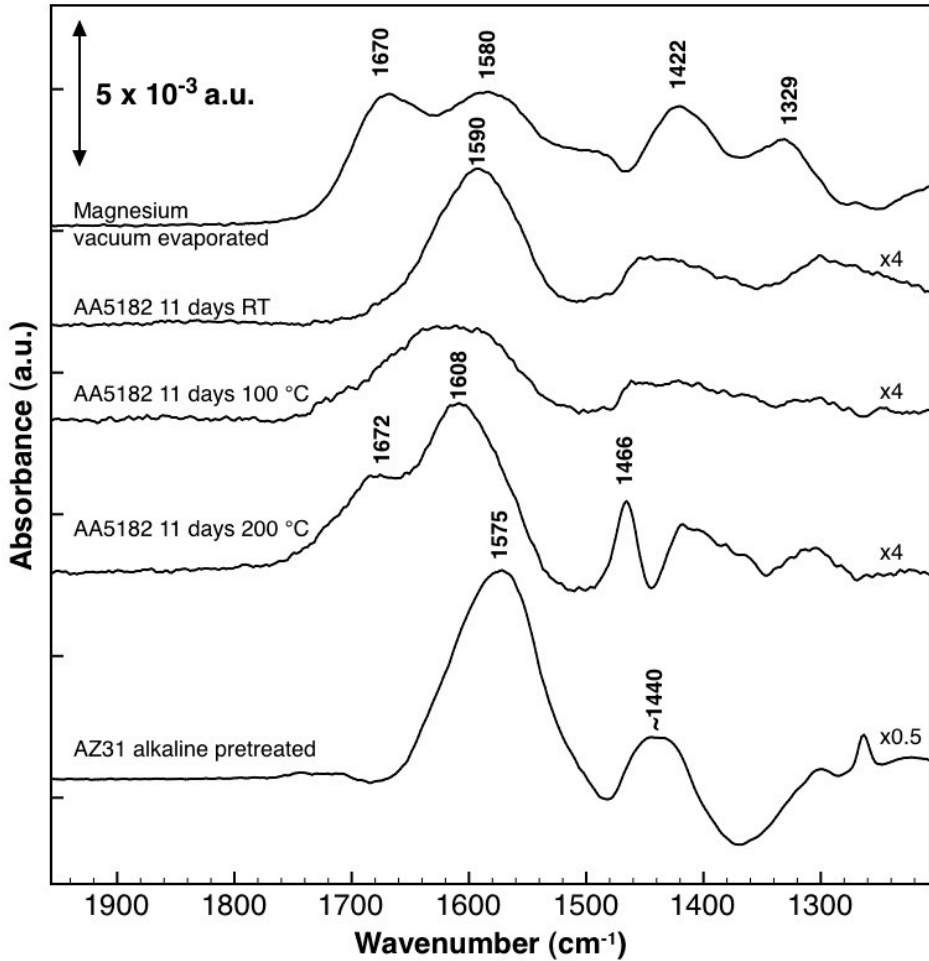
\* $\nu_{\text{s}}$  and  $\nu_{\text{as}}$  are the symmetrical and asymmetrical stretching peak positions of the given ion

Table 6.2 shows the calculated distance of the carboxylic acid bonding peaks  $\Delta\nu$  ( $\nu_{\text{as}} - \nu_{\text{s}}$ ). The interpretation of these distances was found in the article by Deacon and Phillips<sup>[21]</sup> In this table, either the most pronounced peak, or the average of the  $\nu_{\text{s}} (\text{COO}^-)$  components was used, as not all components are well resolved for all samples.

**Table 6.2** Configuration of succinic acid molecules calculated from the position ( $\text{cm}^{-1}$ ) of the main peaks  $\Delta\nu$  ( $\nu_{\text{as}} - \nu_{\text{s}}$ ) for different chemical pre-treatments. Note that all calculations indicate a bridging bidentate configuration. (bb = bridging bidentate)

Alkaline Pretreated AA5182	Vacuum Evaporated Aluminium	Dehydroxylated AA5182	Pseudo-boehmite AA5182	Acid pre treated AA5182	Assignment*
1585	1606	1606	1583	1601	$\nu_{\text{as}} (\text{Al-COO}^-)$
1462(m) 1419	1460 (m) 1431	1462 1423(m)	1470(m) 1416	1472 (m) 1419	$\nu_{\text{s}} (\text{Al-COO}^-)$
166 (bb)	175 (bb)	144 (bb)	167 (bb)	182 (bb)	$\nu_{\text{as}} - \nu_{\text{s}}$

\* $\nu_{\text{s}}$  and  $\nu_{\text{as}}$  are the symmetrical and asymmetrical stretching peak positions of the given ion



**Figure 6.4** Typical overview of the relevant part of the FTIR spectra for vacuum evaporated pure Mg, AA5182 with succinic acid molecules after aging at RT, 100°C and 200°C, and alkaline pre-treated AZ31. Note the differences in scale, indicated by the multiplication factor.

### 6.2.2 FTIR-RAS analysis of bonding of succinic acid on heat-treated aluminium alloy surfaces, vacuum evaporated magnesium and AZ31

Figure 6.4 gives a similar overview as figure 6.3 of the 2000-1200  $\text{cm}^{-1}$  part of the FTIR spectrum after deposition of succinic acid, but now AA5182 samples were aged for 11 days at 100°C and 200°C. For reference, also an AZ31 sample was used, which has the composition given before, to be able to compare to magnesium-rich engineering materials. A vacuum evaporated pure magnesium

sample was added for comparison with the pure metal. In addition to the four peaks found in the chemically pre-treated samples, figure 6.5 shows another peak most pronouncedly in the vacuum evaporated magnesium as well as in the sample aged at 200°C. The sample aged at 100°C shows a band-broadening with respect to the sample aged at room temperature. Table 6.3 gives (similar) assignments of the peaks according to literature to those given in Table 6.1.

**Table 6.3** FTIR peak positions (cm<sup>-1</sup>) as measured after various pre-treatments and succinic acid deposition from THF and rinsing in THF.

Vacuum Evaporated Magnesium	11 days aged at RT AA5182	11 days aged at 100°C AA5182	11 days aged at 200°C AA5182	Alkaline pre-treated AZ31	Assignment*
1671	-	-	1683		$\nu_{as}(\text{COO}^-)$
	1593	1612	1608	1576	$\nu_{as}(\text{COO}^-)$
1482 (m)	1454	1457	1466	1448	$\nu_s(\text{COO}^-)$
1423	1427	1423	1418	1429	
1330	1301	1301	1307	1302	$\nu_s(\text{COO}^-)$ or $\text{CH}_2$ wagging

\* $\nu_s$  and  $\nu_{as}$  are the symmetrical and asymmetrical stretching peak positions of the given ion

Again, the peaks found are assigned to similar bonds as found on the non-aged samples. It has to be noted that the vertical scale of figure 6.3 is about 10 times smaller than the vertical scale of figure 6.2. Like in figure 6.2, scaling took place for some spectra. The vacuum evaporated magnesium substrate shows a large peak at 1670 cm<sup>-1</sup>. Combined with the 1330 cm<sup>-1</sup> peak this can be assigned to carboxylic acid bonds in a unidentate configuration on magnesium (see figure 6.5).

The peak around 1600 cm<sup>-1</sup> found in the room temperature sample is considerably less wide than the peak after aging at 100°C. This peak splits into two peaks after the 200°C pretreatment. Also, the peaks around 1440, 1420 and 1300 cm<sup>-1</sup> become sharper. Overall, from figure 6.4 and the calculated peak-to-peak distances ( $\Delta\nu$  (cm<sup>-1</sup>) in Table 6.4), it can be seen that, since the peaks are broad (100 cm<sup>-1</sup>), there can be several peaks underneath one bigger peak. The distribution of the magnesium in the heat-treated samples is more towards to the surface (enrichment). In this AA5182 sample there can be enrichment on the surface, which adds clearly another, less well-resolved peak to the one found around 1600 cm<sup>-1</sup>. This suggests that, like in the vacuum evaporated magnesium sample, there is more unidentate binding of magnesium instead of bridging bidentate. This is somewhat in disagreement with Fotea et al.<sup>[22]</sup> who have attributed the 1380 cm<sup>-1</sup> to contamination from the air. This contamination bonded as unidentates, which are

called “monodentates” in the mentioned article. The vacuum evaporated magnesium surface however also shows unidentate bonding. AZ31 was also expected to show this type of bonding and although the  $\nu_{as}$  peak is broad, no clear evidence of the distinct unidentate peak can be given. An explanation for the missing of this peak is that the outer oxides are dominantly aluminium oxides, as was found before<sup>[23]</sup>.

**Table 6.4** Configuration of succinic acid molecules calculated from the position ( $\text{cm}^{-1}$ ) of the main peaks  $\Delta\nu$  ( $\nu_{as} - \nu_s$ ) for different pretreatments. Note that all calculations indicate a bridging bidentate configuration. \*averaged (bb = bridging bidentate, ud = unidentate)

Alkaline Pretreated AZ31	11 days aged at RT AA5182	11 days aged at 100°C AA5182	11 days aged at 200°C AA5182	Vacuum Evaporated Magnesium	Assignment*
1576	1593	1612	1608	1565	$\nu_{as}$ (Mg/Al-COO <sup>-</sup> )
1448 1429	1454 1427	1456 1423	1466 1418 (m)	1482 (m) 1422	$\nu_s$ (Mg/Al-COO <sup>-</sup> )
146*	153*	146	146	142 (bb)	$\nu_{as} - \nu_s$
-	-	~1680	1683	1671	$\nu_{as}$ (Mg-COO <sup>-</sup> )
-	-	1301	1307	1330	$\nu_s$ (Mg-COO <sup>-</sup> )
-	-	~380 (ud)	367 (ud)	341 (ud)	$\nu_{as} - \nu_s$

\* $\nu_s$  and  $\nu_{as}$  are the symmetrical and asymmetrical stretching peak positions of the given ion

### 6.2.3 FTIR-RAS analysis of bonding of dimethyl terephthalate (DMT) on pretreated aluminium alloy surfaces

Figures 6.7 and 6.8 show the results of the FTIR measurements with DMT molecules. In the total spectra taken, which were from 600 - 3500  $\text{cm}^{-1}$ , several zones of peaks could be distinguished. Around 3500  $\text{cm}^{-1}$  were OH related peaks: water and hydroxyl bonds. The 2700 - 2800  $\text{cm}^{-1}$  range contained the  $\text{CH}_2/\text{CH}_3$  bonds and below 1300  $\text{cm}^{-1}$  C-H type bond resonance and Al-O bonds were found. For the sake of brevity only the range is shown where bonding frequencies are expected. In both figures 6.5 and 6.6 one large band can be seen, which is split up into several peaks. For AA1050, alkaline and boiling pre-treatment show peaks in the 1300 - 1700  $\text{cm}^{-1}$  range. Acid pre-treatment shows no signals, even after 4 times magnification. For AA5182, the peaks for alkaline and boiling pre-treatment are more clearly discernible from the broad bands. Also the acid pre-treatment

shows some (small) peaks. In general peaks at around  $1500\text{ cm}^{-1}$  and  $1400\text{ cm}^{-1}$  indicate carboxylic acid bonding.

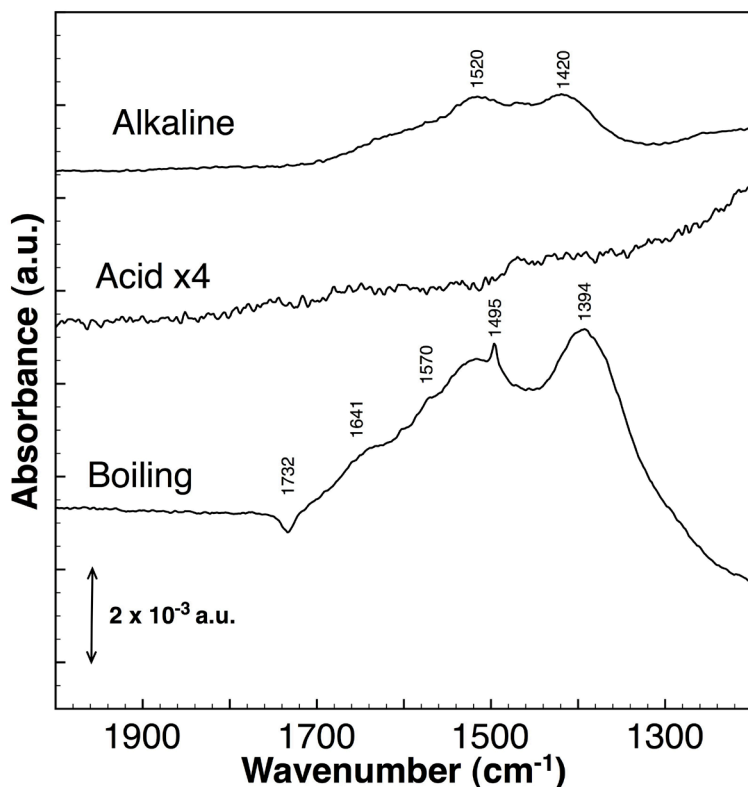


**Figure 6.5** FTIR spectra of DMT molecules on AA1050 after pre-treatments.

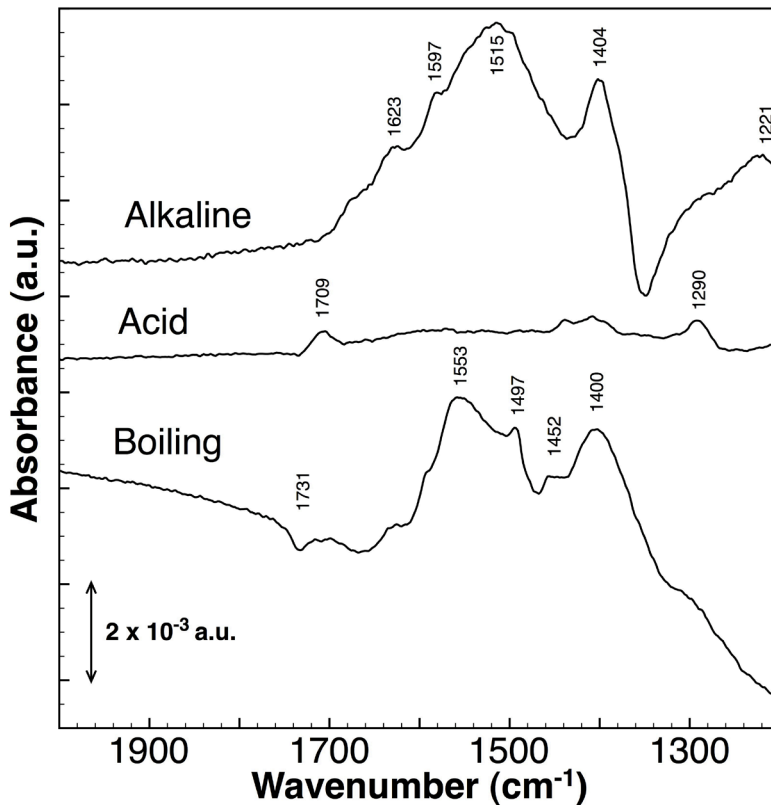


**Figure 6.6** FTIR spectra of DMT molecules on AA5182 after pre-treatments.

### 6.3 Discussion

The AES results from chapter 4 show that the oxide film composition can vary considerably with temperature treatment. Although at the outer surface of the alloy there is still  $\text{Al}_2\text{O}_3$  present, but in the 4 nm thick oxide, magnesium is dominantly present. After the 200°C treatment, magnesium (hydro)oxide is present almost exclusively, probably in the form of  $\text{Mg}(\text{OH})_2$  due to reaction with the atmospheric water.

#### 6.3.1 Bonding of succinic acid on heat-treated aluminium alloy surfaces, vacuum evaporated magnesium and AZ31

Combining these results with the FTIR spectra and the assignments of the symmetrical and asymmetrical stretching vibrations, it is assumed that the aluminium bonds remain in both unidentate and bridging bidentate configurations



(figure 6.7). It is supposed that the magnesium-rich oxides at the surface cause the unidentate (figure 6.8) coupling possibilities for the succinic acid molecules.

In summary, the results show that the bonding of succinic acid to the various pre-treated surfaces is predominantly via bidentates and therefore similar to the bonding on AA1050.

Bonding configurations on AA5182 are thus classified as unidentate and bridging bidentate, where the alkaline and the boiled samples have relatively more unidentate on aluminium, as results from the shift to lower peak positions around  $1570\text{ cm}^{-1}$ .

This is in accordance with what Nara et al.<sup>[24]</sup> found, after ab initio calculations of acetic acid on magnesium. They determined that the frequency shift for bridging bidentate for a magnesium-carboxylic acid complex would be around  $1400\text{ cm}^{-1}$ , with a very small peak-to-peak distance of approximately  $30\text{ cm}^{-1}$ . For a unidentate bond,  $\nu_s$  was found at lower wavenumber, around  $1300\text{ cm}^{-1}$ , while the symmetrical stretching was found at considerably higher wavenumber than for bridging bidentate symmetrical stretching around  $1650\text{ cm}^{-1}$ . This is however only the case for simulated surfaces, which are assumed perfect with respect to atomic configuration and oxide. Experiments show that all kinds of reactions (for instance with  $\text{CO}_2$  from the air) and configurations (Mg-Mg bonds with varying lengths) are possible.

The difference in the configurations for the mixed Al-Mg surfaces was first assumed to be caused by the larger size in an octahedral configuration of the magnesium ion as opposed to the size of the aluminium ion,  $86\text{ pm}$  and  $67.5\text{ pm}$ <sup>[25]</sup>, respectively. The larger size of the magnesium ion makes the bridging of the carboxylic acid group from the succinic acid energetically unfavorable. Also, the polarizability of Mg with respect to that of Al contributes to this preference ( $10.6$  and  $6.8$ )<sup>[25]</sup>. Magnesium attracts carboxylic acid ions more, thus altering the distance and angle of the bond. Furthermore, magnesium is probably present in a complex carbonate-hydrate form, which allows for easier unidentate coupling, since the OH-groups are not so closely packed. Since there is still aluminium present at the surface, this will give also contribute to an image of a bridging bidentate configuration. Pure magnesium also shows bidentate configuration.

The change in surface chemistry might have consequences for the adhesion of coatings, since the bond strength depends on the ability of the individual molecules to bond with as many carboxylic groups as possible. Although Dudev and Lim<sup>[26]</sup> did not find a large difference in bonding energy.

This would suggest that adhesion of a coating is possible with any pretreated surface. Unidentate bonding mode succinic acid molecules will be less stable than bidentate or chelating components, because they are attached to the surface by

only one bond. No conclusion can be drawn however on the number of these molecules, which means the adhesion force of a coating cannot be predicted yet.

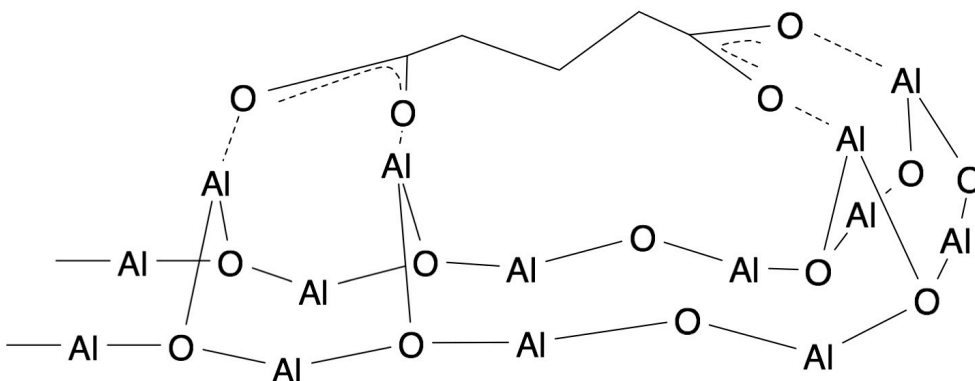


**Figure 6.7** Illustration of bidentate bonding on aluminium rich surfaces

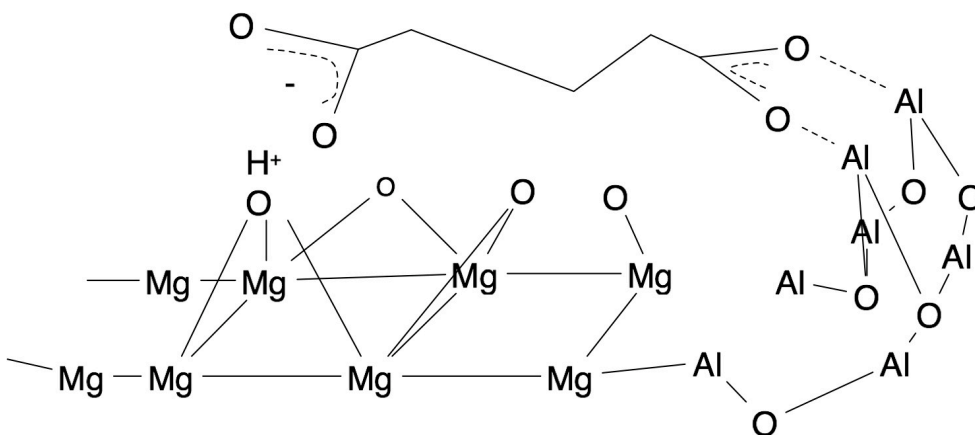


**Figure 6.8** Illustration of unidentate bonding on magnesium rich surfaces

### 6.3.3 Bonding of dimethyl terephthalate (DMT) on pretreated aluminium alloy surfaces

Table 6.5 and 6.6 give an overview of the peaks assigned from figures 6.7 and 6.8, respectively. The variation in peak positions is relatively minor and uniform over the two alloys. Therefore similar mechanisms of bonding of the DMT molecules are assumed. Aromatic ring vibrations were assigned to peaks in the  $1500\text{ cm}^{-1}$  range, as was also found in literature<sup>[11]</sup>.

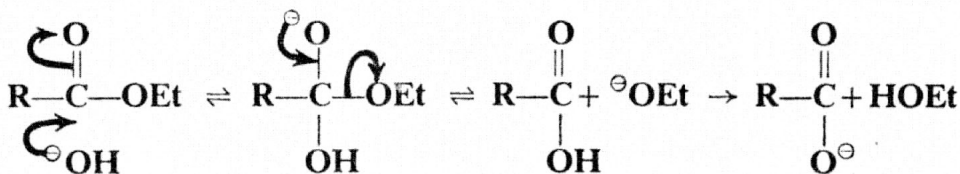
More predominantly, various peaks in the spectra were assigned to symmetrical  $\nu_s$  ( $\text{COO}^-$ ) and a-symmetrical  $\nu_{as}$  ( $\text{COO}^-$ ) vibrations of carboxylic acid bonds. Although no carboxylic acids are present, this can be explained as follows: on alkaline and boiling samples, a strong alkaline surface is present with a high amount of surface hydroxyls<sup>[4]</sup>. Since the experiments were done in air, it was assumed that there was a layer of water on the surface, which is known from literature<sup>[27]</sup>. This surface is considered wet enough to have not only aluminium ions, but also free hydroxide molecules. It is a dynamic equilibrium in which hydroxides are formed and dissolved. In the case of the presence of a DMT molecule with two ester groups, the free hydroxide ions can be involved in a saponification reaction (see figure 6.9). In this type of reaction, the free hydroxide ion separates the ester group into a carboxylic acid and an alcohol group, in this case methanol. The carboxylic acid then bonds via a Lewis acid-base connection, much like succinic acid with two carboxylic groups to the hydroxylated surface. This of course is a statistical occurrence, but the last step of the reaction is irreversible, i.e. once a carboxylic acid is formed, no carbonyl groups can be re-formed. The peak assignments also show there is still some carbonyl bonding taking place, but this is minor and almost not present in the acid pre-treated surfaces.

**Table 6.5** Overview of peak assignment (in  $\text{cm}^{-1}$ ) of DMT molecules on AA1050 s = strong, w = weak \*negative

Alkaline	Boiling	Acid	Assignment
1420	1394	-	$\nu_s$ (Al- $\text{COO}^-$ )
shoulder	1495	-	aromatic ring
1520s	1520s	-	
shoulder	1570s	-	$\nu_{as}$ (Al- $\text{COO}^-$ )
shoulder	1641s	-	aromatic ring
-	1732s*	-	C=O

**Table 6.6** Overview of peak assignment (in  $\text{cm}^{-1}$ ) of DMT molecules on AA5182 s = strong, w = weak \*negative

Alkaline	Boiling	Acid	Assignment
1221	shoulder	-	$\nu(\text{C-O})$
shoulder	shoulder	1290	$\nu_s(\text{COO}^-)$
1400s	1404s	1398w	$\nu_s(\text{COO}^-)$
shoulder	1452s	1441w	
shoulder	1497s	-	aromatic ring
1515s	shoulder	-	
shoulder	1553s	-	$\nu_{as}(\text{COO}^-)$
1579s	shoulder	-	
1632s	1632w	-	
shoulder	1663w*	-	
shoulder	shoulder	1709w	Bonded $\text{C=O}$
shoulder	1731w*	-	Free $\text{C=O}$

**Figure 6.9** Generalized reaction of an ester group which undergoes saponification in the presence of a (strong) ionic base, separating the ester into a carboxylic acid and an alcohol, McMurry<sup>[28]</sup>.

In the spectra, methanol could not be detected, this was due to the rinsing off after the reaction, which would wash away methanol, since it was neither chemically nor physically bound to the surface. Furthermore, toluene is a good solvent to methanol.

The range in which the symmetrical and a-symmetrical stretching vibrations occur of the carboxylic acid groups suggest bonding to aluminium sites as well as magnesium, as was reported before<sup>[18]</sup>. The nature of these bonds is tentatively assumed to be bridging bidentates (see figure 6.10). No evidence of free carbonyl groups was found, suggesting that all DMT molecules still present after rinsing were bound by two sides onto the surface, whereby the aromatic ring is assumed to be flat on the surface<sup>[11]</sup>.

Therefore, the alkaline and boiling pre-treatment show bonding of DMT molecules by Lewis acid-base interaction, while the acid pre-treatment does not.

Although Beentjes<sup>[29]</sup> has questioned the occurring of a bond between the surface hydroxyls and PET coatings as published by Bou et al.<sup>[30]</sup>, it is doubtful that bonding happens through carboxylic end-groups only, due to their low concentration.

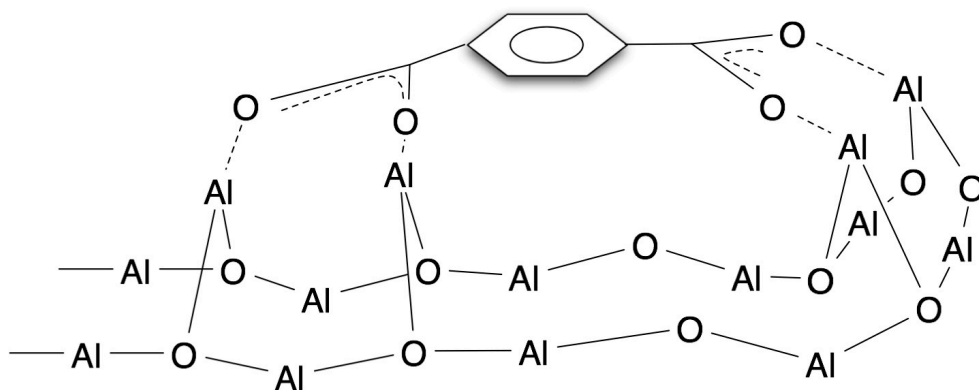


**Figure 6.10** Illustration of DMT molecule bonding on aluminium surfaces.

## 6.4 Conclusions

### 6.4.1 Bonding of succinic acid on presented surfaces

Succinic acid molecules can bond to vacuum evaporated aluminium and magnesium as well as to AA5182 surfaces. The mode in which they bond depends on the composition of the surface. Surfaces rich in magnesium display the same properties in this respect as the ones rich in aluminium.

Succinic acid molecules on the various samples, all pretreated AA5182 as well as pure vacuum-evaporated aluminium and magnesium, show a similar bonding, i.e. a mixed unidentate and bridging bidentate configuration. There are small differences in the peak-to-peak distances due to the differences in the oxide configuration, be it more magnesium or more aluminium rich. The general trend points in the direction of a smaller difference in wavenumbers for magnesium and heat-treated AA5182. This is due to the difference in oxide configuration that varies with the Al/Mg ratio.

Enriching the surface in magnesium clearly shows that the unidentate configuration on magnesium adds a peak in the spectrum to the existing mixed uni- and bidentate state on aluminium-magnesium alloys.

### 6.4.2 Bonding of DMT on presented surfaces

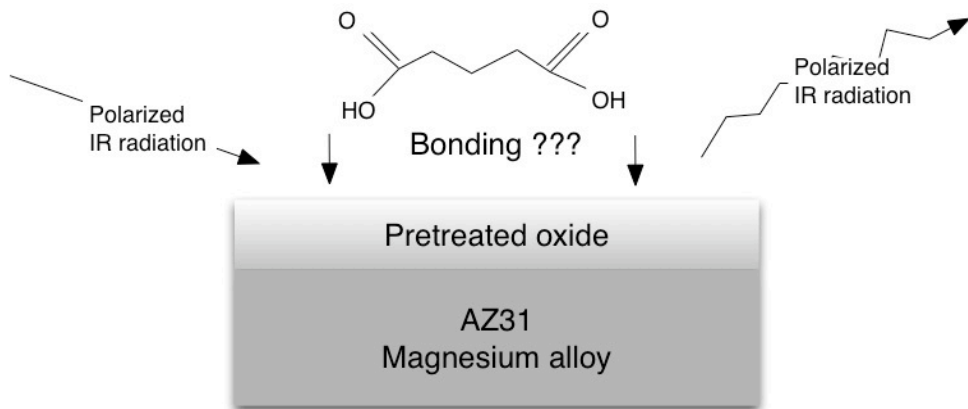
The influence of the pre-treatment of AA1050 and AA5182 on bonding of DMT molecules and PETG coatings on these alloys was investigated. FTIR spectra showed that bonding of DMT molecules could occur by bridging bidentate bonds of carboxylic acid Lewis acid-base (formed after saponification of the ester bonds in the presence of the strong base on the surface). Both for AA1050 and AA5182, alkaline and boiling pre-treatment showed evidence of bonding, while acid pre-treatments did not. Results of mechanical testing of the adhesion of PETG coatings to these surfaces will be discussed in chapter 8. The chemical bonding of DMT molecules on the aluminium surfaces was successfully linked to macroscopical adhesion behavior of PETG coated systems.

## References

- [1] M. Pourbaix, *Atlas of Electrochemical Equilibria in Aqueous Solutions* **1966**, Pergamon Press, Oxford.
- [2] G. Olafsson, M. Jagerstad, R. Oste, B. Wesslen, *Journal of Food Science* **1993**, *58*, 215.
- [3] J.K. Jethwa, A.J. Kinloch, *Journal of Adhesion* **1997**, *61*, 71.
- [4] J. Kurdi, H. Ardelean, P. Marcus, P. Jonnard, F. Arefi-Khonsari, *Applied Surface Science* **2002**, *189*, 119.
- [5] R.E. Galindo, H. Schut, A. van Veen, R. Rastogi, W.P. Vellinga, H.E.H. Meijer, *Thin Solid Films* **2005**, *478*, 338.
- [6] M.R. Alexander, G.E. Thompson, G. Beamson, *Surface and Interface Analysis* **2000**, *29*, 468.
- [7] J. van den Brand, P.C. Snijders, W.G. Sloof, H. Terryn, J.H.W. de Wit, *Journal of Physical Chemistry B* **2004**, *108*, 6017.
- [8] J. van den Brand, S. Van Gils, P.C.J. Beentjes, H. Terryn, V. Sivel, J.H.W. de Wit, *Progress in Organic Coatings* **2004**, *51*, 339.
- [9] G.W. Critchlow, D.M. Brewis, *International Journal of Adhesion and Adhesives* **1996**, *16*, 255.
- [10] J.F. Watts, M.M. Chehimi, E.M. Gibson, *Journal of Adhesion* **1992**, *39*, 145.
- [11] M. Brogly, M. Nardin, J. Schultz, *Journal of Adhesion* **1996**, *58*, 263.
- [12] C.W. Lin, W.L. Lee, *Journal of Applied Polymer Science* **1998**, *70*, 383.
- [13] D.L. Allara, R.G. Nuzzo, *Langmuir* **1985**, *1*, 45.
- [14] L. Philippe, C. Sammon, S.B. Lyon, J. Yarwood, *Progress in Organic Coatings* **2004**, *49*, 302.
- [15] M. Ohman, D. Persson, *Electrochimica Acta* **2007**, *52*, 5159.
- [16] J. van den Brand, O. Blajiev, P.C.J. Beentjes, H. Terryn, J.H.W. de Wit,

- Langmuir* **2004**, *20*, 6318.
- [17] J. van den Brand, O. Blajiev, P.C.J. Beentjes, H. Terryn, J.H.W. de Wit, *Langmuir* **2004**, *20*, 6308.
- [18] F.M. de Wit, J.M.C. Mol, H. Terryn, J.H.W. de Wit, *Journal of Adhesion Science and Technology* **2008**, *22*, 1089.
- [19] W.P. Vellinga, A. Fedorov, J.T. De Hosson, *Journal of Computer-Aided Materials Design* **2007**, *14*, 37.
- [20] Y.T. Tao, *Journal of the American Chemical Society* **1993**, *115*, 4350.
- [21] G.B. Deacon, R.J. Phillips, *Coordination Chemistry Reviews* **1980**, *33*, 227.
- [22] C. Fotea, J. Callaway, M.R. Alexander, *Surface and Interface Analysis* **2006**, *38*, 1363.
- [23] J.H. Nordlien, K. Nisancioglu, S. Ono, N. Masuko, *Journal of the Electrochemical Society* **1996**, *143*, 2564.
- [24] M. Nara, H. Torii, M. Tasumi, *Journal of Physical Chemistry* **1996**, *100*, 19812.
- [25] D.R. Lide, *CRC Handbook of Chemistry and Physics 88th Edition*, Taylor and Francis Group LLC, **2007**.
- [26] T. Dudev, C. Lim, *Journal of Physical Chemistry B* **2004**, *108*, 4546.
- [27] J.C.M. Bolger, A. S. , *Molecular structure and electrostatic interaction at polymer-solid interfaces*, Elsevier, New York, **1969**.
- [28] J. McMurry, *Organic Chemistry*, Brooks/Cole Publishing Company, Monterey, California, **1984**.
- [29] P. Beentjes, PhD thesis thesis, Durability of polymer coated steel in diluted acetic acid environment, Delft University of Technology (Delft), **2005**.
- [30] M. Bou, J.M. Martin, T. Lemogne, *Applied Surface Science* **1991**, *47*, 149.

# Chapter 7 - Bonding and stability of succinic acid on magnesium alloy





## **Synopsis**

The influence of pre-treatments on bonding of succinic acid molecules to pre-treated magnesium alloy AZ31 is studied. The configuration of succinic acid bonded to all pre-treated surfaces is again studied by FTIR-RAS like in the previous chapter. Also, aging of samples in air before bonding, after immersion for 15 minutes in demineralized water is explored. Morphological changes are visualised by SEM and AFM. The latter method is also used to quantify roughness after pre-treatments.

## 7.1 Introduction

In this chapter the influence of surface pre-treatment on bonding of organic molecules on magnesium aluminium alloy AZ31 is investigated. The goal is to be able to compare the results of bonding of succinic acid molecules on these substrates to the previously reported aluminium-magnesium alloys as well as pure vacuum evaporated magnesium. The work was therefore limited to relatively simple treatments applied to the magnesium alloy surface, similar to the ones on aluminium alloys in chapter 6. The treatments chosen for this work were again alkaline (NaOH, pH = 12), acid (HNO<sub>3</sub>) and immersion in boiling water surface treatment. Succinic acid was again chosen as a model molecule for coatings. Bonding of these organic molecules was investigated by means of Fourier Transform Infrared Spectroscopy Reflection Adsorption Spectroscopy (FTIR-RAS), in a similar way as was done in chapter 6. Also, the influence of exposing samples to water after and air before bonding is reported. Finally, characterization of morphology of the surfaces after pre-treatments was done by SEM and AFM.

## 7.2 Results

### 7.2.1 FTIR-RAS analysis of bonding of succinic acid to chemically pretreated magnesium alloy surfaces

Figure 7.1 shows an overview spectrum of the full range of an alkaline pretreated and succinic acid covered AZ31 sample. The vertical axis gives the intensity of the peaks or absorbance, in arbitrary units and the horizontal axis shows the wavenumbers (in cm<sup>-1</sup>) range. There are four regions of interest indicated, namely the areas under 3500-3000 cm<sup>-1</sup>, 3000 - 2700 cm<sup>-1</sup>, 2000 - 1200 cm<sup>-1</sup> and 1200 - 1000 cm<sup>-1</sup> regions. The 3500 - 3000 cm<sup>-1</sup> region is related to the loss of hydroxyl groups with respect to the pre-treated sample, be it from the bonding of succinic acid molecules or the desorption of water in the solvent. The 3000 - 2700 cm<sup>-1</sup> region contains some CH<sub>2</sub>/CH<sub>3</sub> peaks of either the succinic acid molecules or the desorption of some aliphatic chains still present after pre-treatment. The focus of the discussion will be on the 2000 - 1200 cm<sup>-1</sup> region, which contains the carboxylic acid stretching vibrations. Finally, the 1200 - 1000 cm<sup>-1</sup> regions contains some aliphatic chains which are due to the presence of the succinic acid molecules.

In Figure 7.2, infrared spectra are shown for succinic acid on three differently prepared AZ31 substrates with respect to a background prior to immersion in the succinic acid solution. In Table 7.1, infrared peak positions were assigned like in

chapter 6. The distances between the main peaks are calculated and related to the molecular configuration similar to paragraph 6.2.1 and table 6.2.

As can be seen in figure 7.2, all spectra show broad bands around  $1570\text{ cm}^{-1}$  and asymmetrically shaped bands between  $1475$  en  $1375\text{ cm}^{-1}$ . Van den Brand<sup>[1]</sup> already described these bands for adsorption of succinic acid on aluminum substrates. He stated that the first one is not due to succinic acid, but indicates that carboxylic acid groups have been de-protonated to form a coordinated bonded carboxylate species. The band is then assigned to the asymmetric carboxylate stretching vibration  $\nu_{\text{as}}(\text{COO}^-)$ . The broad band around  $1475\text{-}1375\text{ cm}^{-1}$  can be assigned to symmetric carboxylate stretching vibration  $\nu_{\text{s}}(\text{COO}^-)$ <sup>[1]</sup>.

Next to the main  $\text{COO}^-$  peaks, for the alkaline and somewhat weaker for acid pretreated samples, a shoulder can be distinguished around  $1720\text{ cm}^{-1}$ , which was assigned by Van den Brand et al.<sup>[1]</sup> previously to a small amount of singly coordinately bonded carboxylic acid groups ( $\text{C}=\text{O}$ ) of the succinic acid molecules while the second carboxylic group is only weakly bonded through a hydrogen bond.

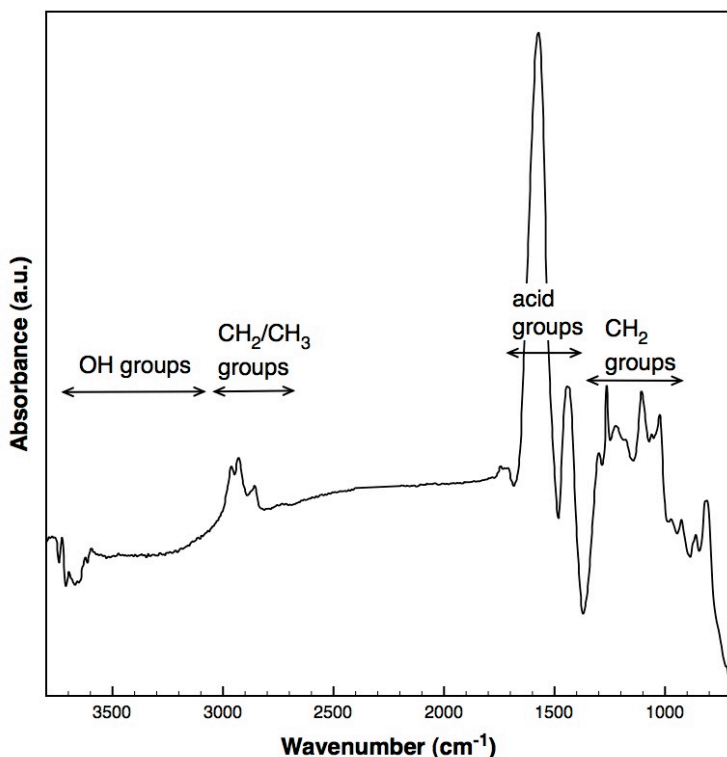


**Figure 7.1** FTIR-RAS overview spectrum of alkaline pretreated AZ31 substrate, recorded with respect to the substrate prior to immersion in succinic acid solution.

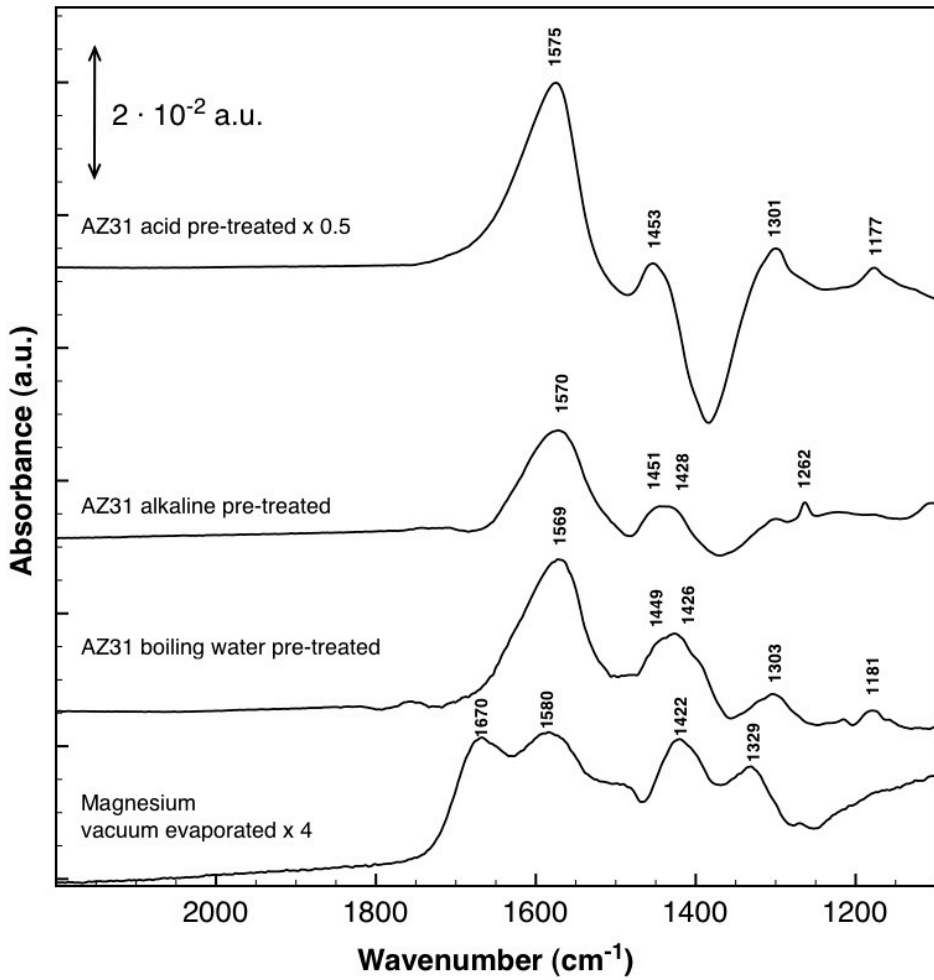


**Figure 7.2** FTIR-RAS spectra of succinic acid on acid, alkaline and boiling pre-treated AZ31 acid pretreated and magnesium vacuum evaporated signals are shown with a different vertical scaling, which is indicated by the multiplication factor.

**Table 7.1** Assignment of peaks to succinic acid interactions with the surfaces after pretreatments from figure 7.2. bb - bridging bidentate, ud - unidentate; m - medium, w - weak- Please refer to section 6.2.1 for further details.

Acid Pretreated AZ31	Alkaline Pretreated AZ31	Boiling water pretreated AZ31	Vacuum Evaporated Magnesium*	Assignment*
-	1720 (w)	1720 (w)	-	$\nu(\text{C}=\text{O})$
1575	1570	1569	1565	$\nu_{\text{as}} (\text{Mg}/\text{Al}-\text{COO}^-)$
1453(m)	1451 (m) 1428	1449(m) 1426	1482 (m) 1422	$\nu_{\text{s}} (\text{Mg}/\text{Al}-\text{COO}^-)$
122 (bb)	142 (bb)	143 (bb)	142 (bb)	$\nu_{\text{as}} - \nu_{\text{s}}$
			1671	$\nu_{\text{as}} (\text{Mg}-\text{COO}^-)$
			1330	$\nu_{\text{s}} (\text{Mg}-\text{COO}^-)$
			341 (ud)	$\nu_{\text{as}} - \nu_{\text{s}}$

\*from chapter 6

## 7.2.2 Aqueous stability of succinic acid on the differently prepared substrates

To investigate the bonding stability of succinic acid, substrates were immersed in triple de-ionized water for a period of up to 15 minutes. In Figure 7.3, infrared spectra obtained initially and after immersion for 15 minutes in triple de-ionized water for succinic acid on various pre-treated AZ31 are shown. As a reference, also a spectrum of freshly cleaned (no pretreatment) AZ31 immersed for 15 minutes in triple de-ionized water was added. A broad combined band between 1500 and 1300  $\text{cm}^{-1}$  was introduced as well as a water bending vibration  $\delta(\text{H}_2\text{O})$  at around 1650  $\text{cm}^{-1}$ .

For boiling water pretreated samples, the broad peak around 1570  $\text{cm}^{-1}$  as seen in figure 7.2 due to asymmetric carboxylate stretching vibration  $\nu_{\text{as}} (\text{COO}^-)$  disappeared after immersion in water for 15 minutes.

For acid pre-treated AZ31 with succinic acid and exposure at room temperature for 15 minutes, a shoulder around 1650  $\text{cm}^{-1}$  is visible after immersion in water. This peak can be assigned to bending vibration  $\delta(\text{H}_2\text{O})$ . However, the peaks around 1562 and 1433  $\text{cm}^{-1}$  as shown figure 7.2 are still visible after 15 minutes immersion in water.

Alkaline pretreated samples showed again some residual peaks of succinic acid as well as a peak at 1710  $\text{cm}^{-1}$  which can be assigned to C=O bond vibrations. Water bands are not clearly visible, but the total background is much less even around these numbers than for instance acid pretreated samples. The alkaline pretreated

sample spectrum is shown with a 4x multiplication due to its comparatively low intensity.

The spectrum for vacuum evaporated magnesium with succinic acid was added for comparison, again shown with a 4x multiplication.

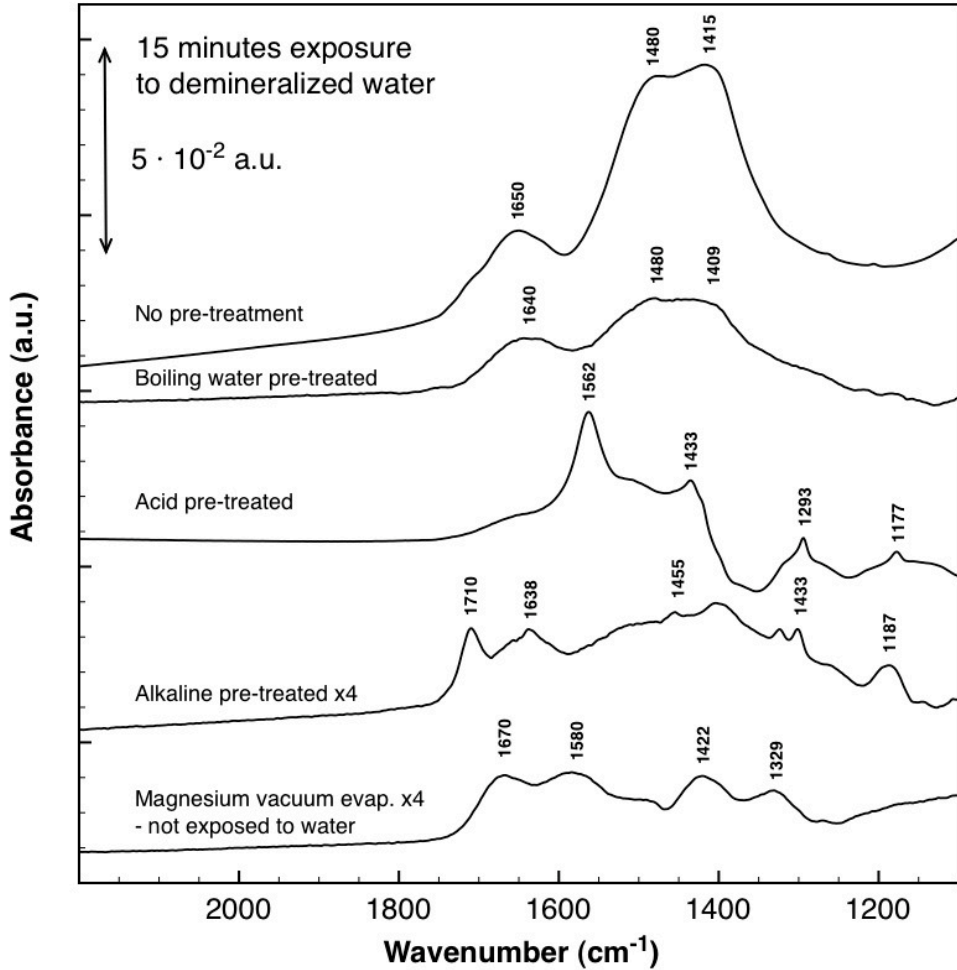


**Figure 7.3** FTIR-spectra of several pre-treated AZ31 samples bonded with succinic acid after immersion in triple deionised water for 15 minutes. For clarity, some spectra are shown with a different vertical scaling, which is indicated by the multiplication factor. Spectra were recorded with respect to a background before immersion in succinic acid.

**Table 7.2** Assignment of peaks to succinic acid interactions with the surfaces after pretreatments and exposure to water for 15 minutes from figure 7.3. Please refer to chapter 6 for the peak assignment of vacuum evaporated magnesium.

Acid Pretreated AZ31	Alkaline Pretreated AZ31	Boiling water pretreated AZ31	No pretreatment	Assignment*
-	1710	-	-	$\nu(\text{C=O})$
1650(w)	1638	1640	1650	$\delta(\text{H}_2\text{O})$
1562	-	-	-	$\nu_{\text{as}}(\text{Mg/Al-COO}^-)$
1433	1455	-	-	$\nu_{\text{s}}(\text{Mg/Al-COO}^-)$
1293	1428 1333	1480 1409	1480 1415	Associated with water

### 7.2.3 Influence of aging in air

Ambient air contains water and several organic and inorganic species. Adsorbed water blocks surface sites, which are then no longer available for organic functional groups. This could result in a decrease of the bonding capacity. Therefore, in this paragraph, the changes to the surfaces that occur due to aging in ambient air with a relative humidity of 30% are studied.

In Figure 7.4, infrared spectra are shown for AZ31 substrates aged for 1, 4, 16 and 48 hours in ambient air. The spectra show the changes that have occurred during the aging period<sup>[2]</sup>. Already after one hour, a clear band around  $1630\text{ cm}^{-1}$  is visible. This band can be assigned to adsorbed water. Also, a broad band around  $3450\text{ cm}^{-1}$  is seen and the intensity is increasing with time. This band is attributed to hydroxyl stretching  $\nu(\text{OH})$ , due to adsorbed water and hydroxide. There is a slight increase in the intensity of both bands, indicating an increase of water adsorbed to the surface as a function of aging time.

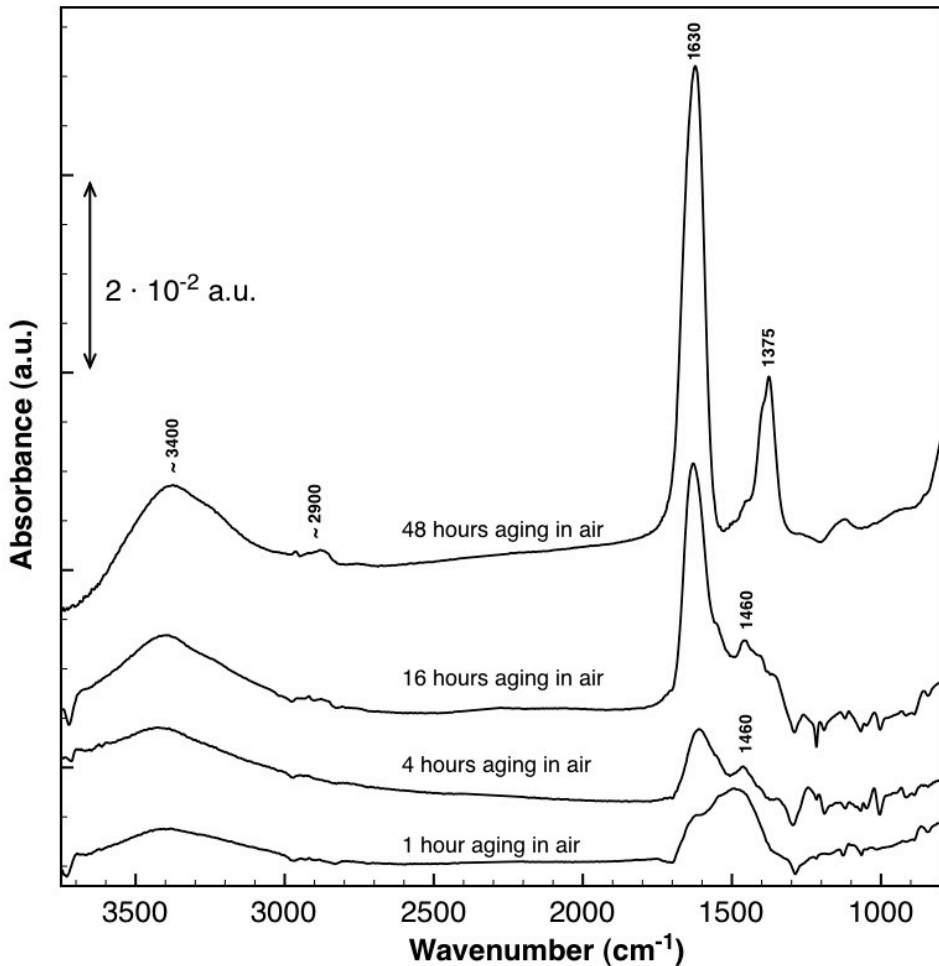


**Figure 7.4** FTIR-RAS spectra from AZ31 substrates after aging in ambient air for indicated periods. Spectra are shown with respect to a background prior to aging and therefore only show the changes that have occurred due to the aging process.

After 48 hours, in the 2850-3000  $\text{cm}^{-1}$  region, growth of peaks assigned to alkyl carbonate is visible. This indicates the presence of contamination on the surface. The band around 1369  $\text{cm}^{-1}$  is related to this and is likely a  $\delta(\text{CH}_3)$  deformation vibration of the organic contaminant.

Van den Brand found in comparable aging experiments with AA1050 a band at 960  $\text{cm}^{-1}$ . This band was growing with aging time and was assigned to the Al-O stretching vibration due to the aluminium oxide layer<sup>[2]</sup>. Although AZ31 contains approximately 3 wt.% aluminium, these peaks were not found in aging experiments on this alloy.



### 7.2.4 Bonding of succinic acid molecules on aged samples

In this paragraph, the bonding capacity of the substrates after water and organic contamination is discussed. Substrates were cleaned according to the procedure described in 3.4.5 and a new background spectrum was recorded. Please note no special pre-treatments were done to the substrates, besides the aging in air at room temperature.

In Figure 7.5, infrared spectra are shown, obtained after adsorption of succinic acid on substrates aged for 1, 4, 16 and 48 hours. Spectra are obtained with respect to a background prior to immersion in succinic acid. Therefore, they show only the changes due to adsorption and not the changes which occurred during the aging period.

Peak positions are similar to the ones found on pre-treated surfaces (see paragraph 7.2.1) and can be assigned identically: the peak around  $1600\text{ cm}^{-1}$  is assigned to the asymmetric carboxylate stretching vibration  $\nu_{\text{as}}(\text{COO}^-)$  and the broad band around  $1475\text{-}1375\text{ cm}^{-1}$  can be assigned to a combination of the symmetric carboxylate stretching vibration  $\nu_{\text{s}}(\text{COO}^-)$  and water.

The peak intensity is generally lower compared to peak intensities in the infrared spectra of succinic acid on the pre-treated surfaces. Moreover, the peak intensity is slightly decreasing with aging time. The bending vibration  $\delta(\text{H}_2\text{O})$  around  $1650\text{ cm}^{-1}$  for water molecules becomes more visible with increasing aging time.

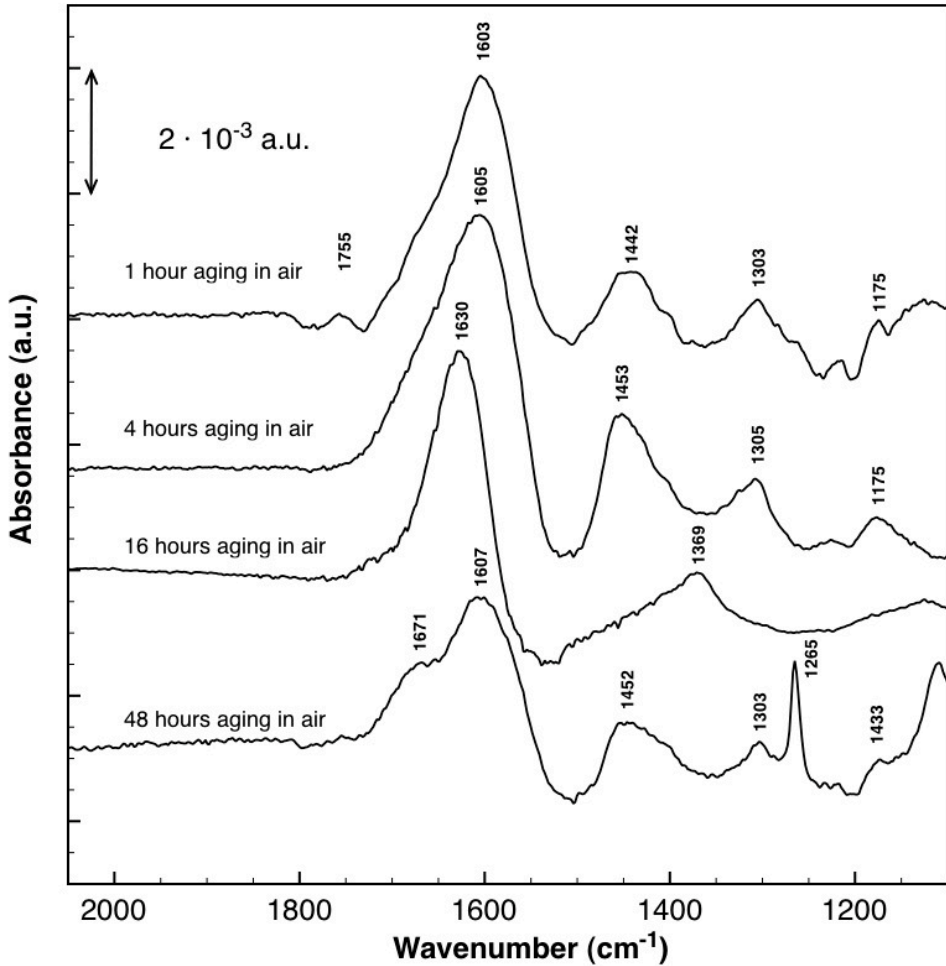


**Figure 7.5** FTIR-RAS spectra of AZ31 after the adsorption of succinic acid on substrates aged in ambient air for the indicated periods. Spectra are shown with respect to a background prior to immersion in succinic acid and therefore only show the changes due to adsorption of succinic acid.

### 7.2.5 Morphological characterization

SEM micrographs are shown in figure 7.6 to illustrate the difference in roughness for both boiling water pretreated (left image) and alkaline pretreatment. Acid pretreated samples resembled the alkaline pretreated ones. Although not as rough as the boiling water pre-treated samples, also alkaline surfaces show some kind of (nano) surface texture.

In order to determine the surface roughness more quantitatively, AFM experiments in contact mode were performed on the freshly pre-treated AZ31 surfaces. In Figure 7.7, the morphology of the differently pre-treated AZ31 surfaces are shown. The subsequently calculated surface roughness of the differently pre-treated samples is shown in Table 7.3.

The boiling pre-treated surface has an average surface roughness of about 15.80 nm and the alkaline pre-treated surface has an average surface roughness of about 4.75 nm. The average surface roughness of the acid pre-treated samples was found to be in between and of the order of 9.18 nm. SEM images of both boiling and alkaline pre-treated surfaces show similarity with images of pre-treated aluminium alloys made by Van den Brand<sup>[3]</sup> and Rider<sup>[4]</sup> respectively. The boiling pre-treated surface is covered with a dense hydroxide structure with big pores.

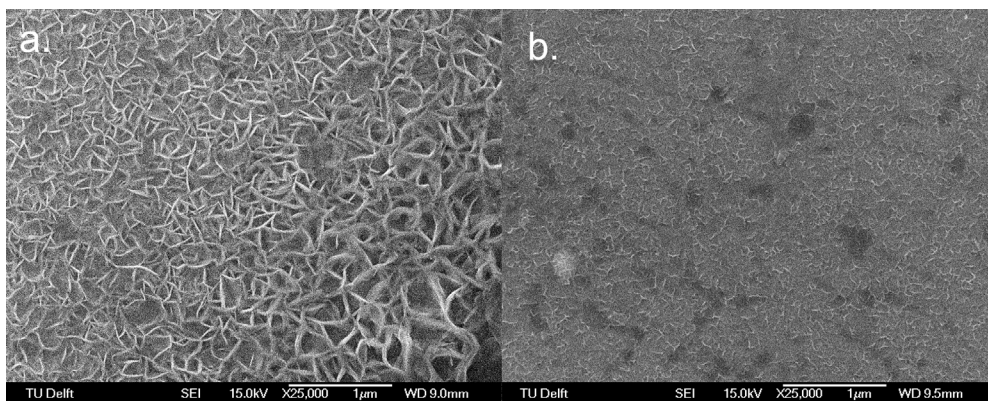


**Figure 7.6** SEM image of AZ31 substrate after immersion in a) boiling water for 60 seconds and b) NaOH pH 12.5 at a temperature of 30°C for 30 seconds.

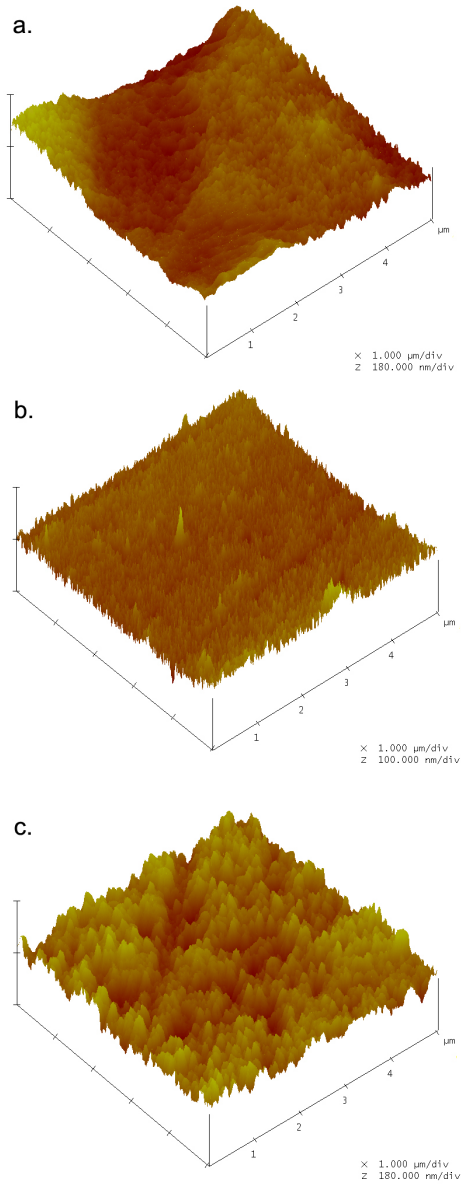


**Figure 7.7** AFM images of AZ31 after (a) acid pre-treatment, (b) alkaline pre-treatment and (c) boiling pre-treatment.

**Table 7.3** Surface roughness of the differently pre-treated samples of AZ31 as measured by AFM in contact mode.  $R_{rms}$  is the root-mean-square and  $R_{ave}$  the average roughness in nm.

Pre-treatment	$R_{rms}$ (nm)	$R_{ave}$ (nm)
Acid	11.5	9.18
Alkaline	6.02	4.74
Boiling	19.8	15.8

### 7.3 Discussion

Oxide composition of magnesium alloys varies with pre-treatment<sup>[5]</sup>. As Nordlien et al.<sup>[6]</sup> have shown, the composition of oxides formed on  $Mg_3Al$  alloys immersed in distilled water can contain up to 20 wt% of aluminium and AZ31 even up to 25 wt% versus magnesium<sup>[7]</sup>.

Blücher et al.<sup>[8]</sup> state that in the presence of water (or humid air) and carbon dioxide,  $Mg_5(CO_3)_4(OH)_2$  is formed on AZ91D surface. In this study, infrared peaks were found around 1530, 1460 and 860  $cm^{-1}$  on infrared spectra of freshly prepared AZ31. These peak positions correspond to wavenumbers found by Lu et al.<sup>[9]</sup> on pure magnesite. After cleaning, the samples were immediately used for the infrared experiments. This means that exposition to air took less than 5 minutes. Nevertheless, between the grinding step and entering the infrared chamber, carbonate was formed on the samples. Infrared spectra of AZ31 aged in air were obtained with respect to a background prior to aging, while infrared spectra of freshly prepared AZ31 were recorded with respect to a clean gold surface. During aging experiments, the carbonate peaks were not seen in the infrared spectra. This means that the amount of carbonates on the magnesium alloy surface did not increase during the aging period. Therefore, carbonates are formed on freshly prepared AZ31 almost immediately after exposition to carbon dioxide containing atmosphere. The amount of carbonates on the surface remains constant during exposition to humid air.

#### 7.3.1 Bonding of succinic acid on AZ31

Infrared spectra were presented for bonding of succinic acid on three differently prepared AZ31 substrates and a substrate without pretreatment. The broad bands around 1570  $cm^{-1}$  were assigned to the asymmetric carboxylate stretching vibration  $\nu_{as}(COO^-)$ . The broad bands around 1475-1375  $cm^{-1}$  were assigned to symmetric

carboxylate stretching vibration  $\nu_s$  ( $\text{COO}^-$ ). In the 1100-1300  $\text{cm}^{-1}$  region peaks related to succinic acid were found, although they differ in intensity and resolution. The peak around 1300  $\text{cm}^{-1}$  is attributed to  $\nu(\text{C-O})$  stretching vibration and the peaks at 1176  $\text{cm}^{-1}$  can be assigned to  $\gamma(\text{CH}_2)$  twisting as was already assigned in chapter 6 and were therefore not mentioned.

Succinic acid molecules did therefore successfully bond to the three differently pre-treated surfaces. The configuration of the succinic acid molecules was similar to the configuration on Al-Mg surfaces, namely by bridging bidentate. This configuration was discussed in section 6.2.1 and assigned to the bonds in table 7.1.

Regarding intensities of the absorption peaks of succinic acid it has to be noted that on acid pre-treated AZ31 about 4-5 times higher peak intensities were found as compared to boiling and alkaline pre-treated surfaces. Because the roughness is on a similar scale, these differences are attributed to a higher concentration of molecules on the surface.

Summarizing, the bonding on the surfaces of AZ31 can be understood as bridging bidentates on either aluminium or magnesium oxide species, like shown schematically in figure 7.8.

However, aqueous stability of succinic acid on the differently pre-treated substrates showed important differences.

### 7.3.2 Bonding stability of succinic acid on pretreated AZ31

Infrared spectra of non-pretreated and boiling water pre-treated surfaces showed similarities after immersion as shown in figure 7.3. The broad peak around 1570  $\text{cm}^{-1}$  due to asymmetric carboxylate stretching vibration  $\nu_{as}$  ( $\text{COO}^-$ ) disappeared already after immersion in water for 15 minutes. A broad combined band between 1500 and 1300  $\text{cm}^{-1}$  was introduced as well as a peak around 1650  $\text{cm}^{-1}$  attributed to water bending vibration  $\delta(\text{H}_2\text{O})$ . This indicates that succinic acid was removed from the surface of the boiling water pre-treated AZ31 samples after immersion in water. This can be explained by the fact that the resulting pseudoboehmite layers on AZ31 are not stable in water. Because of the open morphology, an alternative explanation would be that there is so much water adsorbed, that these intensities completely overshadow the succinic acid bonds.

Since the peaks assigned to succinic acid on acid pretreated surfaces are still visible after immersion, these surfaces seem to offer some resistance to water, probably because of removal of relatively more magnesium, leaving more aluminium, which is stable in water of  $\text{pH} = 7$ . Also, as can be seen in figure 7.2, the peak intensities of the absorption peaks of succinic acid on acid pre-treated AZ31

were about 4-5 times higher and therefore the amount of molecules is higher to begin with for the acid pretreated samples than for the others.

Alkaline pretreated samples showed a resistance to water between boiling water and acid pretreated samples; there are still succinic acid bonds distinguishable and even a C=O vibration. Therefore, some of the molecules are still bonded with one side of the acid group and some are displaced by water.

Combining these observations, carboxylic acid groups were found to be attached better and therefore offer more resistance to immersion in water, on acid pretreated surface than on alkaline or boiling water pre-treated AZ31.

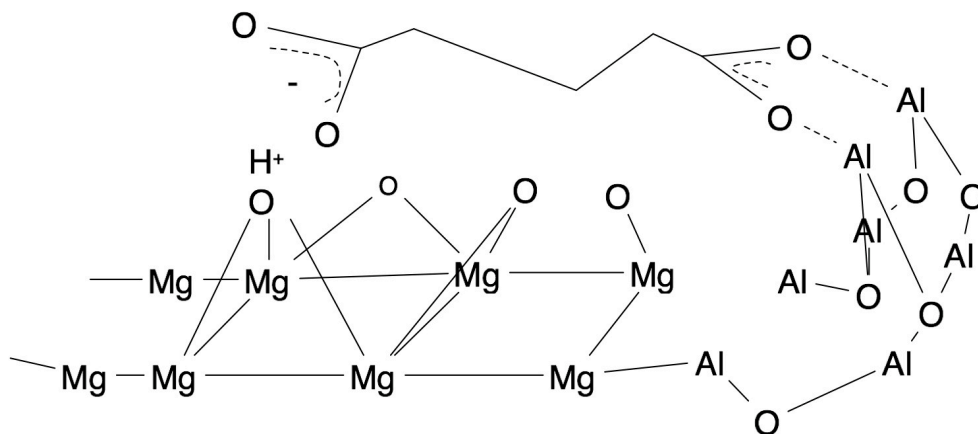


**Figure 7.8** Impression of the configuration of succinic acid molecules on a mixed Mg/Al surface.

### 7.3.3 Influence of aging on bonding

Aging of samples resulted in an increase in water and organic contamination in the spectra in figure 7.4. On this contaminated surface, it was however still possible to bond succinic acid molecules, as evidence of bonds is shown in figure 7.5. However, after 48 hours, bonding has deteriorated in a sense that water bonds around  $1650\text{ cm}^{-1}$  are displacing the succinic acid molecules. It is already known from practice that pre-treated substrates should not be left unprotected for too long if coating or adhesive bonding has to be successfully conducted.

## 7.4 Conclusions

Succinic acid was bonded to AZ31 substrates following acid, alkaline and boiling water pre-treatments. As shown with FTIR-RAS, the distances of the main carboxylic acid peaks are in the range of  $120 - 140\text{ cm}^{-1}$ . Therefore, the molecules are bonded in a bridging bidentate fashion to the surface. The question remains

which metal-oxide atoms they are bonded to, since the AZ31 alloys is known to have a complex, mixed magnesium/aluminium (hydr)oxide. However, for the acid pre-treatments, peaks were significantly higher. This cannot be attributed to a much higher roughness, as these lie in the same range for both alkaline and acid pretreatments. Therefore the assumption is that bonding takes place on more of the aluminium that is left.

After exposition of the surfaces to air up to 48 hours succinic acid still bonded to the substrate. Carbonates were formed on a freshly prepared AZ31 substrate almost immediately after exposition to an atmosphere containing CO<sub>2</sub>. During aging experiments, the amount of carbonates on the surface remained constant.

Peak intensities on infrared spectra of succinic acid on AZ31 after aging in ambient air, decreased with increasing aging times. This indicates that bonding of succinic acid to AZ31 surfaces, aged in ambient air, is deteriorating with aging time, as was seen before<sup>[2]</sup>.

The stability of the bonding of succinic acid to the acid pre-treated surface remained stable in the presence of water for immersion times of 15 minutes. In contrast, alkaline and boiling pre-treated surfaces, did not show stable bonding in the presence of water. Therefore, it can be expected that also a polymer with carboxylic acid as bonding molecules, will not show a stable bond to these surfaces when exposed to water.

### **Acknowledgements**

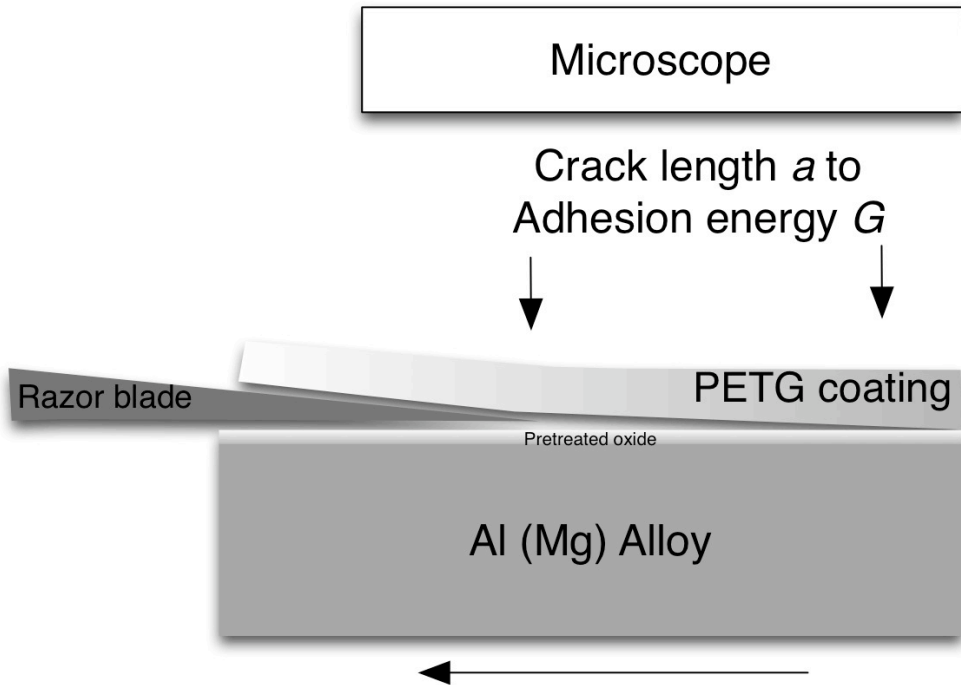
This chapter includes part of the work done by J.J. Kleikers for his TU Delft Master thesis.



## References

- [1] J. van den Brand, O. Blajiev, P. C. J. Beentjes, H. Terryn, J. H. W. de Wit, *Langmuir* **2004**, *20*, 6308.
- [2] J. van den Brand, S. Van Gils, P. C. J. Beentjes, H. Terryn, J. H. W. de Wit, *Applied Surface Science* **2004**, *235*, 465.
- [3] J. van den Brand, S. Van Gils, H. Terryn, V. G. M. Sivel, J. H. W. de Wit, *Progress in Organic Coatings* **2004**, *51*, 351.
- [4] A. N. Rider, D. R. Arnott, *International Journal of Adhesion and Adhesives* **2000**, *20*, 209.
- [5] H. A. Al-Abadleh, H. A. Al-Hosney, V. H. Grassian, *Journal of Molecular Catalysis a-Chemical* **2005**, *228*, 47.
- [6] J. H. Nordlien, K. Nisancioglu, S. Ono, N. Masuko, *Journal of the Electrochemical Society* **1996**, *143*, 2564.
- [7] J. H. Nordlien, K. Nisancioglu, S. Ono, N. Masuko, *Journal of the Electrochemical Society* **1997**, *144*, 461.
- [8] D. B. Blucher, J. E. Svensson, L. G. Johansson, M. Rohwerder, M. Stratmann, *Journal of the Electrochemical Society* **2004**, *151*, B621.
- [9] Z. Lu, A. Schechter, M. Moshkovich, D. Aurbach, *Journal of Electroanalytical Chemistry* **1999**, *466*, 203.

## Chapter 8 - Adhesion of PETG



This chapter is based on (parts of) “The influence of pre-treatments of aluminium alloys on bonding of PET coatings” by F.M. de Wit, Ö. Özkanat, J.M.C. Mol, H. Terryn and J. H.W. de Wit, published in *Surface and Interface Analysis* 42, 316–320, 2010 and furthermore reference is made to “Adhesion at Al-hydroxide-polymer interfaces: influence of chemistry and evidence for self-pinning” by W.P. Vellinga, G. Eising, F.M. de Wit, J.M.C. Mol, H. Terryn, J.H.W. de Wit and J.Th.M. De Hosson, published in *Materials Science and Engineering* 527, issue 21-22, 5637-5647, 2010

## **Synopsis**

Adhesion of PETG coatings is investigated with the novel ADCB method. This method allows for the visual characterization of the delamination crack front which can then be related to the energy necessary for delamination. Release energies after pre-treatments are compared and evaluated in relation to both the composition of the oxide from chapter 4 as well as to the semi-quantitative FTIR-RAS results from chapter 6. Also, morphological characterization by SEM of the (failed) surfaces is presented.

## 8.1 Introduction

This chapter is dedicated to the macroscopic behavior of coatings on pre-treated surfaces of AA1050 and AA5182. In this chapter, the adhesion of PETG coatings is evaluated with the novel ADCB method. As shown before, one way of protecting aluminium alloys is by using an organic coating. To obtain good protection, coatings need to be good barriers to water and gasses and have additional properties (e.g. active protection by inhibitors). It is of high importance that coatings adhere well to substrates. The adhesion and potential delamination of organic coatings on aluminium are therefore important topics in the food and beverage industry<sup>[1]</sup> and where adhesives are concerned, e.g. in transport<sup>[2]</sup>.

Some studies have combined analysis of surface composition and mechanical tests, with various pre-treatments<sup>[3, 4]</sup> and used the theory of acid-base characteristics of both substrate and several polymers on steel<sup>[5]</sup>. The delamination of coatings or adhesion is also studied using mechanical testing methods, like T-peel testing<sup>[6, 7]</sup>, pull-off and tape tests<sup>[8]</sup>, cross-hatch and n-methylpyrrolidone (NMP)<sup>[9]</sup>. Brogly et al.<sup>[10]</sup> have studied the relationship between bonding thin layers of poly(ethylene-co-vinyl acetate) (EVA) and the mechanical adhesion of EVA coatings on pure aluminium.

PETG coatings on steel were studied extensively by Van den Bosch<sup>[11]</sup>. He showed the presence of fibrils in 180° peel tests<sup>[12]</sup>.

For this chapter, substrates and a coating were chosen which were studied before: AA1050 (99.5 wt% pure Al), AA5182 (4.8 wt% Mg) from chapter 4 and glycol-modified polyethylene terephthalate (PETG)<sup>[13]</sup>. As a model molecule dimethylterephthalate (DMT) was chosen in chapter 6, since this represents the most likely and abundant bonds in a PET coating.

Surface roughness and oxide composition for pretreated AA1050 was already determined before. It was found that both acid and alkaline surface pretreatments did not result in a large increase of geometric surface area. Treatment with boiling water however showed an almost 15 times increase in roughness. This is due to the porous nature of the resulting pseudoboehmite layer. Also, oxide composition was determined with XPS. Analysis showed then that the hydroxyl fraction increased significantly for alkaline as well as for boiling water pretreatments. Table 8.1 contains the summary of these measurements done by Van den Brand<sup>[14, 15]</sup>.

The surface content of magnesium of this alloy was already shown to depend on certain heat pre-treatments by Auger Electron Spectroscopy (AES)<sup>[16]</sup> in chapter 4. After chemical pre-treatments the magnesium contents also vary<sup>[16]</sup>, which was

predicted by the Pourbaix diagrams of Al and Mg ( $\text{Mg}(\text{OH})_2$  is stable only above  $\text{pH} = 12$ )<sup>[17]</sup>.

**Table 8.1** Results of XPS and BET measurements on AA1050 samples for different pretreatments, Van den Brand et al.<sup>[14, 15]</sup>.

Pretreatment	Al 2p binding energy FWHM (eV)	OH <sup>-</sup> fraction	Geometric area increase factor
Acid	74.6	0.35	1.4
Alkaline	74.7	0.43	1.6
Boiling water	73.9	0.47 0.04 H <sub>2</sub> O	14.6

For macroscopical adhesion, the method of Asymmetric Double Cantilever Beam (ADCB) is used to study the delamination properties of the pre-treated and coated samples. This method allows for studying the crack propagation in transparent coatings in real-time using a camera<sup>[13, 18]</sup>.

This chapter extends chapter 6 by adding the comparison of quantifiable, macroscopic adhesion testing of PETG to bonding of DMT model molecules, containing the groups which are responsible for bonding of the coating to the oxide surfaces.

## 8.2 Results

### 8.2.1 Energy release rates from ADCB

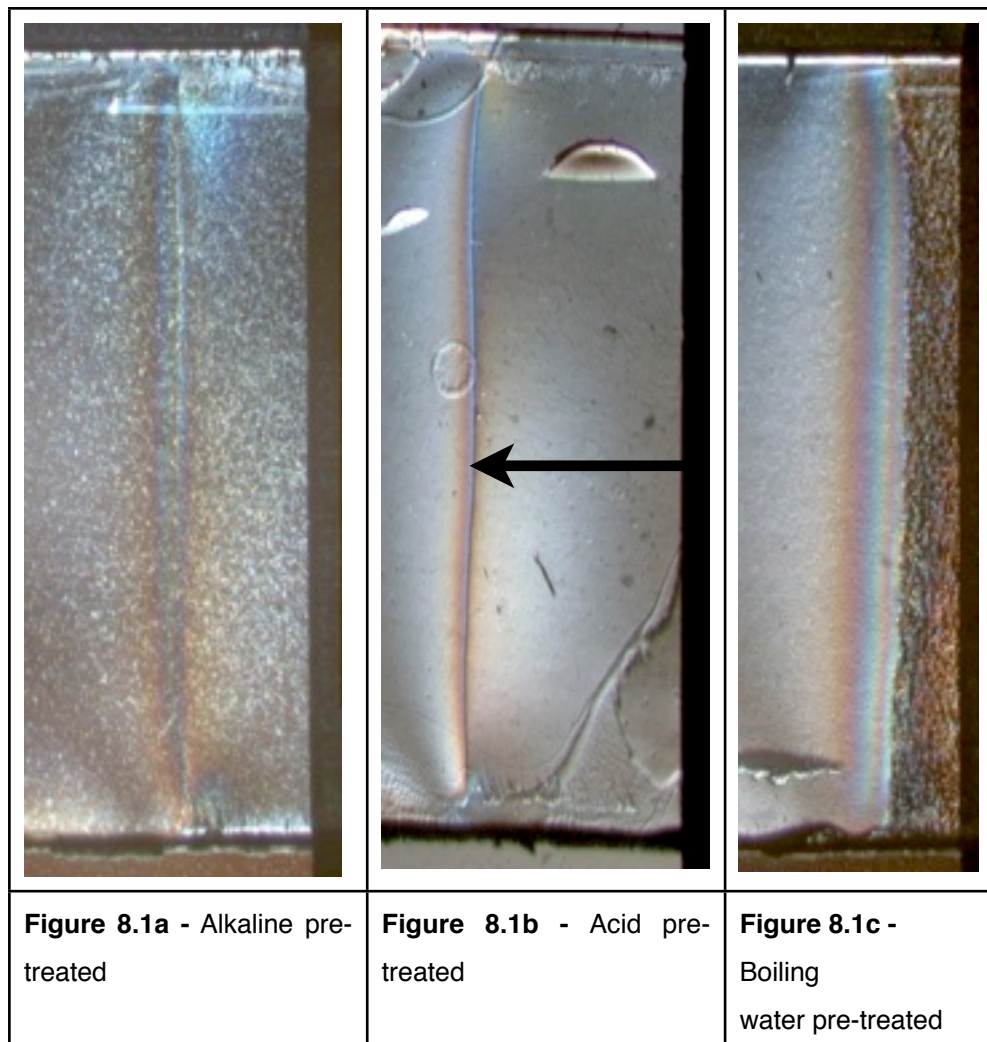
For all systems, several pretreated samples were tested with ADCB as described in chapter 3 in paragraph 3.4.3. To illustrate the outcomes, in this paragraph some typical results will be discussed.

Figures 8.1 a-c show stills taken by optical microscope of selected ADCB experiments which were found representative for the various studied systems. Since measurements were dynamic, these only show the behavior at a certain moment during the experiments on the surface. The delamination front can be observed because of a polarizer in the microscope and this is the point where the coating detached from the substrate. As can be seen in figure 8.1b, there are

several defects possible which hinder proper determination of crack length. These are e.g. closed-in bubbles from air entrapment between coating and surface, uneven crack front and pinning at the sides of the sample. Despite the presence of some flaws, energy release rates were calculated, taking into account average crack lengths. Then crack length  $a$  is determined from several stills. Crack length is determined from the knife's edge (the dark part at the right hand side of the images). The length between the edge of the knife and the delamination front is measured in pixels and converted to meters. This is used as parameter  $a$  in equation 3.1. Several points were measured over the total running time, which was as long as it took for the whole coating to delaminate, or when the length of the attached coating was close to the total crack length. Only points where no failure due to embedded air or severe asymmetrical crack-growth occurred were used. Experiments were repeated several times for the same pre-treatments.

When comparing figures 8.1 a - c, next to the delamination length, another difference can be noted. The structure of the aluminium surface varies from macroscopically even for acid pretreated to rough for boiling water pretreated. Alkaline pretreated samples showed a more homogeneous pattern. Please note, this is the surface where traces of PET coating may be left, as seen through the transparent coating, on top of the natural roughness of the pre-treated aluminium. Figures with larger magnifications of the surfaces will be shown in the next paragraph.

As for the delamination lengths, these were used as input parameter  $a$  in equation 3.1. This resulted in values as displayed in table 8.2.



**Figures 8.1a-c.** Example images from the optical microscope of each denoted pre-treated AA5182 sample. The arrow indicates the length of the crack front from the knife's edge and direction in which the front runs.

**Table 8.2.** Calculated adhesion energy  $G$  from ADCB experiments with formula 3.1 for PETG coatings on AA1050 and AA5182 averaged with standard-deviations.

Pre-treatment	AA1050	AA5182
Acid	$10 \pm 2 \text{ J/m}^2$	$8 \pm 2 \text{ J/m}^2$
Alkaline	$21 \pm 3 \text{ J/m}^2$	$30 \pm 3 \text{ J/m}^2$
Boiling	$79 \pm 15 \text{ J/m}^2$	$73 \pm 13 \text{ J/m}^2$

For both alloys boiling water pre-treated samples showed the highest energy release rates, while acid pre-treated samples showed the lowest. It can also be

observed that values of  $G$  after acid and boiling water pre-treatments are of similar magnitude for AA1050 and AA5182. Alkaline pre-treated samples showed lower energy release rates for AA1050 than for AA5182. Furthermore, both alkaline and boiling water pre-treated AA5182 showed higher energy release rates than acid pre-treated AA5182.

### **8.2.2 Morphological analysis of delamination on aluminium surfaces**

The surfaces of the tested materials were evaluated post-mortem with SEM to determine if the materials failed adhesively, cohesively or both. Figures 8.2 to 8.7 show the surfaces approximately 950 times magnified in secondary electron image (SEI) mode.

Figures 8.2 to 8.4 show an increase in polymer coverage for AA1050 material, evident from the lighter spots (due to electron accumulation because of the low conductivity). After acid pre-treatment the surface shows relatively small spots of polymer. Similar spots are found after alkaline pre-treatments, but these spots increase both in size and number as compared to acid pre-treated samples. After boiling pre-treatment, the size of the spots increases and the shapes changes to a more patchy nature. Also long-stretched sometimes triangular shapes with a spot at the start dominate the overall surface. The AA5182 samples like in figure 8.5 show almost no polymer left on the surface after acid pre-treatment. The alkaline pre-treatment images like figure 8.6 show the presence of relatively large areas with an elevated centre. Furthermore, some smearing due to possible contact with the knife blade is visible here. Finally, boiling pre-treated samples like shown in figure 8.7 showed a patchy and rough surface.

Figures 8.8 and 8.9 show a 3300 time magnification of an acid pre-treated and a 1000x magnification of an alkaline pre-treated AA5182 sample. On both a bonded patch with a ruptured extension is found. These spots appeared all over the mentioned surfaces, although at lower magnifications they are harder to distinguish.



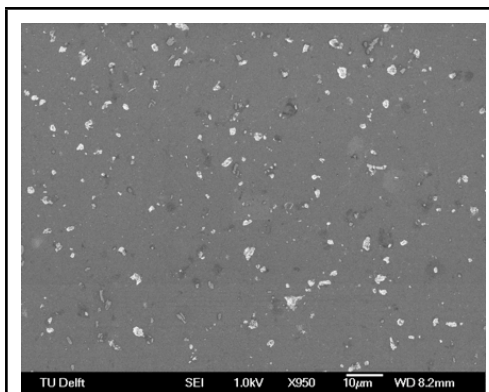


**Figure 8.2** SEM image of acid pre-treated AA1050

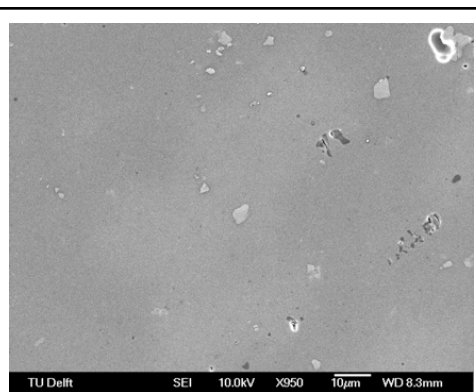


**Figure 8.5** SEM image of acid pre-treated AA5182

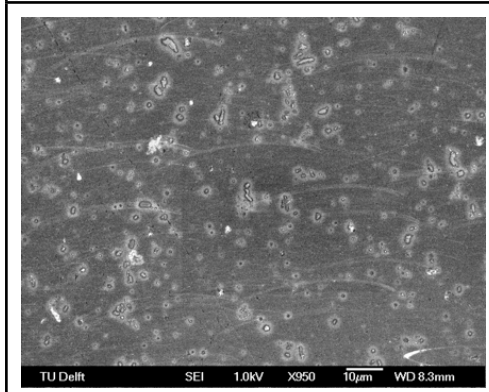


**Figure 8.3** SEM image of alkaline pre-treated AA1050

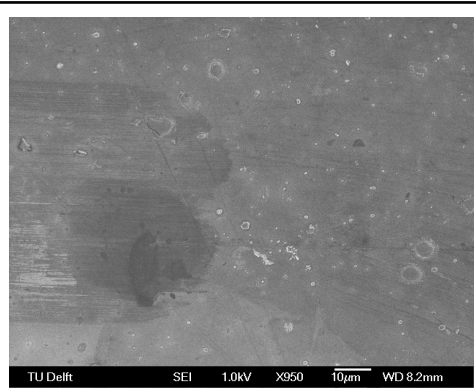


**Figure 8.6** SEM image of alkaline pre-treated AA5182

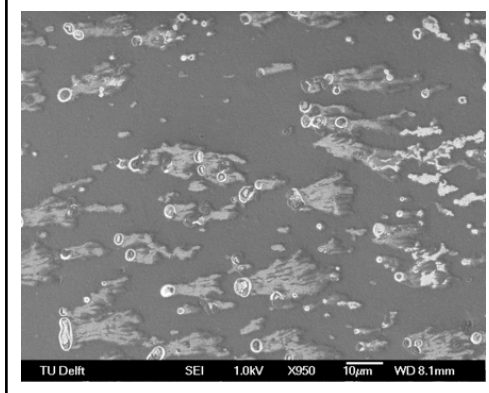


**Figure 8.4** SEM image of boiling pre-treated AA1050

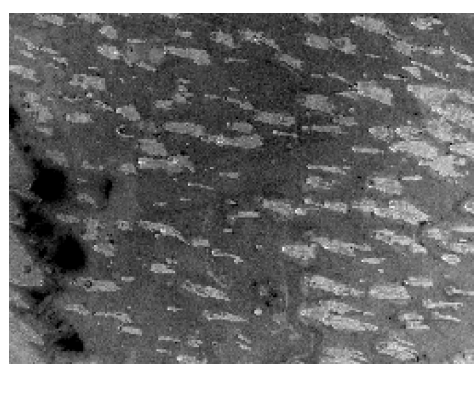


**Figure 8.7** SEM image of boiling pre-treated AA5182 (similar scale as 8.6)

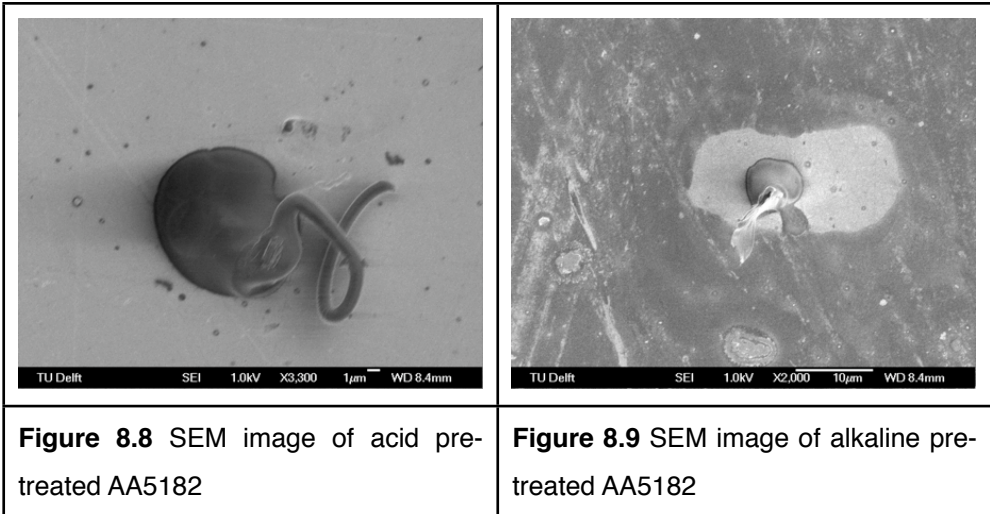


Table 8.3 contains the visually estimated percentages of failure mode as determined from post-mortem SEM images. For both alloys, adhesive failure was the dominant mode after acid and alkaline pre-treatments. Because the large amount of PETG left on the boiled water pretreated samples, the failure mode was shifted increasingly to cohesive failure.

**Table 8.3.** Estimated percentages (%) of cohesive/adhesive failure determined visually from SEM images.

Pre-treatment	AA1050	AA5182
Acid	10/90	5/95
Alkaline	20/80	30/70
Boiling	40/60	80/20

## 8.3 Discussion

### 8.3.1 Interpretation of ADCB results

Acid pretreatment showed the lowest adhesion energy for both AA1050 as well as AA5182 samples. The acid pre-treated samples of the two alloys furthermore showed little difference in adhesion energy. Therefore, the behavior can be considered similar: adhesion is relatively poor. The fact that these energies are of comparable strength, is reasonable because the surface of AA5182 is depleted of Mg after acid treatment and the chemistry of both surfaces has become rather similar. PETG coatings were assumed to be Lewis bases, determined by inverse

gas chromatography (IGC)<sup>[19]</sup>. Since adhesion clearly is possible with a smooth surface of pure aluminium (IEP at pH = 9.5)<sup>[20]</sup>, it is tentatively assumed that the polymer is indeed a weak base.

Alkaline pretreated surfaces of AA1050 showed a higher adhesion energy than the acid pretreated ones (Table 8.2). This is attributed to the increased density of hydroxyl groups on the surface as was shown in XPS measurements<sup>[15]</sup>. This explains also why for an alkaline pre-treatment, adhesion increases: a more alkaline surface adheres better to a less alkaline polymer. The difference of almost a factor 2 between the AA1050 and the AA5182 alloys is assumed to be due to the difference in surface composition as found by AES depth profiling. Magnesium is an even stronger base than aluminium (IEP at pH > 12) <sup>[21]</sup> and it is therefore assumed that attractive forces are higher, there are more bonding possibilities or they are more abundant. Furthermore, magnesium hydroxides are stable above pH = 12.

The boiling water pre-treatment produced a pseudoboehmite structure of small needle-like oxides with a high surface area as expected<sup>[22]</sup>. AES measurements from chapter 4 on AA5182 indicated that there is negligible magnesium content in the pseudo-boehmite layer, so presumably surface chemistry of the pseudo-boehmite layers on AA1050 and AA5182 is similar. Judging from SEM images their geometry is also similar. Together this explains the fact that the energy release rates are of similar magnitude. There is more variation in adhesion energy, because of a more uneven front as can be seen in 8.1c. Macroscopical roughness can even be observed in figure 8.1c. where a considerable roughening is visible underneath the coating at the interface. Also note the much smaller distance of the delamination front from the knife. The better adhesion is a result of very high number of OH groups (strong base) in the pseudoboehmite as well as an increased surface area. Due to the larger difference in IEP value between the oxide and the PETG coating stronger hydrogen bonds are expected to form<sup>[23]</sup>, improving adhesion.

Overall, adhesion energies on the boiling water pretreated surfaces are the highest, regardless of alloy.

It was already reported in literature on AA1050 with epoxy<sup>[4]</sup> that boiling results in better adhesion as compared to some organic molecule pre-treatments. Also boiled AA2024 with epoxy adhesive gave better results than without boiling<sup>[7]</sup>. Lunder and coworkers<sup>[24]</sup> have also found that an alkaline pre-treatment combined with desmutting of an AA6060 alloy can result in a better adhesion of epoxy, better than chromating and on par with Ti/Zr pre-treatments.

Additionally, Kinloch and coworkers<sup>[25]</sup> have found that although magnesium might increase the initial adhesion of an epoxide adhesive, the more magnesium at the surface, the more sensitive the joint is to environmental influences. This can also be

linked to the poor carboxylic acid bonding stability in water on AZ31 that was reported in chapter 7.

Recently, McCafferty<sup>[21]</sup> has shown that there is a correlation between the isoelectric point (IEP) of the surface of a metal oxide and adhesion of acid (pressure sensitive adhesive (PSA), Scotch) and alkaline coatings (poly (methyl methacrylate), PMMA). The adhesion on different (pure) metals was studied, such as Ti, Fe and Al. PMMA (alkaline) coatings were found to adhere significantly better to acid surfaces than to alkaline surfaces. And vice versa, acid coatings adhered better to alkaline than to acid surfaces. Also, epoxy coatings were shown before to adhere best after boiling in water, rendering the surface more alkaline<sup>[7]</sup>.

Adhesion energy of adhesively joint bonds on aluminium alloy were already reported to be more than 3000 J/m<sup>2</sup>, although determined with a tapered-double cantilever-beam (TDCB)<sup>[2]</sup>. Epoxy adhesive on boiled samples showed adhesion energy around 1400 J/m<sup>2</sup> <sup>[2]</sup>. These are designed for bonds with high loads, whereas coatings usually are not loaded mechanically. An exception is the food- and beverage industry. Strålin and Hjertberg<sup>[26]</sup> have found that for T-peel tests on LDPE foils bonded to aluminium foil, cohesive failure of the LDPE could be achieved by pretreating the aluminium foil with boiling water for 60s. Furthermore, they found a correlation between application temperature and adhesion energy, which they explained by more penetration into the pseudoboehmite layers.

The considerably lower energies that were found in these experiments are due to the fact the studied system was not designed with high loading in mind but mainly to show the differences between pretreatments.

Finally, too high adhesion energies would lead to very small values of  $a$  in an ADCB experiment, which would make measuring precise delamination lengths much more inaccurate.

### **8.3.2 Morphological analysis of delamination on aluminium surfaces**

Comparing the pre-treatments between the AA1050 and AA5182 alloys, acid pretreatment showed a similar (low) level of adhesion energy. However, from SEM images, it is clear that a slightly different mechanism is responsible for the bonding at a molecular level. In the AA1050, an average bonding on the whole surface had taken place, where locally the coating was attached, but failure was dominated by adhesive failure. While on the AA5182 the majority of the failure can be classified as adhesive failure, on a microscopic level, the coating failed cohesively, i.e. after plastic deformation of a locally well-adhering spot, like can be seen in figure 8.8.

Alkaline pre-treatment resulted in a better adhesion for both alloys, however, again the bonding mechanism is different: the AA1050 alloy displays a rather large amount of small areas of well-bonded spots. The AA5182 alloy showed larger patches which adhered well and failure took place in the centre of a patch. Again, the coating was elongated and failed after plastic deformation. It is unclear if the shorter and more rough failure at the tip of the extension is because of the better adhering of the surrounding patch or if this is due to higher forces because of the larger area. It is however tentatively assumed that local phenomena observed in SEM of bonding in patches on AA5182 suggest that local composition of the metal oxide or polymer is more favorable for bonding.

The greater change in failure mode is observed for the boiling pre-treatment. Here, AA1050 displays a smeared-out adhesive patch, at the beginning of which there is a locally deformed piece of coating. The AA5182 failure mode was much more patchy, where larger areas were cohesively destroyed. As shown by Vellinga et al.<sup>[27]</sup> there are many regimes in which the polymer can behave quite different from the bulk on these small scales. This is evidence of local concentration of adhesive bonding to the extent that not the adhesive strength, but rather the local plastic deformation is favored to take up the (macroscopic) delamination energy.

On the boiled samples there are comet shaped features, of which the “head” is centered probably on a precipitate and the “tail” stretches from the “head” in the direction opposed to the crack front movement. This has been named microscopic self-pinning in literature<sup>[28]</sup>. It was shown by Vellinga et al.<sup>[27]</sup> that a broken hydroxide surface resulted, as aluminium was found on the PETG coating side by SEM-EDX. This would suggest a better adhesion of the coating to the oxide than the oxide to the underlying coating. Another possibility is that the PETG forms a interphase with the pseudoboehmite. Since this mixed material has a considerably higher Young’s modulus than the PETG (aluminium oxide E-modulus is in the range of 350GPa), much less elongation is possible. Failure will then be brittle as opposed to the necking behavior of PETG. This follows the rationale of 2.3.6 and figure 2.9. In literature, examples of cohesive failure of aluminium oxides are abundant, but more related to the behavior of anodizing layers. These highly loaded layers for e.g. aerospace adhesive bonding applications, are known to fail when too thick.

### **8.3.3 Comparison to FTIR-RAS results from chapter 6**

As shown in chapter 6, quality of bonding of DMT molecules varied with pretreatment. FTIR-RAS measurements were an average of interactions on approximately 1 cm<sup>2</sup> of surface, while the ADCB data was also collected over a

similar sized surface. Recall figure 6.7 and 6.8, where FTIR-RAS spectra of DMT bonding on pretreated substrates were shown. Here, relatively speaking, the acid surfaces showed no discernible FTIR response on AA1050 and very low peaks were observed on AA5182. For alkaline pretreated surfaces, both AA1050 and AA5182 showed clear FTIR response, which was attributed to carboxylic bonding. FTIR signals on AA5182 were significantly more pronounced than on AA1050, leading to the speculation that there were more molecules present and bonded on the surface of AA5182. FTIR signals for boiling water pretreated surfaces were of a similar magnitude as those on the alkaline pretreated surfaces. Because of the behavior in ADCB experiments, where adhesion was quantified, it can be reasoned that bonding of representative molecules at least gives a direction of adhesion for a polymeric coating system. While it is not possible to predict the overall quality, a distinction can be made between poor chemical bonding, leading to predominantly adhesive failure, and good chemical bonding, leading to mixed cohesive /adhesive failure

#### **8.4 Conclusions**

Adhesion of PETG coatings depending on pre-treatment of AA1050 and AA5182 substrates was investigated. The results of ADCB tests showed measurable and reproducible differences in delamination energy in the pre-treated samples after adhesion of PETG and subsequent delamination. The energy used for delamination of the PETG coating is about a factor two higher for the Mg-rich AA5182 than for the AA1050 after alkaline pre-treatment. Boiling water treatment showed considerably higher adhesion energy values. This is attributed to both chemical composition of the surface and a surface area increase. However, the regime with which the coatings fail varies locally. In some of the samples, delamination over large areas is observed, leading to more cohesive failure in the polymer layer or mixed pseudoboehmite/PETG interphase failure. Furthermore, local delamination has shown several interesting features, where fibrils, gum-like threads, were still locally bonded. One can imagine these to have stretched until failure, passing through the macroscopically observable behavior or thread-like fibrils as was shown before in literature. Since these isolated spots show such high bonding and subsequent adhesion, it is speculated that the local composition of the oxide was favorable for bonding. This might be the location of an intermetallic particle with a different oxide composition.

Failure on the pseudoboehmite, boiled water pretreated surfaces, showed the highest energy for delamination. After closer examination with SEM, it was found

that not only the coating failed cohesively at some spots, also the oxide layer itself. This means that the adhesion in total did not reach its full height; the oxide was the weak link in the chain, probably because of its brittleness and relatively high thickness. An interphasial region might be present, which has properties of the combined components: aluminium oxides and PETG. This shows that, although chemical bonding is necessary to obtain adhesion, in the complete system, the weakest link is the point that fails because it cannot dissipate the energy that is put into it from macroscopic loading.

Finally, FTIR spectra from chapter 6 showed that bonding of DMT molecules could occur by bridging bidentate bonds of carboxylic acid (formed after saponification of the ester bonds in the presence of the strong base on the surface). Both for AA1050 and AA5182, alkaline and boiling pre-treatment showed evidence of bonding, while acid pre-treatments did not. The chemical bonding of DMT molecules on the aluminium surfaces was successfully linked to macroscopical adhesion behavior of PETG coated systems, because where the coating failed predominantly adhesively, no or little bonding was found.

### **Acknowledgements**

Gert Eising is kindly acknowledged for the work on the ADCB setup and the testing. Thanks goes out to Willem-Pier Vellinga for his help with the interpretation of the data and SEM images and his submission as first author of the journal article. Furthermore I would like to thank prof. De Hosson for his stimulation and approval of the internship of Gert Eising at Delft University of Technology.

---

**References**

- [1] G. Olafsson, M. Jagerstad, R. Oste, B. Wesslen, *Journal of Food Science* **1993**, *58*, 215.
- [2] J. K. Jethwa, A. J. Kinloch, *Journal of Adhesion* **1997**, *61*, 71.
- [3] G. W. Critchlow, D. M. Brewis, *International Journal of Adhesion and Adhesives* **1996**, *16*, 255.
- [4] J. van den Brand, S. Van Gils, P. C. J. Beentjes, H. Terryn, V. Sivel, J. H. W. de Wit, *Progress in Organic Coatings* **2004**, *51*, 339.
- [5] J. F. Watts, M. M. Chehimi, E. M. Gibson, *Journal of Adhesion* **1992**, *39*, 145.
- [6] D. M. Brewis, G. W. Critchlow, *International Journal of Adhesion and Adhesives* **1997**, *17*, 33.
- [7] C. Spadaro, C. Dispenza, C. Sunseri, *International Journal of Adhesion and Adhesives* **2008**, *28*, 211.
- [8] S. M. Mirabedini, J. D. Scantlebury, G. E. Thompson, S. Moradian, *International Journal of Adhesion and Adhesives* **2005**, *25*, 484.
- [9] J. van den Brand, S. Van Gils, H. Terryn, V. G. M. Sivel, J. H. W. de Wit, *Progress in Organic Coatings* **2004**, *51*, 351.
- [10] M. Brogly, M. Nardin, J. Schultz, *Journal of Adhesion* **1996**, *58*, 263.
- [11] M. J. van den Bosch, PhD thesis thesis, Interfacial delamination in polymer coated metal sheet, Eindhoven University of Technology (Eindhoven), **2007**,
- [12] M. J. van den Bosch, P. J. G. Schreurs, M. G. D. Geers, *Journal of the Mechanics and Physics of Solids* **2008**, *56*, 3259.
- [13] W. P. Vellinga, A. Fedorov, J. T. De Hosson, *Journal of Computer-Aided Materials Design* **2007**, *14*, 37.
- [14] J. van den Brand, O. Blajiev, P. C. J. Beentjes, H. Terryn, J. H. W. de Wit, *Langmuir* **2004**, *20*, 6318.
- [15] J. van den Brand, P. C. Snijders, W. G. Sloof, H. Terryn, J. H. W. de Wit, *Journal of Physical Chemistry B* **2004**, *108*, 6017.
- [16] F. M. de Wit, J. M. C. Mol, H. Terryn, J. H. W. de Wit, *Journal of Adhesion Science and Technology* **2008**, *22*, 1089.
- [17] M. Pourbaix, *Atlas of Electrochemical Equilibria in Aqueous Solutions* **1966**, Pergamon Press, Oxford.
- [18] B. Bernard, H. R. Brown, C. J. Hawker, A. J. Kellock, T. P. Russell, *Macromolecules* **1999**, *32*, 6254.



- [19] L. Jia, Y. P. Wang, B. Wang, M. J. He, Q. R. Zhang, B. L. Shi, *Journal of Macromolecular Science Part B-Physics* **2008**, *47*, 378.
- [20] E. McCafferty, J. P. Wightman, *Journal of Colloid and Interface Science* **1997**, *194*, 344.
- [21] E. McCafferty, *Journal of the Electrochemical Society* **2003**, *150*, B342.
- [22] R. S. Alwitt, *In Oxides and Oxide Films vol. 4* **1976**, J.W. Diggle A.K.Vijh (eds).
- [23] J. C. M. Bolger, A. S. , *Molecular structure and electrostatic interaction at polymer-solid interfaces*, Elsevier, New York, **1969**.
- [24] O. Lunder, F. Lapique, B. Johnsen, K. Nisancioglu, *International Journal of Adhesion and Adhesives* **2004**, *24*, 107.
- [25] A. J. Kinloch, H. E. Bishop, N. R. Smart, *Journal of Adhesion* **1982**, *14*, 105.
- [26] A. Stralin, T. Hjertberg, *Journal of Adhesion Science and Technology* **1993**, *7*, 1211.
- [27] W. P. Vellinga, G. Eising, F. M. de Wit, J. M. C. Mol, H. Terry, J. H. W. de Wit, J. T. M. de Hosson, *Materials Science and Engineering a-Structural Materials Properties Microstructure and Processing* **2010**, *527*, 5637.
- [28] T. D. Bruns, L. C. Grubisha, J. M. Trappe, J. F. Kerekes, E. C. Vellinga, *Mycologia* **2010**, *102*, 438.

## **Chapter 9 - Summarizing conclusions**



## Introductory chapters

As described in the chapter 1, adhesion is a very important field of expertise, albeit very wide. Previous research with a similar approach, i.e. study of molecular *bonding* and macroscopic coating *adhesion* on a relatively pure aluminium alloy, indicated that the two are linked. Varying pretreatments and thus the chemical composition of the oxides (especially the OH<sup>-</sup> concentration) was found to lead to differences in bonding of polymer-like molecules. Macroscopically, it was established qualitatively that an increase in OH<sup>-</sup> at the surface also increased macroscopic adhesion.

However, aluminium alloying elements and their effect on both bonding as well adhesion were not taken into consideration. Therefore, the research of this thesis is an extension to the previous work, studying the adhesion of polymer coatings and bonding of representative model molecules on two aluminium alloys. As alloying element magnesium was chosen because of its relatively high solid solubility in aluminium and its homogeneous distribution (precipitates are approximately 1 - 5  $\mu\text{m}$ ) and its industrial relevance. So choices were made for substrates, model molecules and coatings. A nearly pure Al-alloy (99.5 wt% Al), which was studied before and an Al-Mg alloy (4.8 wt% Mg) were compared. Representative molecules and coatings were chosen. Also, bonding behavior on an Mg-Al alloy was studied.

Pre-treatments were given to the alloys and the bonding of molecules was compared *qualitatively* while the macroscopic adhesion of two coatings was studied *quantitatively*. For one system both properties were coupled, i.e. the bonding of the molecules was linked to macroscopic adhesion.

A schematic overview of the contents of the thesis was given in figure 1.1.

In chapter 2 an overview of the literature related to the background of the work shown in this thesis was given. In this chapter a description was given of the relevant properties of oxides on aluminium alloys with an extensive discussion on theories of bonding and adhesion. Finally some macroscopic testing methods were evaluated.

In chapter 3 all experimental information was given, including details of materials, surface treatments and equipment used.

## Surface Characterization (chapters 4 and 5)

The concentration of magnesium in oxide surfaces of aluminium-magnesium alloy AA5182 can be changed by different pre-treatments. As already reported in literature, both heat pre-treatments as well as chemical pre-treatments change the composition of oxides of aluminium alloys. For AA5182, heat pre-treatments,

especially if carried out for long times, increase the concentration of magnesium at the surface most at elevated temperatures. After 11 days at 200°C, the ratio Mg:Al reaches 1:1 at the surface. After the 200°C treatment, magnesium is present almost exclusively, tentatively in the form of  $\text{Mg}(\text{OH})_2$  due to reaction with the atmospheric water.

Chemical pre-treatments also alter the surface, by favorably removing either aluminium or magnesium. Alkaline pre-treatment enriches the surface considerably in magnesium (hydr)oxide, higher than the level of aluminium oxide. However, this is probably present in a thick smut. Boiling completely removes the magnesium and leaves a thick pseudoboehmite layer. Acid pre-treatment mostly removes the magnesium, resulting in a thin  $\text{Al}_2\text{O}_3$  oxide. And finally, dehydroxylating results in the forming of a magnesium metal surface, where neither magnesium nor aluminium oxides are present. Schematically, the overview of the results is shown in figure 9.1.

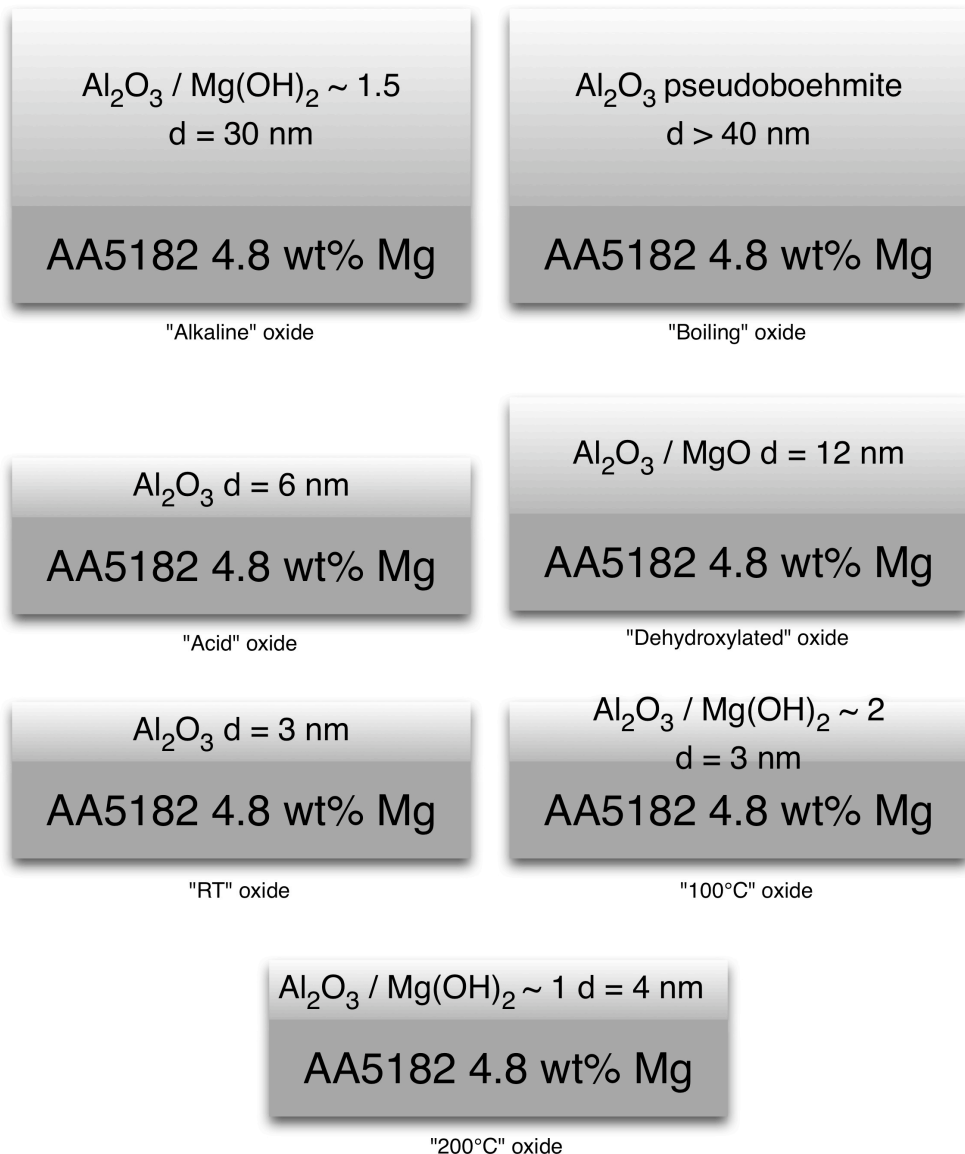


**Figure 9.1** Graphical overview of composition as determined by AES after given pre-treatments (copy of figure 4.4)

Next in chapter 5, open circuit potential (OCP) measurements were used to determine the IEPS of various pretreated surfaces of AA1050 and AA5182. First, the relation between  $E_{\text{pit}}$  and IEPS and was established from revisiting the literature. Working under the assumption that in a chloride containing electrolyte,  $E_{\text{corr}}$  as determined in OCP measurements equals  $E_{\text{pit}}$ , results of OCP measurements on several pre-treated substrates were discussed. Determining

initial and final OCP after 24/48 hours in  $K_2SO_4$  electrolyte showed the presence of Mg (enrichment) in AA5182 samples by lower OCP values as predicted by theory.

A clear relation between measured final OCP values ( $E_{corr} = E_{pit}$ ) and IEPS was established in acidified chloride containing electrolytes. Calculations using AES information on initial surface elemental concentrations (chapter 4), based on  $E_{pit}$  resulted in reasonable oxide compositions. The presence of  $Mg(OH)_2$  and  $MgCO_3$  was quantified for all pretreated samples, in good agreement with the tentative presence of these species as discussed in chapter 4.

Prediction of  $E_{pit}$  from  $E_g$  and IEPS or  $pH_{pzc}$  was shown to be possible only if one does take into account the mixed nature of the oxides and carbonates on the surface based on preexisting knowledge from other sources. When this however is taken into account, fast and simple OCP measurements, can show to some extent quantitatively the composition of mixed Al/Mg surfaces.

### **Nanoscopic/molecular interactions at the interface (chapters 6 and 7)**

#### *Bonding of succinic acid on different surfaces*

With FTIR-RAS it was shown that succinic acid molecules can bond to vacuum evaporated aluminium and magnesium as well as to AA5182 surfaces. The mode in which they bond depends on the composition of the surface. Surfaces rich in magnesium display the same properties in this respect as the ones rich in aluminium.

Succinic acid molecules on the various samples, all pretreated AA5182 as well as pure vacuum-evaporated aluminium and magnesium, show a similar bonding, i.e. a mixed unidentate and bridging bidentate configuration. There are small differences in the peak-to-peak distances due to the differences in the oxide configuration, be it more magnesium or more aluminium rich. The general trend points in the direction of a smaller difference in wavenumbers for magnesium and heat-treated AA5182. This is due to the difference in oxide configuration that varies with the Al/Mg ratio.

Enriching the surface in magnesium clearly shows that the unidentate configuration on magnesium adds a peak in the spectrum to the existing mixed uni- and bidentate state on aluminium-magnesium alloys. For all substrates bonding was observed in accordance with the discussion in chapter 2 where it was established that a predominant ionic interaction would take place.

#### *Bonding of DMT on different surfaces*

The influence of the pre-treatment of AA1050 and AA5182 on bonding of DMT molecules and PETG coatings on these alloys was investigated. FTIR spectra

showed that bonding of DMT molecules could occur by bridging bidentate bonds of carboxylic acid with Lewis acid-base interactions (formed after saponification of the ester bonds in the presence of the strong base on the surface). Both for AA1050 and AA5182, alkaline and boiling pre-treatment showed bonding, while for acid pre-treatments this could not be detected. This is in accordance with expectations as discussed in chapter 2 where for DMT (with  $pK_B = -7.2$ ) only weak dipole interactions would result with such surfaces. Results of mechanical testing of the adhesion of PETG coatings to these surfaces are discussed later, where the chemical bonding of DMT molecules on the aluminium surfaces will be linked to macroscopical adhesion behavior of PETG coated systems.

#### *Bonding and stability of succinic acid on magnesium alloy*

Succinic acid was bonded to AZ31 substrates following acid, alkaline and boiling water pre-treatments. As shown with FTIR-RAS, the distances of the main carboxylic acid peaks are in the range of 120 - 140  $\text{cm}^{-1}$ . Therefore, the molecules are bonded in a bridging bidentate fashion to the surface. The question remains which metal-oxide atoms they are bonded to, since the AZ31 alloys is known to have a complex, mixed magnesium/aluminium (hydr)oxide. However, for the acid pre-treatments, peaks were significantly higher. This cannot be attributed to a much higher roughness, as these lie in the same range for both alkaline and acid pretreatments. Therefore the assumption is that bonding takes place on more of the aluminium that is left.

After exposition of the surfaces to air up to 48 hours succinic acid still bonded to the substrate. Carbonates were formed on a freshly prepared AZ31 substrate almost immediately after exposition to an atmosphere containing  $\text{CO}_2$ . During aging experiments, the amount of carbonates on the surface remained constant.

Peak intensities on infrared spectra of succinic acid on AZ31 after aging in ambient air, decreased with increasing aging times. This indicates that bonding of succinic acid to AZ31 surfaces, aged in ambient air, is deteriorating with aging time.

The stability of the bonding of succinic acid to the acid pre-treated surface remained stable in the presence of water for immersion times of 15 minutes. In contrast, alkaline and boiling pre-treated surfaces, did not show stable bonding in the presence of water. Therefore, it can be expected that also a polymer with carboxylic acid as bonding molecules, will not show a stable bond to these surfaces when exposed to water. This is in accordance with the calculations in chapter 2 that resistance of succinic acid to water displacement on  $\text{Al}_2\text{O}_3$  will be limited to a pH



range of 4-8, while for  $\text{Mg}(\text{OH})_2$  it is a range of 4-12. However the  $\text{Mg}(\text{OH})_2$  is not stable below  $\text{pH}=12$ , therefore bonding will be undermined by Mg dissolution.

### **Macroscopical/mechanical testing of adhesion (chapter 8)**

Adhesion of PETG coatings depending on pre-treatment of AA1050 and AA5182 substrates was investigated. The results of ADCB tests showed measurable and reproducible differences in delamination energy in the pre-treated samples after adhesion of PETG and subsequent delamination. The energy used for delamination of the PETG coating is about a factor two higher for the Mg-rich AA5182 than for the AA1050 after alkaline pre-treatment. Boiling water treatment showed considerably higher adhesion energy values. This is attributed to both chemical composition of the surface and a surface area increase. However, the regime with which the coatings fail varies locally. In some of the samples, delamination over large areas is observed, leading to more cohesive failure in the polymer layer or mixed pseudoboehmite/PETG interphase failure. Furthermore, local delamination has shown several interesting features, where fibrils, gum-like threads, were still locally bonded. One can imagine these to have stretched until failure, passing through the macroscopically observable behavior or thread-like fibrils as was shown before in literature. Since these isolated spots show such high bonding and subsequent adhesion, it is speculated that the local composition of the oxide was favorable for bonding. This might be the location of an intermetallic particle with a different oxide composition.

For the pseudoboehmite, boiled water pretreated surfaces, the highest delamination energy was found. After closer examination with SEM, it was found that not only the coating failed cohesively at some spots, also the oxide layer itself. This means that the adhesion in total did not reach its full height; the oxide was the weak link in the chain, probably because of its brittleness and relatively high thickness. An interphasial region might be present, which has properties of the combined components: aluminium oxides and PETG. This shows that, although chemical bonding is necessary to obtain adhesion, in the complete system, the weakest link is the point that fails because it cannot dissipate the energy that is put into it from macroscopic loading.

Finally, FTIR spectra from chapter 6 showed that bonding of DMT molecules could occur by bridging bidentate bonds of carboxylic acid (formed after saponification of the ester bonds in the presence of the strong base on the surface). Both for AA1050 and AA5182, alkaline and boiling pre-treatment showed evidence of bonding, while acid pre-treatments did not. The chemical bonding of DMT molecules on the

aluminium surfaces was successfully linked to macroscopical adhesion behavior of PETG coated systems, because where the coating failed predominantly adhesively, no or little bonding was found.



---

## Epilogue and outlook

Adhesion is a multi-material, multi-scale problem. This makes it a very exciting topic for materials scientists. Variations in materials are however almost infinite. In this thesis therefore specifics valid only for chosen aluminium/magnesium systems were shown. It was concluded that both chemical *bonding* of DMT model molecules to the mentioned metallic surfaces and mechanical *adhesion* of PETG coatings depend on the kind of pretreatment (surface composition) of the aluminium alloy. The presence of an alloying element (Mg) complicates the experiments, since it can change the composition drastically, depending on pretreatment. Furthermore, while *bonding* is a necessity, *adhesion* (energy) also depends on the dissipation of energy in the polymer system. The proper choice and formulation of coatings are therefore not only important from a corrosion protection point of view, but also for the mechanical properties related to adhesion.

It can be expected that similar results could be obtained for different materials combinations.

This thesis was building on previous *kennis en kunde* (loosely translated as: knowledge and experience) in the corrosion groups at Delft University of Technology and Vrije Universiteit Brussel on aluminum alloys. At these two groups, more experimental work is in progress on a variety of materials and systems, which is confirming the expectations.

More generally, trends of course can and were indicated for any combination of metals and polymers like was done in papers by McCafferty: “acid” polymers adhere well to “alkaline” surfaces and vice versa. But it is surprising how such concepts have not found widespread use, neither in academia nor in industry. More *valorization* of these general principles is therefore needed.

Failure of *any* metal-polymer coating system can be ascribed to failure of the weakest link in the system at any time of its functional life. Closer inspection of the failure mechanism can lead to prevention of failure of the system by changing the pretreatment, optimizing the oxide, tailoring the coating itself or a combination of the three.

Of course there are many topics still left untouched.:

---

A knowledge gap exists between nanoscale chemistry (molecular motion, bonding) and averaged, macroscopical, mostly mechanical tests. Adhesion at the *meso* scale of several hundred nanometers to several micrometers needs closer examination, since for bonding and dissipation of energy in the systems, this is the relevant scale. With better understanding at the mesoscale, the properties of total systems could be improved or tailored better to the environments the system will be exposed to (temperature, humidity, mechanical loads, etc.). More understanding at this scale could also benefit research into polymer composite materials greatly.

As an extension to the previous, local bonding properties need to be related to local composition (variations) as well as local adhesion. For metals, oxides on precipitates are such local variations. So for research into the local bonding mechanism either the precipitates need to be made larger, which is technically possible, or local FTIR-RAS measurements should enable showing the distribution of molecules. This could lead to a better understanding of the local failure mode of coated systems of e.g. engineering materials, such as AA2xxx and AA7xxx. Ultimately this will also lead to the understanding of other metal/polymer combinations at the mesoscale, leading to better life time expectancy of coating systems.

---

## Summary

The aim of this PhD work was to obtain more knowledge on adhesion between polymers and aluminium alloys. Especially, studying the influence of the industrially important alloying element magnesium, was taken into account. Furthermore, the relation between (chemical) bonding and (macroscopic) adhesion on selected aluminium/magnesium alloys was topic of investigation.

In the first chapters (2 and 3) the background of bonding and adhesion as deduced from literature as well as the setup of the experiments is presented. The approach taken in literature using the bonding of specific molecules, which represent the functional groups of organic coatings, as well as the use of mechanical testing methods of adhesion of coating systems and the correlation between the two are elaborated upon.

Since there was not yet an established technique available to study adhesion under an organic coating in-situ, the experimental approach followed in this PhD was to use model molecules to study molecular bonding as a function of pre-treatments of the substrates. Mechanical adhesion was studied by a novel technique and a semi-quantitative link between bonding and adhesion is shown for a specific system.

Chapter 4 is dedicated to the determination of the composition of the aluminium-magnesium oxides by Auger analysis. In chapter 5 an attempt is made to determine the composition through electrochemical methods. It was found that both chemical as well as thermal treatments can result in a significant increase in magnesium at the surface of a aluminium alloy which contains 5 wt% magnesium.

The bonding on the varying (oxide) surface compositions is described in chapters 6 and 7. In chapter 6, the bonding of representative model molecules was studied for alloy compositions ranging between pure aluminium and pure magnesium. This work was aimed at the effect of the compositional changes (also induced by (wet) chemical and physical (temperature) pre-treatments) on bonding mechanisms. Two model molecules were used of which one represented the later discussed PETG coating. In chapter 7 bonding of succinic acid molecules is then studied on pretreated magnesium-aluminium alloys and their stability in aqueous environment.

Finally, in chapter 8, results of adhesion tests of a PETG coating on aluminium magnesium alloys by Asymmetrical Double Cantilever Beam (ADCB) are presented. These are then coupled to the results from chapter 6. Here, the link between chemical bonding and adhesion is made insofar that poor bonding properties translate to poor adhesion results and the presence of chemical bonding is a

---

necessity for mechanical adhesion. Some more detailed local observed phenomena are discussed.

The last chapter summarizes the conclusions from the other chapters and some new directions for research and future applications are discussed.

---

# Samenvatting

Het doel van dit promotie-onderzoek was meer kennis te vergaren op het gebied van hechting tussen polymeren en aluminium legeringen. In het bijzonder is er rekening gehouden met de invloed van het industrieel belangrijke legeringselement magnesium. Bovendien is het onderwerp van onderzoek de relatie tussen (chemische) binding en (macroscopische) hechting op deze geselecteerde aluminium/magnesium legeringen en gecoate systemen.

In de eerste hoofdstukken (2 en 3) wordt de achtergrond van binding en hechting zoals bekend uit de literatuur en de experimentele opzet gepresenteerd. De benadering in de literatuur van de binding van moleculen die model staan voor functionele groepen van organische deklagen en van mechanische testmethoden voor hechting van coatings en tevens de correlatie tussen die twee worden verder besproken.

Omdat er nog geen betrouwbare meetmethode beschikbaar was om hechting onder een organische deklaag in-situ te bestuderen, is als aanpak gekozen om met model moleculen de invloed van verschillende voorbehandelingen op de binding te bestuderen. Mechanische hechting werd met een nieuwe methode bestudeerd en een semi-kwantitatieve relatie tussen binding en hechting voor een specifiek systeem werd gevonden.

Hoofdstuk 4 is gewijd aan het bepalen van de samenstelling van de aluminium-magnesium oxides met behulp van Auger analyse. In hoofdstuk 5 wordt een poging gedaan de samenstelling met elektrochemische methoden te bepalen. Zowel chemische als warmtebehandelingen bleken te kunnen leiden tot een significante toename van magnesium aan het oppervlak van een aluminium legering die 5 gewichtsprocent magnesium bevat.

De binding op de verschillende (oxide) oppervlak samenstellingen wordt beschreven in hoofdstuk 6 en 7. In hoofdstuk 6 is de binding van representatieve model moleculen op samenstellingen die tussen puur aluminium en puur magnesium lagen bestudeerd. Dit is gebruikt om inzicht te krijgen in de effecten die samenstellingsveranderingen (ook veroorzaakt door (nat) chemische en fysische (warmte) voor-behandelingen) hadden op de bindingsmechanismen. Twee moleculen zijn gebruikt, waarvan er een de PETG coating representeert die later gebruikt wordt. In hoofdstuk 7 is de binding bestudeerd op voorbehandelde magnesium-aluminium legeringen en hun stabiliteit in waterige omgeving.

Tenslotte worden in hoofdstuk 8 de resultaten van hechtingstesten met Asymmetrical Double Cantilever Beam (ADCB) met een PETG coating en



---

aluminium-magnesiumlegeringen gepresenteerd. Deze worden dan gekoppeld aan de resultaten van hoofdstuk 6. Hier wordt ook de link gelegd tussen chemische binding en hechting met dien verstande dat slechte bindingseigenschappen zijn terug te vinden in slechte hechtings resultaten en dat de aanwezigheid van chemische binding een noodzakelijke voorwaarde is voor mechanische hechting. Tevens worden enkele gedetailleerde waarnemingen op lokale schaal besproken. In het laatste hoofdstuk worden de conclusies uit de andere hoofdstukken samengevat en worden enkele nieuwe richtingen voor onderzoek en toekomstige toepassingen besproken.

---

## Publications related to this work

### ***Journal papers***

*The influence of Chemical Pretreatment and Magnesium Surface Enrichment on Bonding of Succinic Acid Molecules to aluminium alloy* by F.M. de Wit, J.M.C. Mol, H. Terryn and J.H.W. de Wit, Journal of Adhesion Science and Technology 22 : 1089 2008

*Adhesion of Model Molecules to Metallic Surfaces, the Implications for Corrosion Protection* by J.H.W. de Wit, J. van den Brand, F.M. de Wit, and J.M.C. Mol, Corrosion Science And Technology 7 : 50 2008

*The influence of pre-treatments of aluminium alloys on bonding of PET coatings* by F. M. de Wit, Ö. Özkanat, J.M.C. Mol, H. Terryn and J.H.W. de Wit, Surface and Interface Analysis 42 : 316 2010

*Adhesion at Al-hydroxide-polymer interfaces: Influence of chemistry and evidence for microscopic self-pinning* by W.P. Vellinga, G. Eising, F.M. de Wit, J.M.C. Mol, H. Terryn, J.H.W. de Wit and J.Th.M. De Hosson, Materials Science and Engineering A 21-22 : 5637 2011

*Influence of pretreatments and aging on the adhesion performance of epoxy-coated aluminium* by Ö. Özkanat, F.M. de Wit, J.H.W. de Wit, H. Terryn and J.M.C. Mol, to be published in Surface and Coatings Technology/Thin Solid Films 2012

### ***Presentations, poster presentations and proceedings at international conferences***

*“Adhesion of succinic acid model molecules on pure magnesium and AA5182”* by F.M. de Wit, J. van den Brand, H. Terryn and J.H.W. de Wit, 1. Korrosionsschutz Symposium, Technische Akademie Wuppertal, Grainau, St. Goar, Germany, April 2005, poster presentation

*“(De)adhesion mechanism of organic molecules on Al-Mg alloys”* by F.M. de Wit, J. Flores, J. van den Brand, H. Terryn and J.H.W. de Wit, International Corrosion

---

Council (ICC) 2005, Beijing, China, September 2005, oral presentation and proceedings

*“Bonding mechanism of organic molecules on Al-Mg alloys”* by F.M. de Wit, J. van den Brand, H. Terryn and J.H.W. de Wit, 4<sup>th</sup> international symposium on Aluminium Surface Science and Technology (ASST), Beaune, France, May 2006, poster presentation

*“Bonding of organic molecules on aluminium and magnesium alloys”* by F.M. de Wit, J.J. Kleikers, J. van den Brand, H. Terryn and J.H.W. de Wit, Coatings Science International (COSI) Noordwijk, June 2006 and EuroCorr 2006, Maastricht, September 2006, oral presentations

*“Die Adhäsion von Polymeren auf Aluminium und Aluminium-Magnesium Legierungen“*, 2. Korrosionsschutz Symposium, Technische Akademie Wuppertal, Grainau, Germany, June 2007, oral presentation in German, invited

*“Adhesion of polymer coatings on aluminium and aluminium-magnesium alloys”* by F.M. de Wit, J.M.C. Mol, H. Terryn and J.H.W. de Wit, European Aluminium Association (EAA), SALSA workshop, Brussels, Belgium, June 2007, oral presentation

*“Bonding of organic molecules on pre-treated aluminium, magnesium and their alloys”* by F.M. de Wit, S. Göthel, T. Hauffman, J.M.C. Mol, H. Terryn and J.H.W. de Wit, Ecasia '07, September 2007, Brussels, Belgium, poster presentation

*“The influence of pre-treatment of aluminium-magnesium alloys on bonding of organic coatings”* by F.M. de Wit, G. Eising, T. Hauffman, W.-P. Vellinga, J.T.M. de Hosson, J.M.C. Mol, H. Terryn and J.H.W. de Wit, EuroCorr 2008 Edinburgh, UK, September 2008, oral presentation and proceedings paper #1306

*“The influence of pre-treatment of aluminium-magnesium alloys on bonding of organic coatings”* by F.M. de Wit, Ö. Özkanat, J.M.C. Mol, H. Terryn and J.H.W. de Wit, 5<sup>th</sup> international symposium on Aluminium Surface Science and Technology (ASST2009), May 2009, Leiden, oral presentation and proceedings

---

# Dankwoord

Er zijn in de loop van de tijd natuurlijk talloze mensen geweest die bewust of onbewust, wetenschappelijk of anderszins, hebben bijgedragen aan (het schrijven van) dit proefschrift. Voor ik begin met de officiële dankzegging, wil ik graag vooraf mededelen dat ik helaas niet al die mensen kan (be)noemen. Ook is mijn geheugen, zoals van eenieder onbetrouwbaar. Voelt u zich niet tekort gedaan, ik doe mijn best en mocht ik u onverhoopt vergeten zijn, schroom dan niet me hierop persoonlijk aan te spreken.

Voor mijn aanstelling als promovendus, financiële tegemoetkoming en ondersteuning tijdens het onderzoek wil ik de medewerkers van stichting M2i bedanken.

Mijn promotoren Prof. Rob Boom en Prof. Herman Terryen wil ik hartelijk danken voor het in mij gestelde vertrouwen en de kritische beoordeling en bijsturing van het onderzoek dat geleid heeft tot dit proefschrift.

De leiders van de groep waar ik mijn onderzoek gestart ben, Corrosie Technologie en Elektrochemie, Prof. Hans de Wit en zijn (inhoudelijke) opvolger Dr. Arjan Mol, wil uitgebreid bedanken voor de mogelijkheden en hulp die zij hebben geboden zowel binnen als buiten de groep. De expertise op het vakgebied en de opgebouwde ervaring waren (niet uitsluitend wetenschappelijk!) elke keer weer als een warm bad. Mijn voorganger en afstudeerbegeleider Jeroen van den Brand heeft mij op het juiste spoor gezet en zonder hem was de aanzet tot dit proefschrift nooit tot stand gekomen. Ik ben hem daar zeer dankbaar voor, al ben ik er zeker van dat hij dat nooit voor ogen had toen hij zelf promoveerde in 2004.

In de groep van Herman Terryen aan de VUB wil ik Jan Wielant en Tom Hauffman hartelijk danken voor het werk dat we samen hebben gedaan.

Willem-Pier Vellinga heeft, naast het zijn van een M2i collega, een zeer belangrijke rol gehad in de ontwikkeling van mijn begrip van hechting en onze samenwerking zal mij lang bijblijven.

Aan het begeleiden van mijn afstudeerders, Jeroen Kleikers, Stefanie Göthel en Gert Eising (samen met W-P. Vellinga) denk ik met plezier terug. De zelfstandigheid die zij in hun onderzoek hebben ontwikkeld heeft mijn vuur voor het geven van onderwijs opgestookt.

Mijn collega's door de jaren heen ben ik dank verschuldigd op talloze momenten, in goede en slechte tijden. Met name wil ik Wouter Hamer en Bart Norbart bedanken voor de samenwerking tijdens de verhuizing van ons laboratorium. Berend Boelen heeft in de laatste fase van mijn onderzoek nog de nodige zaken bij Tata Steel in

---

IJmuiden in gang gezet om tot betere resultaten te komen. Önnaz Özkanat wil ik hartelijk danken voor de samenwerking die geleid heeft tot het artikel waar ik co-auteur van ben in 2012. Voor de dagelijkse gang van zaken wil ik voor de prettige samenwerking door de jaren heen Peter, Xiaolong, Santiago, Raymond, Ivan, Andy, David, Anne, Emre, Vanya, Georgina, Deniz en nog vele anderen bedanken.

Tijdens het laatste gedeelte van het schrijven van dit proefschrift was ik in dienst bij het Hechtingsinstituut. Mijn dank gaat uit naar prof. Rinze Benedictus, Hans Poulis en Bas Out voor de samenwerking op het gebied van hechting in praktische zin. Ook al heb ik het proefschrift in mijn eigen tijd geschreven, hun bijdrage heeft zeker tot een beter begrip van hechting geleid!

Tenslotte wil ik mijn familie bedanken, in de eerste plaats mijn ouders, Hans en Barbara de Wit voor de morele ondersteuning en het (eindelozes) geduld en vertrouwen. Dankzij hen en natuurlijk mijn “kleine” broer Joost heb ik geleerd dat er meer is dan alleen exacte wetenschap, waarin ook Marjolein een belangrijke plek heeft ingenomen in de loop van de tijd.

Elke dag komen Yue en ons gezin voor mij op de eerste plaats. Yue is al die jaren voor mij de belangrijkste persoon geweest, soms op de voorgrond maar meestal als stille kracht op de achtergrond. Ze was er op de momenten dat ik ondersteuning nodig had, maar zij zorgde ook voor inspiratie die leidde tot het nodige doorzettingsvermogen. Haar geduld en inzet in lastige tijden hebben ervoor gezorgd dat ik mijn prioriteiten op orde heb gehad. Aan onze kinderen, Johannes en Daphne, die ontstaan zijn tijdens (het bewerken van) dit proefschrift, heb ik motivatie, inspiratie en de nodige positieve afleiding te danken. Voor en door jullie is dit proefschrift af gekomen. Waarvoor mijn oneindige dank.

---

# Curriculum Vitae

## Frederik Mathijs de Wit

Born in Utrecht, The Netherlands, December 16th 1979

### Education

1991 - 1997

Marnix Gymnasium, Rotterdam

1997 - 2004

Material Science & Engineering, Delft University of

Technology

### Professional Experience

2004 - 2009

PhD. candidate Materials innovation institute (M2i)  
at Delft University of Technology

2009 - 2012

Researcher / project leader Adhesion Institute,  
Delft University of Technology

From October 2012

Docent Werktuigbouwkunde (Mechanical  
Engineering), Haagse Hogeschool, Delft